NAS CR-135003
TRW ER-7861

ULTRAHIGH VACUUM, HIGH TEMPERATURE, LOW CYCLE FATIGUE OF COATED AND UNCOATED RENE' 80

FINAL REPORT

prepared for

NATIONAL AERONAUTICS AND SPACE ADMINISTRATION

UNDER CONTRACT NAS-3-17830

TRW MATERIALS TECHNOLOGY LABORATORIES
CLEVELAND, OHIO

Request for copies of this report should be referred to

National Aeronautics and Space Administration
Office of Scientific and Technical Information
Attention: AFSS-A
Washington, D. C. 20546

1. Report No.	2. Government Accession No.	3. Recipient's Catalog No.
NAS-CR-135003		

4. Title and Subtitle

ULTRAHIGH VACUUM, HIGH TEMPERATURE, LOW CYCLE FATIGUE OF COATED AND UNCOATED RENE' 80

5. Report Date

April 1976

6. Performing Organization Code

7. Author(s)

C. S. Kortovich

8. Performing Organization Report No.

TRW ER-7861

9. Performing Organization Name and Address

TRW Inc.
TRW Equipment
23555 Euclid Avenue
Cleveland, Ohio 44117

10. Work Unit No.

11. Contract or Grant No.

NAS-3-17830

13. Type of Report and Period Covered

FINAL
17 June 1974 - 17 February 1976

12. Sponsoring Agency Name and Address

U.S. Army Air Mobility R&D Laboratory
Moffett Field, California 94035

14. Sponsoring Agency Code

15. Supplementary Notes

Project Manager, G. R. Halford, Materials Structures Division
NASA Lewis Research Center
Cleveland, Ohio 44135

16. Abstract

A study was conducted on the ultrahigh vacuum strain controlled low cycle fatigue behavior of uncoated and CODEP B-1 aluminide coated Rene' 80 nickel-base superalloy at 1000°C (1832°F) and 871°C (1600°F). The results indicated little effect of coating or temperature on the fatigue properties. There was, however, a significant effect on fatigue life when creep was introduced into the strain cycles. The effect of this creep component was analyzed in terms of the method of Strainrange Partitioning. The longest lives were obtained with $\Delta\varepsilon_{pp}$ type cycling, while the $\Delta\varepsilon_{cc}$ cycle caused a reduction of fatigue life of about 1/2 order of magnitude with respect to the $\Delta\varepsilon_{pp}$ life. The $\Delta\varepsilon_{cp}$ type cycle caused a life reduction of slightly less than 1 order of magnitude with respect to the $\Delta\varepsilon_{pp}$ life, while the $\Delta\varepsilon_{pc}$ type cycle provided a fatigue life approximately 1 order of magnitude below that of the $\Delta\varepsilon_{pp}$ life.

Metallographic evaluation indicated that microstructural damage varied with cycle type and test temperature. Specimens tested with the $\Delta\varepsilon_{pp}$ type deformation exhibited a transgranular fracture mode. Specimens with the $\Delta\varepsilon_{pc}$ type deformation exhibited an intergranular fracture mode with extensive grain boundary sliding resulting in steps or grain extrusions particularly at 1000°C (1832°F). Specimens tested with the $\Delta\varepsilon_{cp}$ type deformation exhibited an intergranular fracture mode while the $\Delta\varepsilon_{cc}$ specimens exhibited different fracture modes depending on test temperature. At 1000°C (1832°F) the fracture mode was intergranular while at 871°C (1600°F) the fracture mode was transgranular.

17. Key Words (Suggested by Author(s))	18. Distribution Statement
Nickel-Base Superalloys Coatings Rene' 80 Low Cycle Fatigue Creep Damage Strainrange Partitioning	Unclassified-Unlimited

19. Security Classif. (of this report)	20. Security Classif. (of this page)	21. No. of Pages	22. Price*
Unclassified	Unclassified	60	3.00

* For sale by the National Technical Information Service, Springfield, Virginia 22161

FOREWORD

The work described in this report was performed in the Materials Technology Laboratory of TRW Inc. under the financial sponsorship of the U.S. Army Air Mobility R&D Laboratory for the National Aeronautics and Space Administration, Contract NAS-3-17830. The program was administered for TRW By Dr. H. E. Collins, Program Manager. The Principal Investigator was Dr. C. S. Kortovich, with technical assistance provided by Mr. J. W. Sweeney. The NASA Technical Manager was Dr. G. R. Halford.

Prepared by C. S. Kortovich
C. S. Kortovich
Principal Engineer

Reviewed by H. E. Collins
H. E. Collins
Section Manager
Physical Metallurgy & Coating Technology Section

Approved by J. A. Alexander
J. A. Alexander
Manager
Materials Research

TABLE OF CONTENTS

		Page
I	INTRODUCTION	1
II	EXPERIMENTAL PROCEDURES	2
	A. Task I - Specimen Preparation	2
	B. Task II - Cyclic Fatigue Tests	5
	C. Task III - Supplementary Mechanical Property Tests	7
III	RESULTS AND DISCUSSION	8
	A. Fatigue Test Results	8
	B. Microstructural Observations	23
	C. Supplementary Mechanical Properties	33
IV	SUMMARY	34
V	REFERENCES	35
	APPENDIX A	36
	APPENDIX B	59

I INTRODUCTION

The use of diffusion aluminide protective coating systems on superalloys in gas turbine engines for the improvement of oxidation and hot corrosion resistance has become quite widespread as a result of increasing cycle temperatures. Although they accomplish this purpose, there is concern that such coatings may degrade the mechanical properties of coated hardware. Of particular concern is a reduction of fatigue resistance in complex geometry hot section components such as turbine blades and vanes which experience severe thermal-mechanical strain cycling during engine service.

The application of a coating to the surface of a material can have a number of effects relevant to the fatigue properties of the coating-substrate system (1). For example, the deformation behavior of the substrate may be changed by the presence of a surface layer having a different elastic modulus and yield strength from that of the substrate. If the fatigue properties of the coating are better than that of the substrate, increased life may be expected. On the other hand, if the fatigue properties are poorer than the substrate, cracks in the coating will serve as surface notches and as paths for the degrading environment to reach the substrate, resulting in reduced fatigue life. In general, the effect that a coating has on the fatigue properties depends on the strainrange, the maximum tensile and compressive strain, temperature, frequency and the nature of the coating itself (1).

The present study was undertaken to provide further insight into the thermal-mechanical fatigue behavior of the nickel-base superalloy Rene' 80 in the coated (CODEP B-1) and uncoated condition. This program involved closed-loop, servo-controlled fatigue testing with independently programmed temperature control and strain cycling to develop baseline data for analysis of thermal fatigue behavior by the method of strainrange partitioning (2). Tests were performed in air and in vacuum to separate the effects of environmental interactions from mechanical effects of the coating on fatigue behavior. Interpretation was made of the influence of thermal cycling on fatigue life within the framework of the strainrange partitioning concept by correlating microstructural damage with various types of reversed inelastic strain cycles involving reversed and unreversed tensile and compressive creep deformation. The program was a cooperative effort between the Materials Technology Laboratory of TRW Inc. and the Materials and Structures Division of the NASA-Lewis Research Center, with vacuum tests being performed at TRW and air testing at NASA. This report presents the results of the vacuum fatigue tests performed at TRW.

II EXPERIMENTAL PROCEDURES

For this program the effect of CODEP B-1 aluminide coating on the thermal-mechanical fatigue behavior of nickel-base superalloy Rene' 80 was evaluated. The program was divided into three tasks, specimen preparation, cyclic fatigue tests and supplementary mechanical property testing. In the following sections the experimental procedures for each task are discussed.

A. Task I - Specimen Preparation

The specimens used for the present study were the individually cast, tubular, hour glass-shaped specimens with threaded ends as per NASA Drawing CB-300740, shown in Figure 1. The specimens were originally cast as solid bars and were then machined to the proper configuration. The composition of the material used for this program is listed in Table I. Uncoated specimens were given the following heat treatment:

1218°C (2225°F)/2 hours vacuum/argon quench to room temperature

1093°C (2000°F)/4 hours vacuum/argon quench to room temperature

1052°C (1925°F)/4 hours vacuum, furnace cool in vacuum to 649°C (1200°F) within 1 hour, air cool to room temperature*

843°C (1550°F)/16 hours vacuum/furnace cool to room temperature

Coated specimens were prepared with the CODEP B-1 aluminide coating. The alumina precoat was deposited on both the internal and external surfaces of the specimens by the electrophoresis technique. All other aspects of the coating application process conformed to General Electric Company Specification No. F50T58-S1. The resulting coating thickness was approximately 0.05mm (0.002 inch). The coated specimens were given the following heat treatment cycle:

1218°C (2225°F)/2 hours vacuum/argon quench to room temperature

1093°C (2000°F)/4 hours vacuum/argon quench to room temperature coating cycle as per Specification No. F50T58-S1

843°C (1550°F)/16 hours vacuum/furnace cool to room temperature

---

* This simulates coating cycle

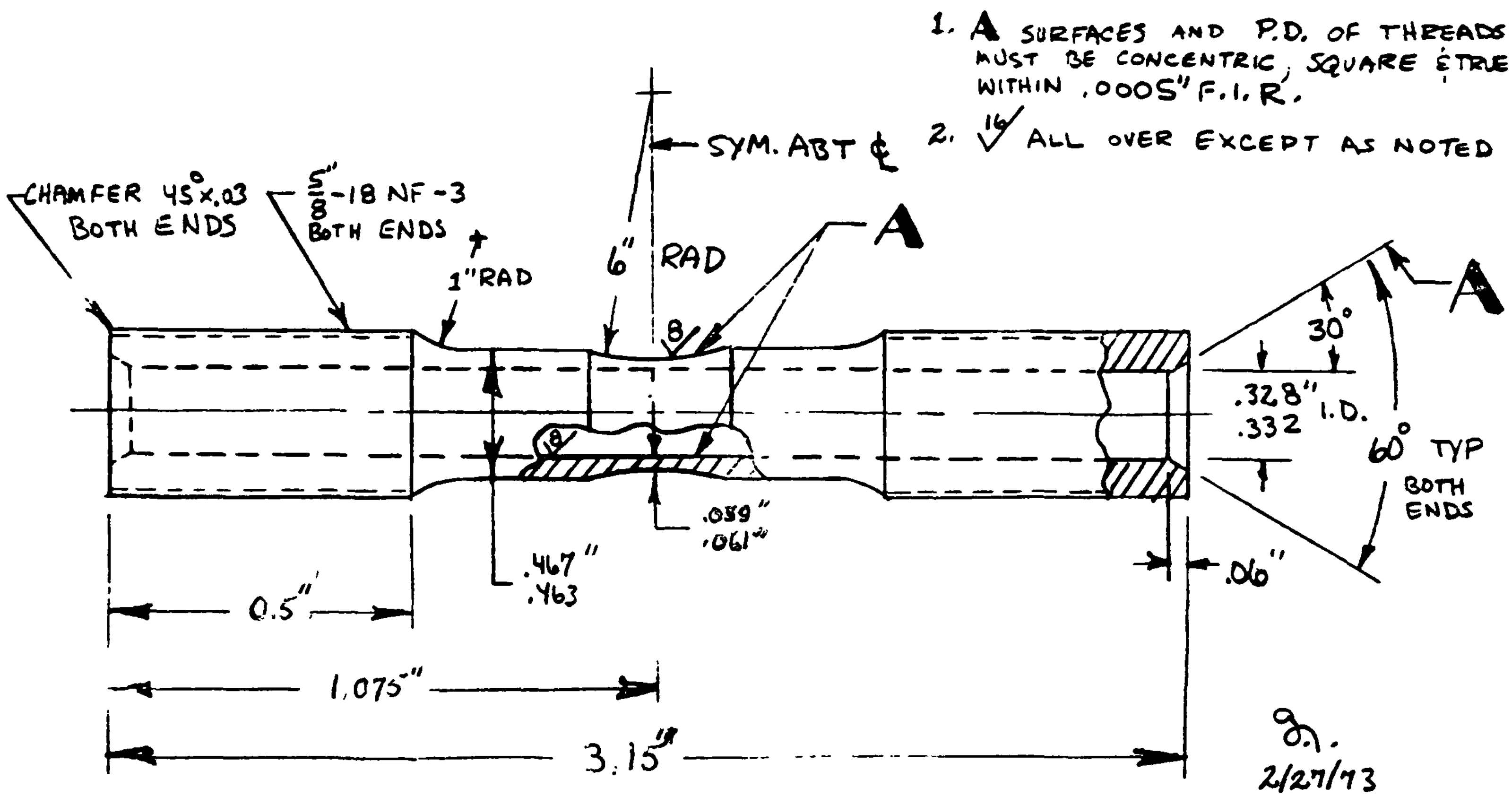

Figure 1. Fatigue test specimen

TABLE I

COMPOSITION OF RENE' 80 MATERIAL UTILIZED FOR LOW CYCLE FATIGUE TEST PROGRAM (w/o)

Element	Composition (1)	Nominal Composition (2)
C	0.17	0.17
Si	<0.05	-
Mn	<0.02	-
Cr	13.80	14.0
Mo	4.11	4.0
Fe	0.13	-
Ti	4.87	5.0
Al	2.99	3.0
Co	9.73	9.5
W	3.94	4.0
Zr	0.043	0.03
B	0.015	0.015
Ni	Balance	Balance

(1) TRW Master Heat BL 5138

(2) ASTM Data Series Publication No DS9E

B. Task II - Cyclic Fatigue Tests

The basic fatigue test program involved isothermal strain cycling to measure the four basic types of creep-fatigue life relationships defined by the strainrange partitioning method (2). The basis of this approach is the concept that two modes of inelastic deformation must be considered during low cycle fatigue, plastic flow and creep. These may exist separately or concurrently, and their interaction can influence the fracture behavior of a material to a considerable degree. Plastic flow is regarded as the sum of all inelastic strain components which occur nearly immediately upon application of stress (time independent) while creep is regarded as the sum of all time-dependent components. A major factor in strainrange partitioning is the shape of the stress-strain hysteresis loop during completely reversed straining and the manner in which the tensile and compressive components of strain are applied.

Strainrange partitioning is based on separation of the reversed inelastic strainrange into components which represent both the direction and the nature of the deformation. The critical point involves how the deformation is reversed in the fatigue cycle. Four basic types of reversed strain are defined:

$\Delta\varepsilon_{pp}$, tensile plastic strain reversed by compressive plastic strain

$\Delta\varepsilon_{cp}$, tensile creep strain reversed by compressive plastic strain

$\Delta\varepsilon_{pc}$, tensile plastic strain reversed by compressive creep strain

$\Delta\varepsilon_{cc}$, tensile creep strain reversed by compressive creep strain

The idealized hysteresis loops for these are shown in Figure 2.

pp strain is experienced at low temperatures, where creep does not occur, or at a high temperature and frequency where thermally activated flow is prohibited. cc deformation occurs in a low frequency, high temperature cycle where the strain rate is low enough that essentially all of the inelastic strain occurs by creep. Pure cp and pc types of deformation would be found in cycles where all of the deformation in one direction occurs at a low temperature and all of the reverse deformation takes place at a high enough temperature and low enough strain rate so that all of the reversed strain occurs by a thermally activated flow mechanism. Another case where this type of deformation might occur would be an isothermal cycle where the tensile and compressive strain rates are not equal so that one half of the cycle sustains more creep deformation than the other half.

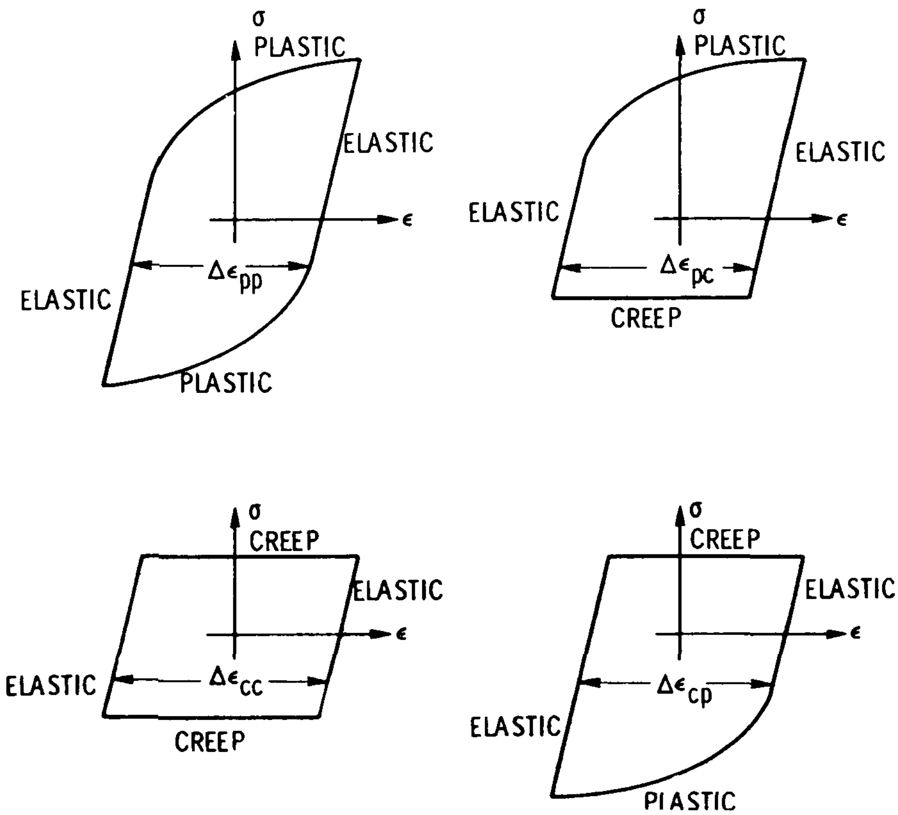

Figure 2. Idealized hysteresis loops for the four basic types of inelastic strainrange.

The basic test program for the present study was conducted at 1000°C (1832°F) and in an ultrahigh vacuum environment below 10^{-7} torr. On the basis of the results obtained from this basic program, similar tests were conducted at 871°C (1600°F) in a poorer vacuum (approximately 10^{-6} torr) to determine the effect of the variation of these parameters on the four basic types of creep-fatigue life relationships defined by the strainrange partitioning method. In order to more completely define the effect of the temperature variable on low cycle fatigue life a series of pp type tests were conducted on uncoated material at a range of temperatures from the ambient to 1000°C (1832°F) in the poorer vacuum.

Equipment and procedures used for the vacuum thermal fatigue tests on this program have been described in detail in previous reports (3,4). Briefly, the test apparatus was designed to perform completely reversed push-pull fatigue tests on hour-glass specimens using independently programmable temperature and strain control. Temperature was programmed using a thyratron-controlled 50 KV AC transformer for direct resistance heating of the specimen, while diametral strain was controlled directly using an LVDT type extensometer coupled to a programmable closed loop electrohydraulic servosystem. The measured specimen diameter was compensated electronically for thermal expansion so that net mechanical strain was controlled directly. Load, diameter and temperature were recorded continuously, with load-diameter hysteresis loops being obtained at periodic intervals during each test. Tests were conducted over a range of strain amplitudes (as measured by the width of the hysteresis loop at zero load) versus cycles to failure. Fatigue failure was defined in all cases as complete separation of the specimens into two pieces. Fractured specimens were sectioned longitudinally and examined metallographically to evaluate the character of the microstructural damage associated with each of the applied cycles.

C. Task III - Supplementary Mechanical Property Tests

Supplementary vacuum tensile and creep-rupture tests were also conducted in this program to provide baseline characterization data. All supplementary tests were conducted in ultrahigh vacuum (below 10^{-7}) at 871°C (1600°F) and 1000°C (1832°F) using tubular hour-glass specimens identical to those used for fatigue tests. Tension tests were conducted on both coated and uncoated specimens using a crosshead extension rate approximately equal to the frequency of the pp type fatigue tests (1.0 Hz). Properties measured were 0.2% offset yield strength, ultimate tensile strength and % reduction of area. Creep-rupture tests were conducted at constant load on coated and uncoated specimens. Reduction of area and rupture life were measured in these tests and a recording against time of the axial creep strain up to failure was also obtained.

III RESULTS AND DISCUSSION

A. Fatigue Test Results

The dynamic stress-strain response (hysterisis loops) for all the fatigue tests conducted in this program are presented in Appendix A along with a list of the elastic modulus at each test temperature used to calculate the elastic strain. In the following discussion PP, PC, CP and CC will refer to $\Delta\varepsilon_{pp}$, $\Delta\varepsilon_{pc}$, $\Delta\varepsilon_{cp}$ and $\Delta\varepsilon_{cc}$ types of deformation, respectively. All PP tests were conducted at approximately 1 Hz. For the PC and CP tests the time required to reverse the creep portion of the cycle by plastic strain and then initiate the creep portion again was 1 second or less. For the CC tests the time required to initiate creep in the reversed direction was also 1 second or less.

The fatigue life results are summarized in Tables II - VI. Table II lists the results of tests conducted at 1000°C (1832°F) and 871°C (1600°F) for uncoated and coated material tested with the PP type cyclic deformation while Tables III, IV and V list results for tests conducted with the PC, CP and CC types of deformation, respectively. Note that in Table III, containing the PC results, eight tests were conducted on uncoated material at 1000°C (1832°F) instead of the usual five. Three extra tests (89U-PC-1, 94U-PC-14 and 97U-PC-15) were conducted here because analysis of the data for the first five tests indicated that drift may have occurred in the zero point for the load and strain control settings resulting in erroneous readings. Thus, the values of total, inelastic and partitioned inelastic strainrange may be in error. Table VI lists the results of tests conducted at a number of different temperatures on uncoated material with the PP type deformation in a poorer vacuum (approximately 10^{-6} torr).

The ultrahigh vacuum fatigue life results from Tables II - V are plotted against longitudinal strainrange in Figures 3-6. For the remainder of the discussion, the term strainrange will always refer to longitudinal strainrange. Each figure contains three different graphs including a plot and a least squares fit of total strainrange versus observed cycles to failure, inelastic strainrange versus observed cycles to failure and partitioned inelastic strainrange versus life relationships computed using the interaction damage rule (5). Figures 3 and 4 contain results for tests conducted at 1000°C (1832°F) for uncoated and coated material, respectively, while Figures 5 and 6 contain results for tests conducted at 871°C (1600°F) for uncoated and coated material, respectively.

TABLE II

SUMMARY OF RENE' 80 FATIGUE TEST RESULTS FOR THE $\Delta\varepsilon_{pp}$ TYPE DEFORMATION

Specimen Number	Test Temperature °F	Test Temperature °C	Half-Life Axial Strain Range (MM/MM) Total	Elastic	Inelastic	Partitioned Inelastic	Half-Life Axial Stress Range Maximum (ksi)	Maximum (MN/M²)	Minimum (ksi)	Minimum (MN/M²)	Total Elapsed Time to Failure (Hours)	Actual Cycles to Failure
						Uncoated Specimens						
4U-PP-3	1832	1000	.00944	.00378	.00566	$F_{pp} = 1$	40.5	279.3	38.4	264.8	.1	306
5U-PP-4	"	"	.00277	.00122	.00155	"	13.4	92.4	12.2	84.1	1.7	6,302
6U-PP-5	"	"	.01250	.00363	.00887	"	40.4	278.6	35.4	243.4	.02	103
7U-PP-6	"	"	.00561	.00265	.00296	"	27.7	191.0	27.7	191.0	.6	2,298
8U-PP-7	"	"	.00247	.00169	.00078	"	17.0	117.2	18.4	124.8	5.9	22,115
21U-PP-8	1600	871	.00851	.00529	.00322	$F_{pp} = 1$	60.5	417.2	60.0	413.7	.2	642
22U-PP-9	"	"	.00241	.00215	.00026	"	26.2	180.7	22.8	156.5	44.0	163,533
41U-PP-10	"	"	.00630	.00451	.00179	"	50.9	350.9	51.8	357.1	.4	1,410
42U-PP-11	"	"	.00296	.00245	.00051	"	23.5	162.1	32.2	222.0	58.5	217,620
74U-PP-13	"	"	.01262	.00657	.00605	"	75.6	521.2	74.0	510.2	.04	145
						Coated Specimens						
43C-PP-1	1832	1000	.00152	.00101	.00051	$F_{pp} = 1$	10.4	71.7	10.8	74.4	55.5	206,460
45C-PP-3	"	"	.00490	.00247	.00243	"	25.9	178.6	25.7	177.2	.6	2,188
47C-PP-4	"	"	.00343	.00177	.00166	"	18.7	128.9	18.3	126.2	2.5	9,412
49C-PP-5	"	"	.00225	.00159	.00066	"	16.9	116.5	16.4	113.1	27.2	101,184
75C-PP-10	"	"	.00961	.00388	.00573	"	41.4	285.5	39.7	273.7	.1	233
51C-PP-6	1600	871	.00672	.00452	.00220	$F_{pp} = 1$	51.5	355.1	51.5	355.1	.5	1,860
52C-PP-7	"	"	.00742	.00512	.00230	"	59.4	409.6	57.2	58.6	.4	1,365
54C-PP-8	"	"	.00410	.00324	.00086	"	33.5	231.0	40.2	277.2	19.4	71,982
55C-PP-9	"	"	.00191	.00145	.00046	"	16.6	112.4	16.4	113.1	114.8	426,870
77C-PP-11	"	"	.01011	.00569	.00442	"	65.6	452.3	64.0	441.3	.1	293

TABLE III

SUMMARY OF RENE' 80 FATIGUE TEST RESULTS FOR THE $\Delta\varepsilon_{pc}$ TYPE DEFORMATION

Specimen No.	Test Temperature °F	°C	Half Life Axial Strainrange (MM/MM) Total	Elastic	In-elastic	Partitioned Inelastic FPC	Partitioned Inelastic Strain-Range	Half Life Axial Stress Range Maximum (ksi)	Maximum (MN/M^2)	Minimum (ksi)	Minimum (MN/M^2)	Total Elapsed Time to Failure (hours)	Actual Cycles to Failure	Partitioned Cycles to Failure
UNCOATED SPECIMENS														
9U-PC-1	1832	1000	.00944	.00191	.00753	.95	.00715	32.9	226.8	7.0	48.3	3.8	479	528
10U-PC-2	"	"	.01999	.00443	.01556	.86	.01338	69.4	478.6	23.1	159.3	1.0	19	18
12U-PC-4	"	"	.01809	.00445	.01364	.92	.01255	71.1	490.2	22.0	151.7	2.0	30	29
23U-PC-6	"	"	.00386	.00177	.00209	.93	.00194	25.6	176.5	11.4	78.6	16.9	9,810	11,202
26U-PC-8	"	"	.00409	.00169	.00240	.90	.00217	28.4	195.9	7.0	48.3	19.1	10,164	13,733
89U-PC-11	"	"	.00579	.00259	.00319	.85	.00271	39.1	270.3	15.0	103.4	4.9	187	161
94U-PC-14	"	"	.00464	.00246	.00218	.86	.00187	34.7	239.2	16.7	115.2	5.8	418	365
97U-PC-15	"	"	.00292	.00181	.00111	.80	.00089	27.3	188.3	10.5	72.4	26.9	1,978	1,713
28U-PC-9	1600	871	.00856	.00478	.00378	.75	.00283	75.4	519.9	33.5	231.0	2.9	148	127
29U-PC-10	"	"	.00330	.00126	.00204	.80	.00164	24.4	168.3	4.2	29.0	7.4	1,415	1,407
91U-PC-12	"	"	.00659	.00402	.00257	.81	.00209	63.6	438.5	27.8	194.7	5.9	356	312
92U-PC-13	"	"	.01064	.00510	.00554	.83	.00460	80.3	553.7	35.7	246.1	1.1	41	35
98U-PC-16	"	"	.00601	.00343	.00258	.71	.00183	56.6	390.2	21.4	147.6	42.8	396	322
COATED SPECIMENS														
56C-PC-1	1832	1000	.00819	.00348	.00471	.72	.00339	50.5	348.2	22.3	153.8	1.0	55	41
57C-PC-2	"	"	.00450	.00242	.00208	.91	.00189	35.1	242.0	15.4	106.2	8.2	386	355
58C-PC-3	"	"	.00581	.00288	.00293	.87	.00255	43.1	297.2	17.0	117.2	3.9	240	213
93C-PC-8	"	"	.00424	.00257	.00167	.85	.00142	44.2	304.8	9.6	66.2	41.2	691	596
96C-PC-10	"	"	.00585	.00289	.00296	.85	.00252	41.0	282.7	19.3	133.1	5.6	262	229
59C-PC-4	1600	871	.01107	.00535	.00572	.80	.00458	91.2	628.8	30.5	210.3	1.8	63	58
61C-PC-5	"	"	.00774	.00480	.00294	.86	.00252	75.5	520.1	33.7	232.3	6.6	282	261
88C-PC-6	"	"	.00485	.00331	.00154	.80	.00123	47.3	326.2	28.0	193.1	66.0	1,855	1,550
90C-PC-7	"	"	.01055	.00510	.00545	.84	.00457	82.2	566.8	33.9	233.7	2.6	48	43
95C-PC-9	"	"	.00835	.00463	.00372	.91	.00339	71.6	493.6	33.8	233.0	2.8	126	118

TABLE IV

SUMMARY OF RENE' 80 FATIGUE TEST RESULTS FOR THE $\Delta\epsilon_{cp}$ TYPE DEFORMATION

Specimen Number	Test Temperature °F	Test Temperature °C	Half Life Axial Strain Range (MM/MM) Total	Elastic	Inelastic	Partitioned Inelastic FCP	Partitioned Inelastic Strain-range	Half Life Axial Stress Range Maximum (ksi)	Maximum (MN/M²)	Minimum (ksi)	Minimum (MN/M²)	Total Elapsed Time to Failure (hours)	Total Time to to Failure	Partitioned Cycle Failure
Uncoated Specimens														
14U-CP-1	1832	1000	.01595	.00328	.01267	.78	.00987	29.2	201.3	39.4	271.2	.5	12	10
16U-CP-3	"	"	.00589	.00211	.00378	.70	.00264	18.6	128.2	25.4	175.2	7.6	601	512
17U-CP-4	"	"	.00409	.00169	.00240	.88	.00210	11.6	80.0	23.7	163.4	8.6	1,385	1,315
39U-CP-8	"	"	.00436	.00193	.00243	.93	.00227	14.3	98.6	26.1	180.0	8.6	527	497
111U-CP-10	"	"	.00957	.00246	.00711	.75	.00533	18.6	128.2	32.8	226.1	1.0	78	61
30U-CP-5	1600	871	.00736	.00447	.00289	.88	.00254	36.4	251.0	65.4	451.0	1.3	193	184
31U-CP-6	"	"	.00588	.00380	.00208	.97	.00202	28.0	193.1	58.4	402.7	4.7	530	520
36U-CP-7	"	"	.00364	.00253	.00111	.83	.00092	18.6	128.2	39.0	268.9	64.1	3,705	3,435
86U-CP-9	"	"	.00772	.00440	.00332	.92	.00306	31.4	216.5	68.8	474.3	3.4	147	138
112U-CP-11	"	"	.00907	.00512	.00385	.78	.00308	41.3	284.8	75.3	519.2	1.8	101	84
Coated Specimens														
65C-CP-3	1832	1000	.00603	.00284	.00319	.86	.00274	16.8	115.8	42.6	293.7	3.8	251	222
66C-CP-4	"	"	.00966	.00358	.00608	.82	.00498	24.8	171.0	50.0	344.7	1.0	66	58
85C-CP-7	"	"	.00568	.00244	.00324	.77	.00250	21.1	145.5	29.8	205.4	4.5	134	106
87C-CP-8	"	"	.00422	.00223	.00199	.85	.00169	18.0	124.1	28.6	197.2	6.2	950	835
113C-CP-9	"	"	.01023	.00368	.00655	.75	.00491	29.0	200.0	47.9	330.3	1.0	45	36
62C-CP-1	1600	871	.00995	.00498	.00497	.92	.00457	40.0	275.8	73.3	505.4	2.7	150	151
64C-CP-2	"	"	.00490	.00358	.00132	.88	.00116	34.9	240.6	46.7	322.0	33.6	1,818	1,630
83C-CP-5	"	"	.00709	.00464	.00245	.86	.00210	28.7	198.0	77.0	530.9	12.1	455	406
84C-CP-6	"	"	.01145	.00616	.00529	.82	.00433	52.0	358.5	88.2	608.1	1.5	29	25
115C-CP-11	"	"	.00907	.00533	.00374	.91	.00340	49.4	340.6	71.9	495.7	1.0	77	71

TABLE V

SUMMARY OF RENE' 80 FATIGUE TEST RESULTS FOR THE $\Delta\varepsilon_{cc}$ TYPE DEFORMATION

Specimen Number	Temperature °F	Temperature °C	Half Life Axial Strain Range (MM/MM) Total	Elastic	Inelastic	Partitioned Inelastic FCC	Strain-Range	FPP	Strain-Range	FPC	Strain-Range	Half Life Axial Stress Range Maximum (ksi)	Maximum (MN/M²)	Minimum (ksi)	Minimum (MN/M²)	Total Elapsed Time to Failure	Actual Cycles to Failure	Partitioned Cycles to Failure
UNCOATED SPECIMENS																		
19U-CC-3	1832	1000	.00457	.00159	.00298	.70	.00209	.20	.00060	.10	.00029	18.7	128.9	14.5	100.0	51.0	420	466
20U-CC-4	"	"	.00233	.00099	.00134	.85	.00114	.10	.00013	.05	.00007	12.4	85.5	8.2	56.5	70.5	8,154	11,993
40U-CC-5	"	"	.00273	.00118	.00155	.75	.00116	.20	.00031	.05	.00008	14.6	100.7	9.8	68.3	152.6	4,783	6,043
67U-CC-6	"	"	.00599	.00093	.00506	.75	.00380	.20	.0010	.05	.00025	11.7	80.7	7.8	53.8	24.8	257	267
119U-CC-11	"	"	.00973	.00251	.00722	.85	.00614	.11	.00079	.04	.00029	27.1	186.9	25.3	174.5	2.6	69	70
71U-CC-7	1600	871	.01368	.00405	.00963	.68	.00655	.25	.00241	.07	.00067	50.9	351.0	41.4	285.5	1.6	26	33
73U-CC-8	"	"	.01193	.00424	.00769	.78	.00600	.11	.00085	.11	.00084	50.0	344.7	46.5	320.7	2.2	35	56
76U-CC-9	"	"	.00784	.00340	.00444	.90	.00400	.03	.00013	.07	.00031	41.9	289.0	35.6	245.4	17.6	166	215
79U-CC-10	"	"	.00507	.00263	.00244	.84	.00205	.12	.00029	.04	.00010	32.3	222.7	27.5	189.7	53.1	637	607
120U-CC-12	"	"	.00622	.00267	.00355	.78	.00277	.20	.00071	.02	.00007	30.9	213.0	29.9	206.1	6.6	181	158
COATED SPECIMENS																		
68C-CC-1	1832	1000	.01135	.00269	.00865	.85	.00736	.08	.00069	.07	.00060	30.3	208.9	26.0	179.3	1.1	17	16
81C-CC-6	"	"	.00790	.00228	.00562	.68	.00384	.08	.00045	.24	.00133	25.9	178.6	21.8	150.3	3.8	76	99
82C-CC-7	"	"	.00445	.00191	.00254	.88	.00223	.06	.00015	.06	.00016	22.5	155.2	17.5	120.7	42.9	621	654
116C-CC-8	"	"	.00754	.00239	.00515	.89	.00458	.06	.00031	.05	.00026*	28.4	195.9	21.6	148.9	4.2	77	78
117C-CC-9	"	"	.00555	.00210	.00345	.75	.00259	.20	.00069	.05	.00017	23.3	160.7	20.5	141.4	12.0	225	233
69C-CC-2	1600	871	.01005	.00420	.00585	.73	.00427	.17	.00099	.10	.00059	49.6	341.9	46.0	317.2	6.0	108	204
72C-CC-3	"	"	.01377	.00543	.00834	.79	.00659	.15	.00125	.06	.00050	64.7	446.1	59.0	406.8	2.5	33	52
78C-CC-4	"	"	.00917	.00413	.00504	.69	.00348	.14	.00071	.17	.00085	50.4	347.5	43.7	301.3	6.7	109	192
80C-CC-5	"	"	.00824	.00404	.00420	.93	.00390	.04	.00017	.03	.00013*	48.3	333.0	43.6	300.6	18.6	171	223
118C-CC-10	"	"	.00582	.00316	.00266	.75	.00200	.19	.00050	.06	.00016	38.2	263.4	33.7	232.3	31.7	554	615

* Partitioned Inelastic $\Delta\varepsilon_{cp}$ Deformation

TABLE VI

SUMMARY OF RENÉ 80 FATIGUE RESULTS FOR $\Delta\varepsilon_{pp}$ TESTS CONDUCTED ON UNCOATED MATERIAL IN POORER VACUUM (APPROXIMATELY 10^{-6} TORR)

Specimen Number	Temperature °F	Temperature °C	Half-Life Axial Strain Range (MM/MM) Total	Elastic	Inelastic	Partitioned Inelastic	Half-Life Axial Stress Range Maximum (ksi)	Maximum (MN/M^2)	Minimum (ksi)	Minimum (MN/M^2)	Total Elapsed Time to Failure (Hours)	Actual Cycles to Failure
99U-PP-14	Room	Room	.00639	.00568	.00071	Fpp = 1	91.2	628.8	79.1	545.4	2.0	6,900
110U-PP-25	Room	Room	.00979	.00828	.00151	Fpp = 1	117.5	810.2	130.6	900.4	0.5	1,306
101U-PP-16	400	204	.00741	.00667	.00074	Fpp = 1	97.0	668.8	96.1	662.6	0.5	1,674
102U-PP-17	"	"	.00769	.00698	.00071	Fpp = 1	97.7	674.3	103.3	712.3	0.6	2,170
1U-PP-1*	1000	538	.00874	.00773	.00101	Fpp = 1	96.3	664	106.7	735.6	0.6	1,621
2U-PP-2*	"	"	.00747	.00654	.00093	Fpp = 1	82.4	568.2	89.3	615.7	0.5	1,950
105U-PP-20	1200	649	.00784	.00669	.00115	Fpp = 1	83.6	576.4	85.5	589.6	0.2	744
107U-PP-22	"	"	.00642	.00539	.00103	Fpp = 1	71.9	495.7	64.5	444.8	1.3	4,402
103U-PP-18	1400	760	.00604	.00488	.00116	Fpp = 1	61.5	424.1	56.3	388.2	1.2	4,216
104U-PP-19	"	"	.00792	.00663	.00129	Fpp = 1	77.8	536.4	82.4	568.2	0.1	496
108U-PP-23	1832	1000	.00343	.00204	.00139	Fpp = 1	22.7	156.5	20.0	137.9	1.6	5,766
109U-PP-24	"	"	.00576	.00280	.00296	Fpp = 1	30.6	210.9	27.9	192.4	0.3	1,240

* This test conducted in ultra-high vacuum, approximately 10^{-7} and below.

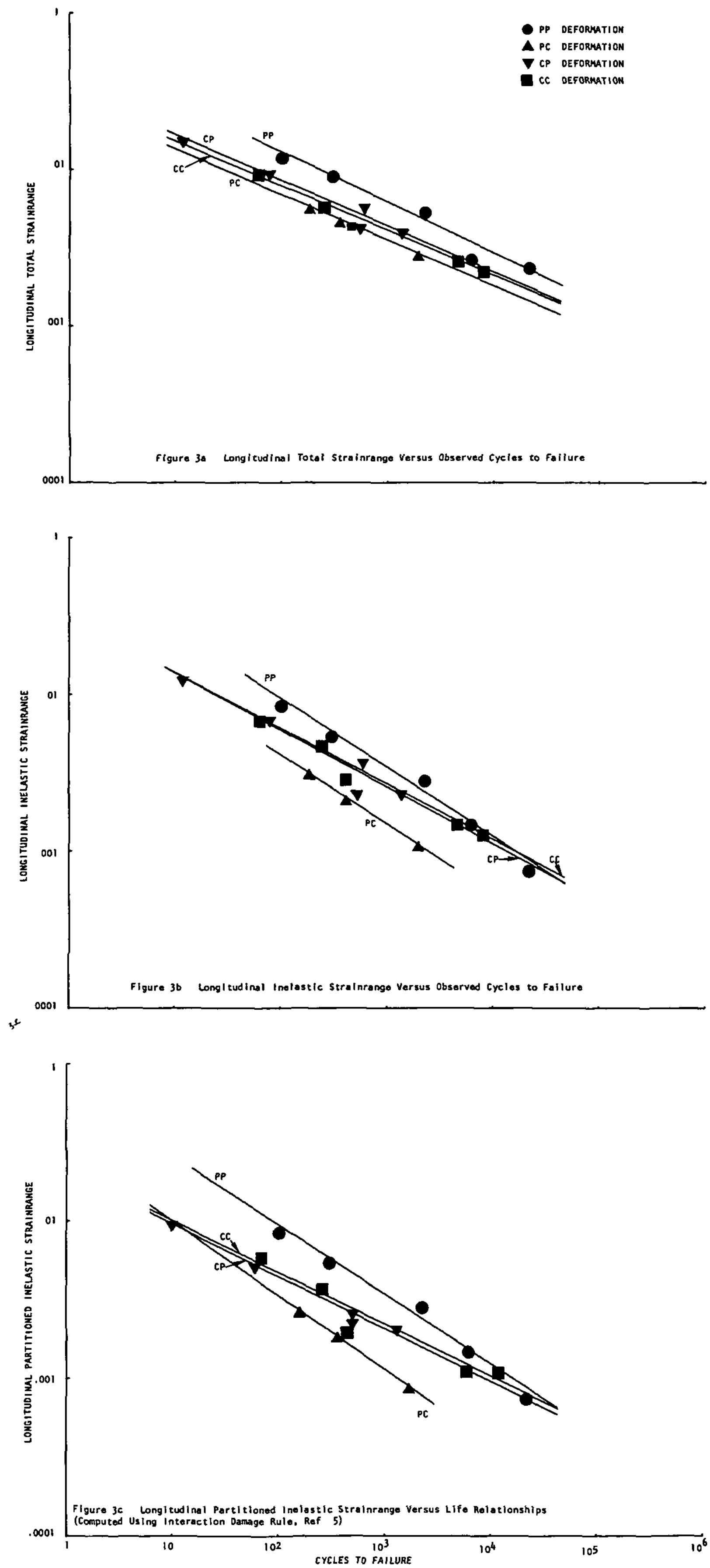

Figure 3. Rene' 80 Fatigue Test Results at 1000°C (1832°F) in the Uncoated Condition.

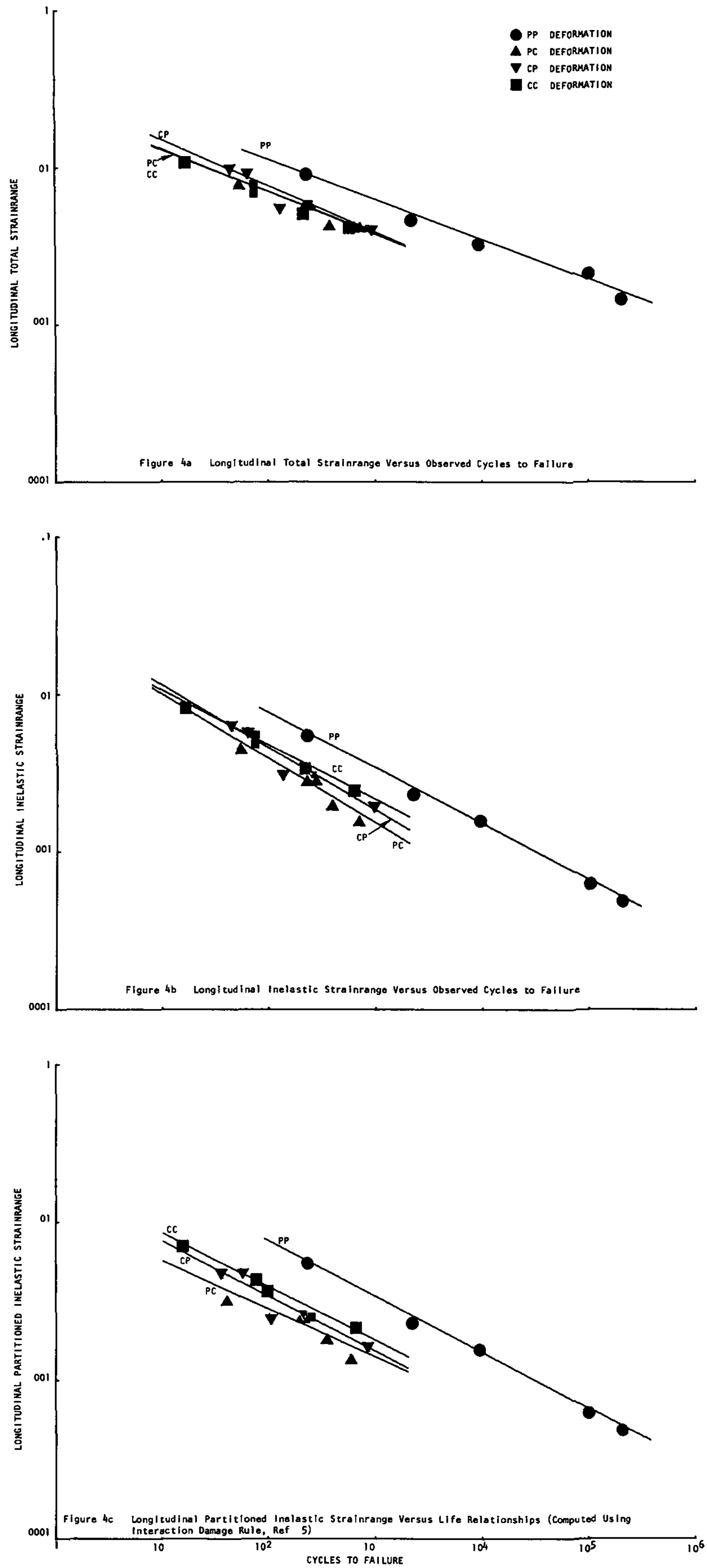

Figure 4. Rene' 80 Fatigue Test Results at 1000°C (1832°F) in the Coated Condition.

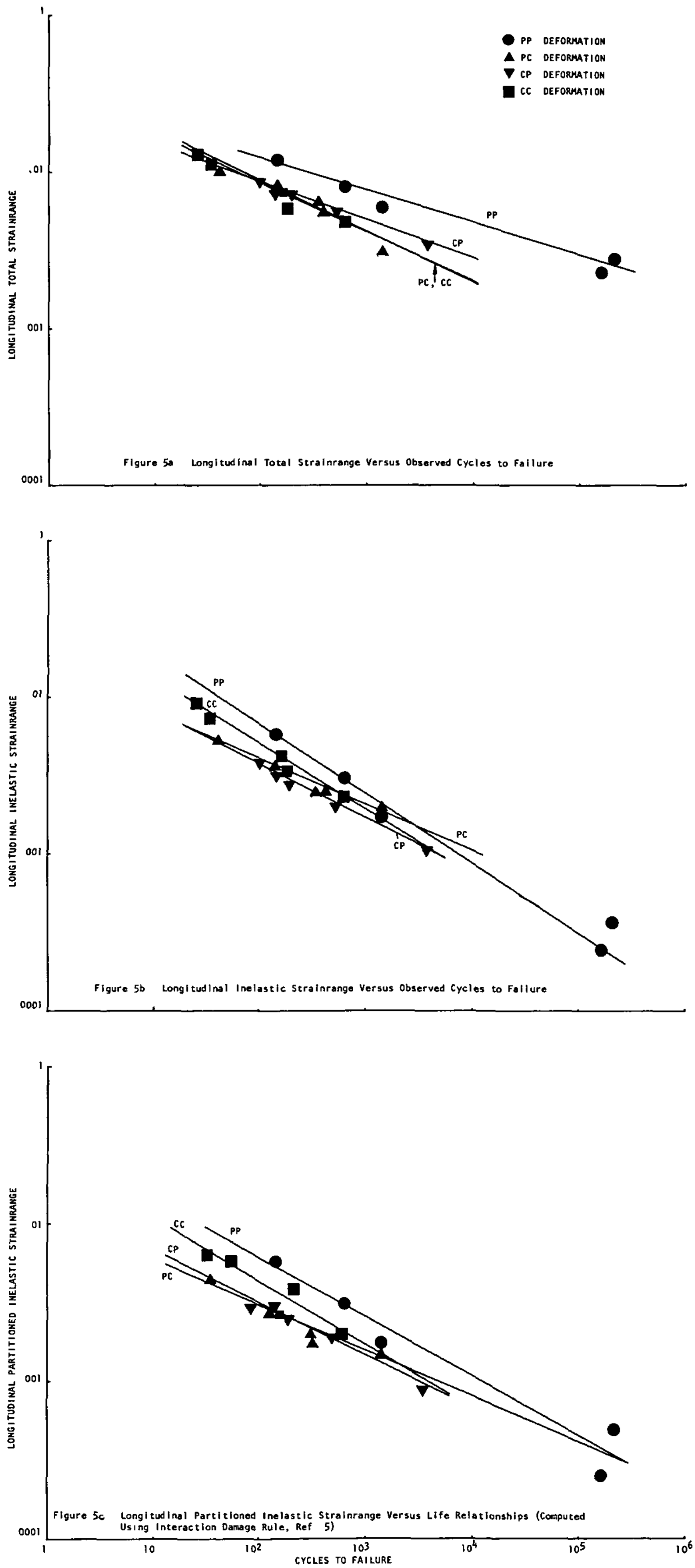

Figure 5a Longitudinal Total Strainrange Versus Observed Cycles to Failure

Figure 5b Longitudinal Inelastic Strainrange Versus Observed Cycles to Failure

Figure 5c Longitudinal Partitioned Inelastic Strainrange Versus Life Relationships (Computed Using Interaction Damage Rule, Ref 5)

Figure 5. Rene' 80 Fatigue Test Results at 871°C (1600°F) in the Uncoated Condition.

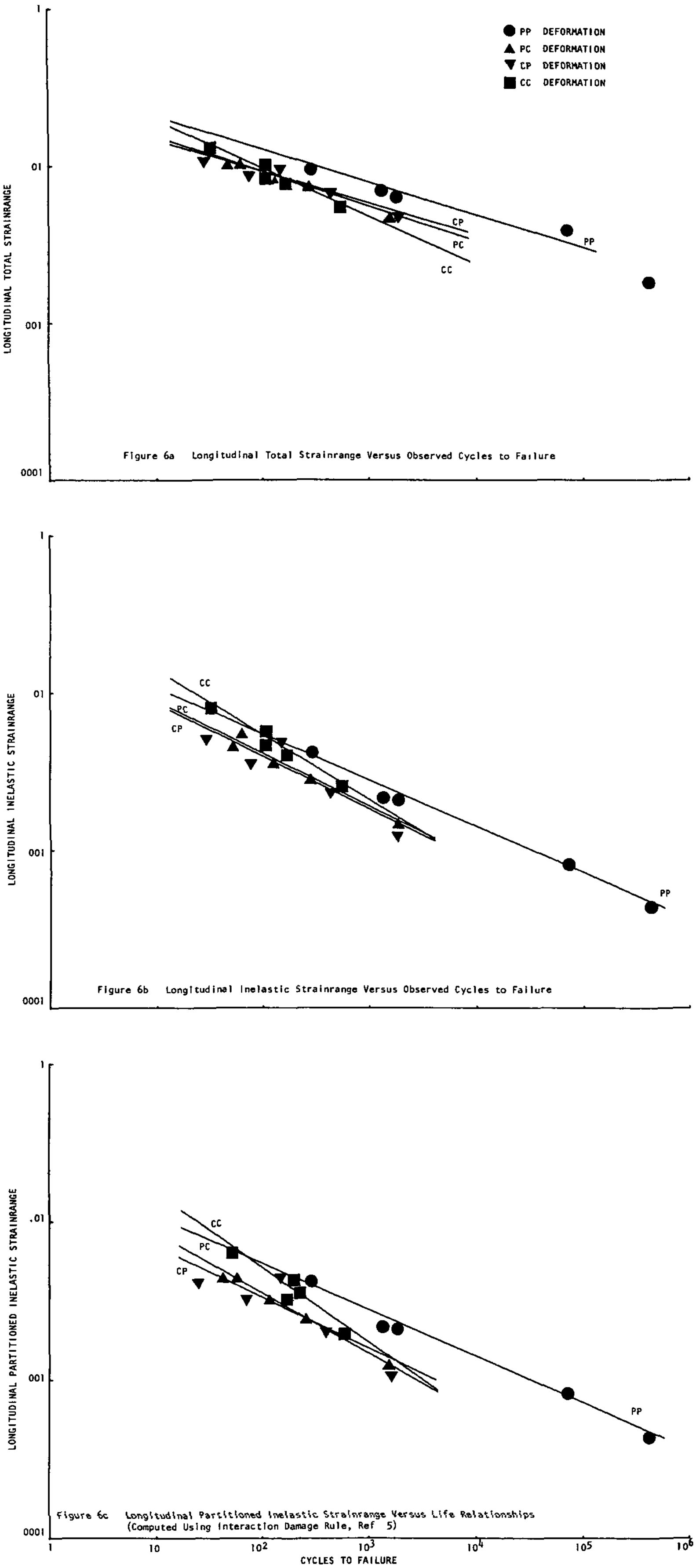

Figure 6. Rene' 80 Fatigue Test Results at 871°C (1600°F) in the Coated Condition.

For tests conducted at 1000°C (1832°F), Figures 3 and 4, the results indicate that the relative positions of the failure lives for the four basic types of strainrange components (PP, PC, CP and CC) changes little as a result of the presence of the aluminide coating. In all instances PP deformation was the least damaging while PC deformation was the most damaging by approximately an order of magnitude difference in number of cycles to failure. The CP and CC lines were quite close together and fell between the PC and PP lines, ranging from 2/3 to 1/2 order of magnitude below the PP line. A difference was observed between coated and uncoated material, however, in that for the values of inelastic and partitioned inelastic strainrange included in this study for uncoated material, the lines for CP and CC approached the PP line at the low strainrange values, Figures 3b and 3c.

Results of tests conducted at 871°C (1600°F), Figures 5 and 6, were consistent with those conducted at 1000°C (1832°F) in that the aluminide coating had little effect on the relative positions of the failure lives for the four basic types of strainrange components. In all cases PP deformation was the least damaging. Unlike the 1000°C (1832°F) results, however, the PC and CP lines were both comparable, ranging from 1/2 to 1 order of magnitude below the PP line. In terms of total and inelastic strainrange, the CC results were somewhat comparable to those for PC and CP, but the partitioned inelastic strainrange results indicated that CC was less damaging than PC and CP by approximately 1/2 order of magnitude at the higher strainrange values. Manson and Halford have made an analysis utilizing Strainrange Partitioning (6) of the low cycle fatigue data generated independently by Lord and Coffin on uncoated Rene' 80 at 871°C (1600°F). They determined that the partitioned lives for the 0.0032 strainrange at this temperature were $N_{pp} = 600$, $N_{cp} = 450$, $N_{cc} = 190$ and $N_{pc} = 80$. With the exception of the N_{cp} results, these values agree quite closely with the data presented in Figure 5c. This indicates that the Method of Strainrange Partitioning may have some potential as a unifying framework around which the many factors concerning fatigue at elevated temperatures can be coherently structured.

In order to illustrate the effect of temperature and coating on these fatigue results in a more graphic manner, the results for each of the basic types of deformation have been plotted separately in Figures 7-10 in terms of total strainrange versus observed cycles to failure and partitioned inelastic strainrange versus life relationship computed using the interaction damage rule (5). For each of these plots a least squares fit was made of all the data. These least squares lines suggest that for all four basic types of deformation, there was little difference between coated and uncoated material at 1000°C (1832°F) and 871°C (1600°F) and further, that there was little effect of temperature on the fatigue results. These results were not unexpected in that the ultrahigh vacuum test atmosphere nullified the effect of oxidation behavior thus minimizing possible differences in fatigue behavior.

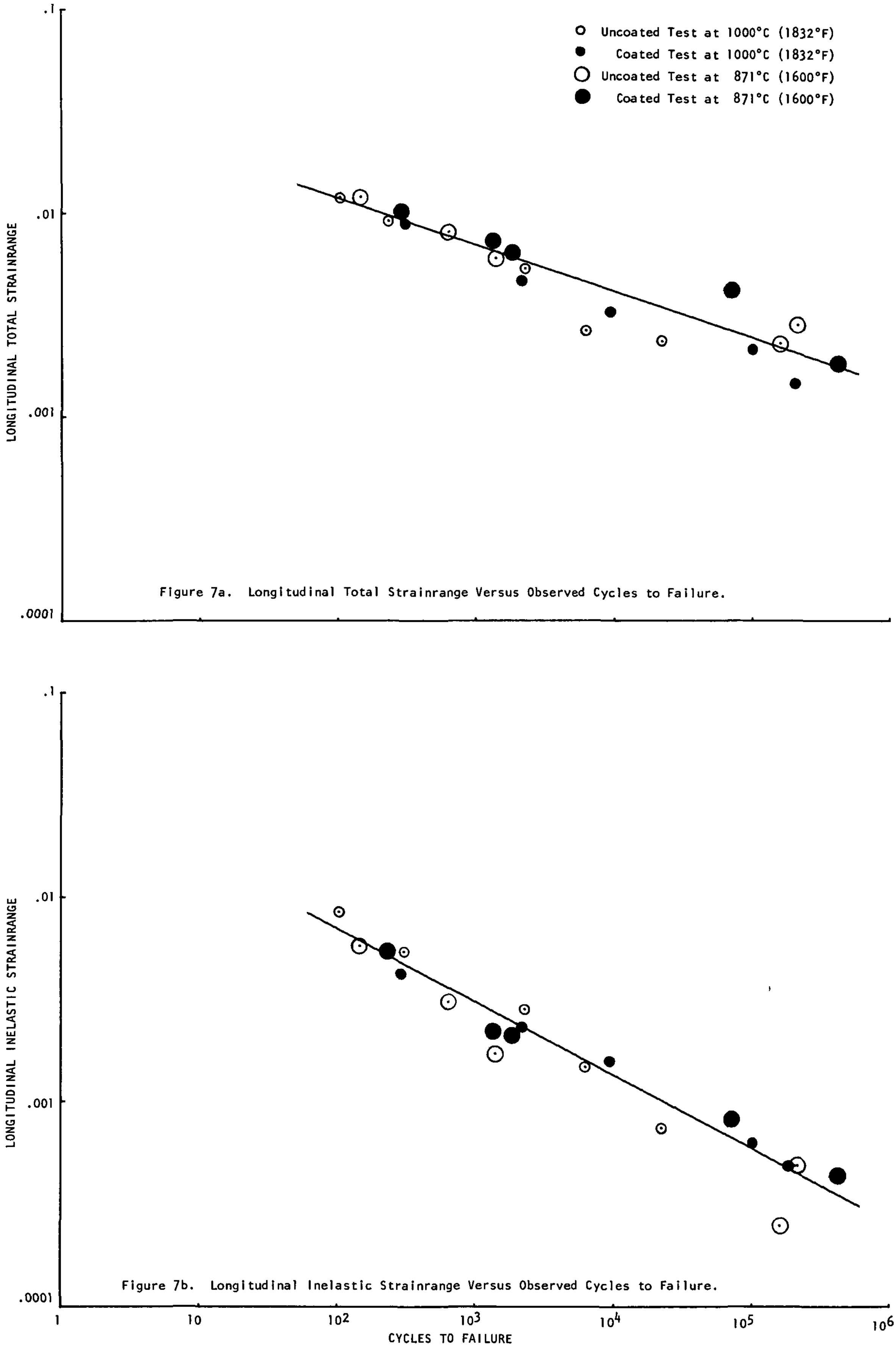

Figure 7a. Longitudinal Total Strainrange Versus Observed Cycles to Failure.

Figure 7b. Longitudinal Inelastic Strainrange Versus Observed Cycles to Failure.

Figure 7. Rene' 80 Fatigue Test Results at 1000°C (1832°F) and 871°C (1600°F) for Uncoated and Coated Specimens Tested with the $\Delta\varepsilon_{pp}$ Type Deformation.

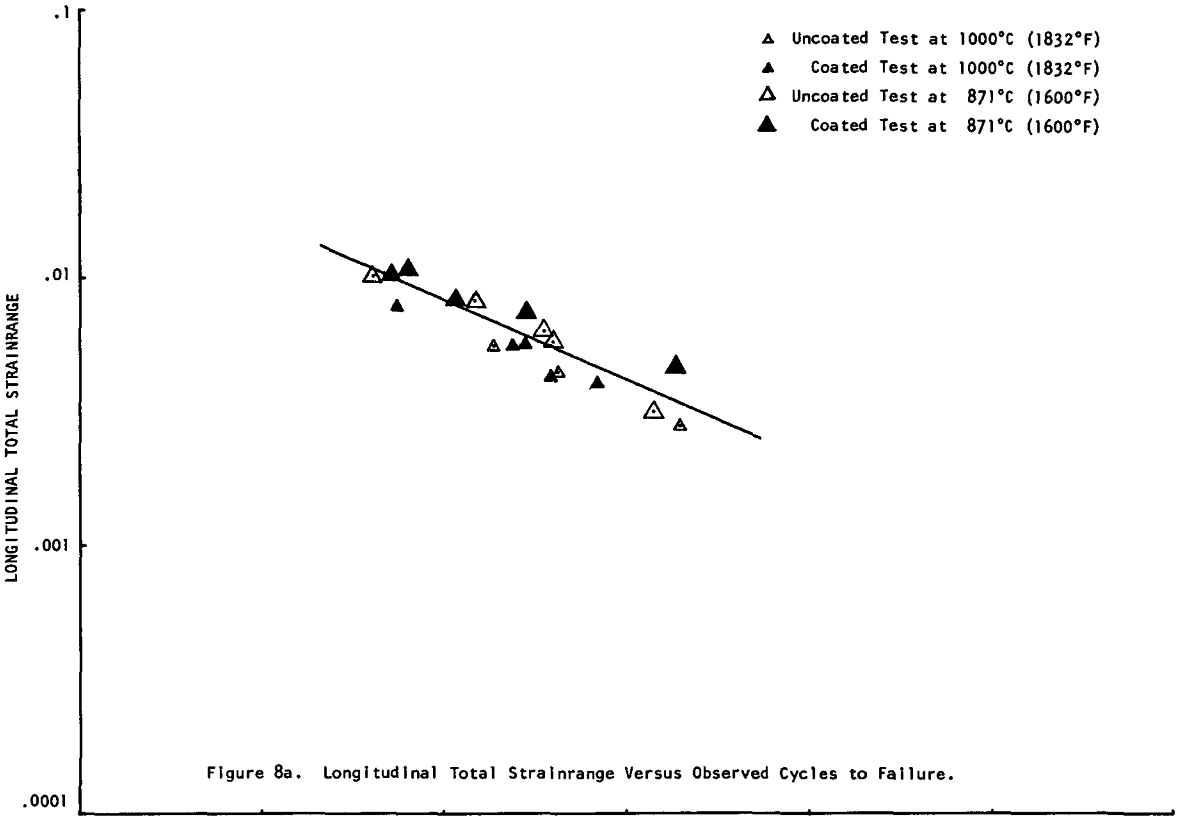

Figure 8a. Longitudinal Total Strainrange Versus Observed Cycles to Failure.

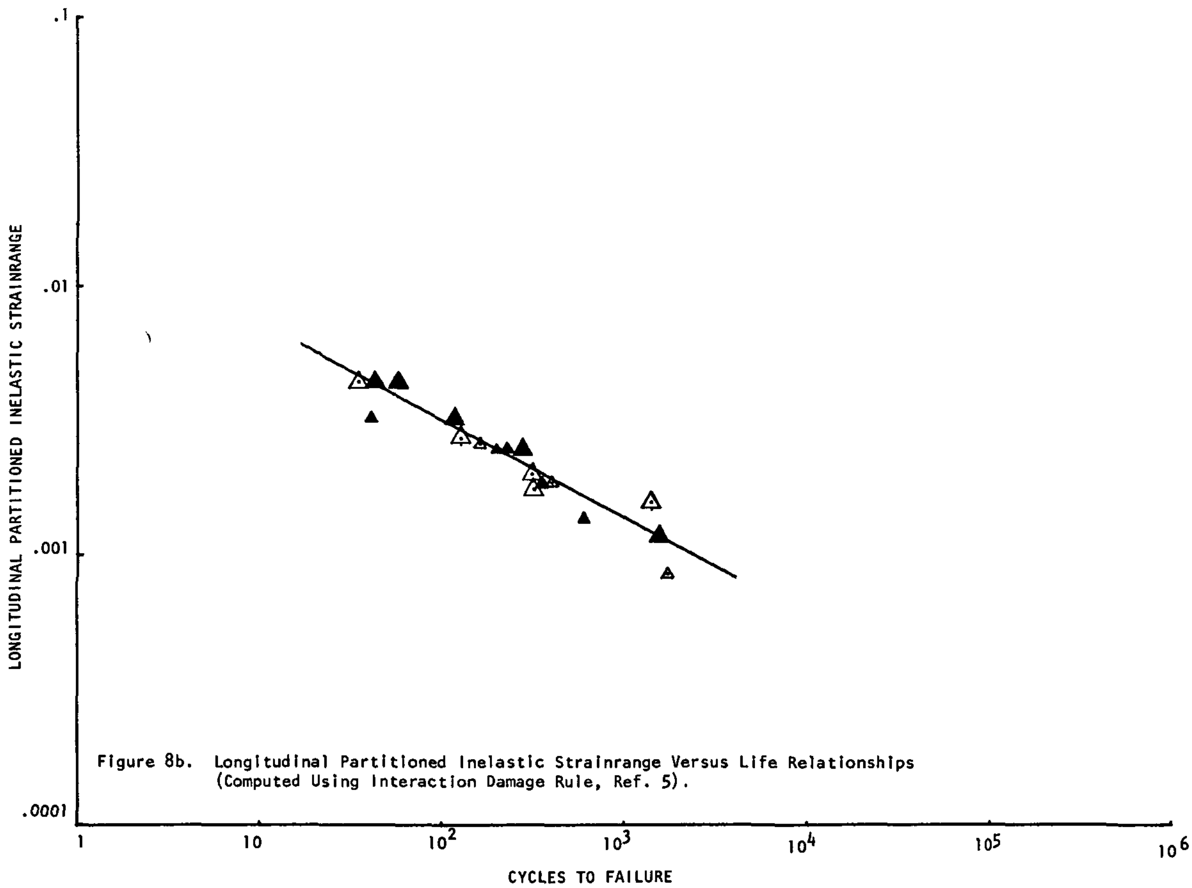

Figure 8b. Longitudinal Partitioned Inelastic Strainrange Versus Life Relationships (Computed Using Interaction Damage Rule, Ref. 5).

Figure 8. Rene' 80 Fatigue Test Results at 1000°C (1832°F) and 871°C (1600°F) for Uncoated and Coated Specimens Tested with the $\Delta\varepsilon_{pc}$ Type Deformation.

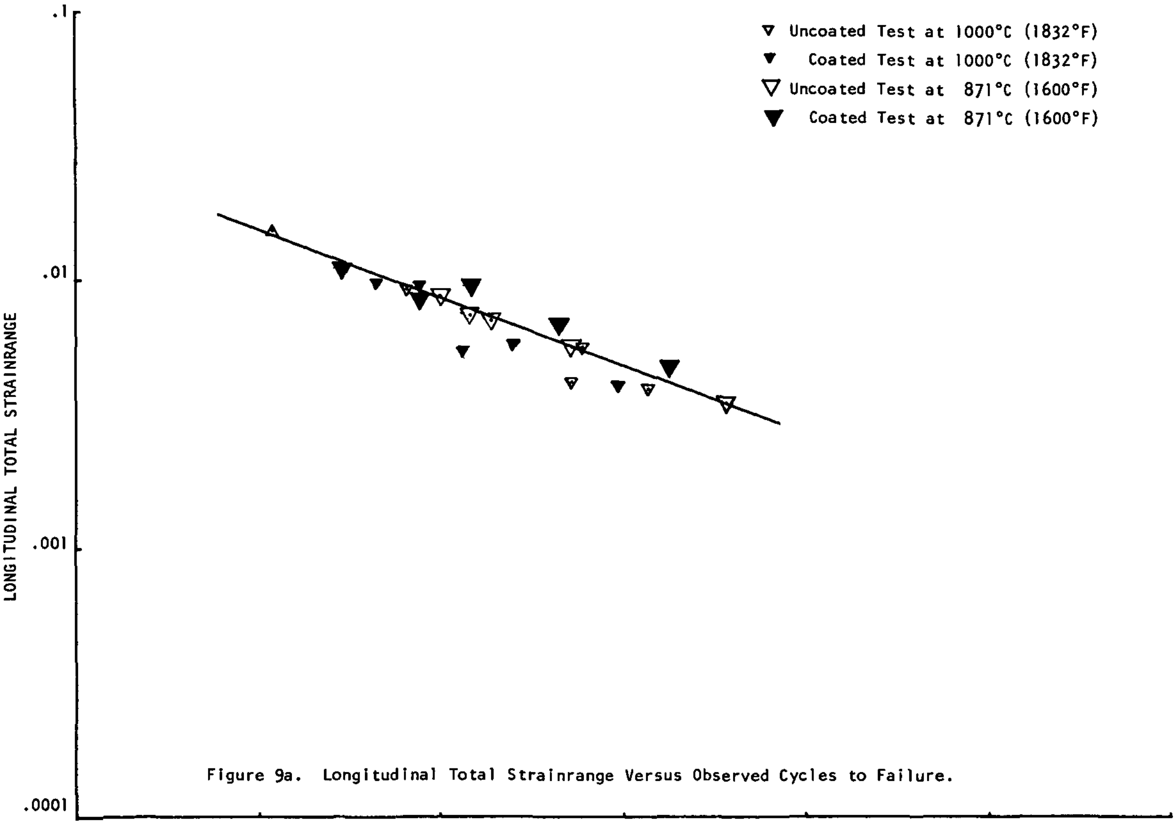

Figure 9a. Longitudinal Total Strainrange Versus Observed Cycles to Failure.

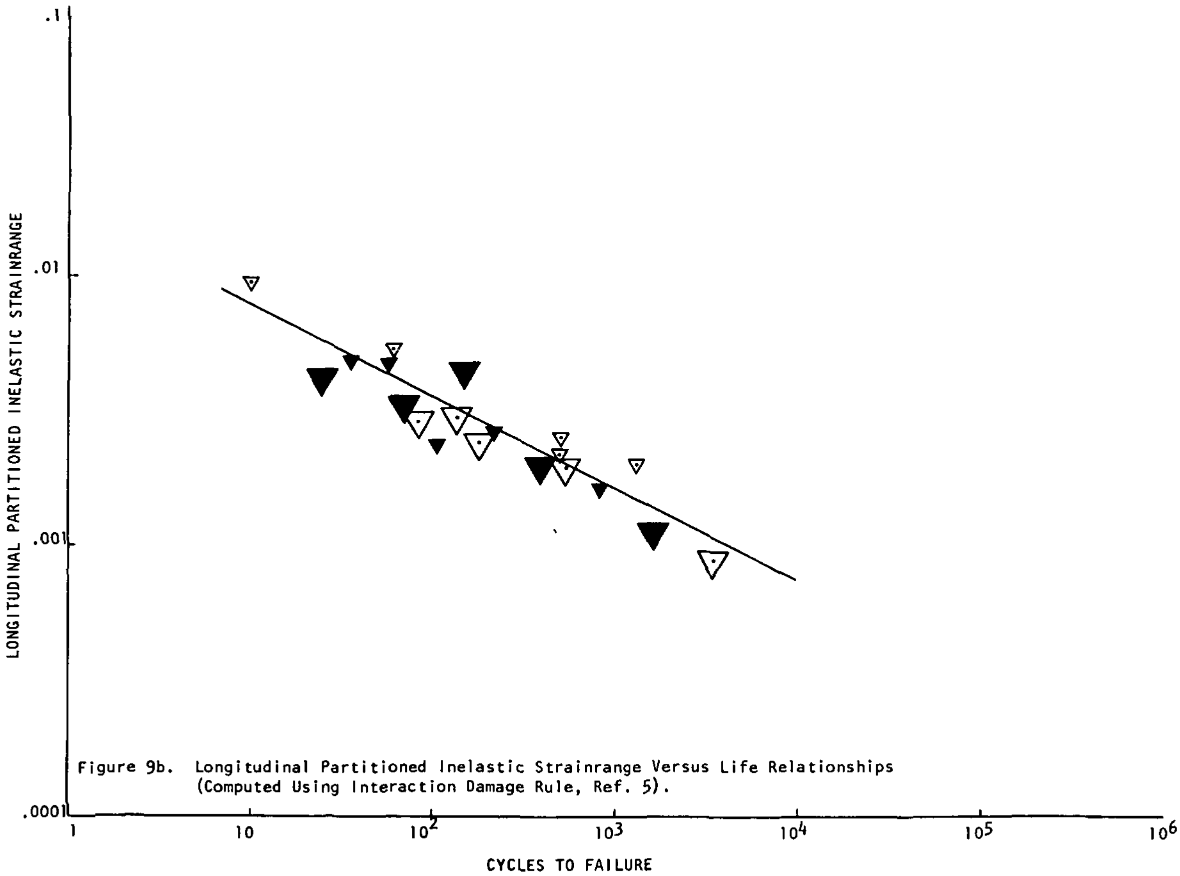

Figure 9b. Longitudinal Partitioned Inelastic Strainrange Versus Life Relationships (Computed Using Interaction Damage Rule, Ref. 5).

Figure 9. Rene' 80 Fatigue Test Results at 1000°C (1832°F) and 871°C (1600°F) for Uncoated and Coated Specimens Tested with the $\Delta\varepsilon_{cp}$ Type Deformation

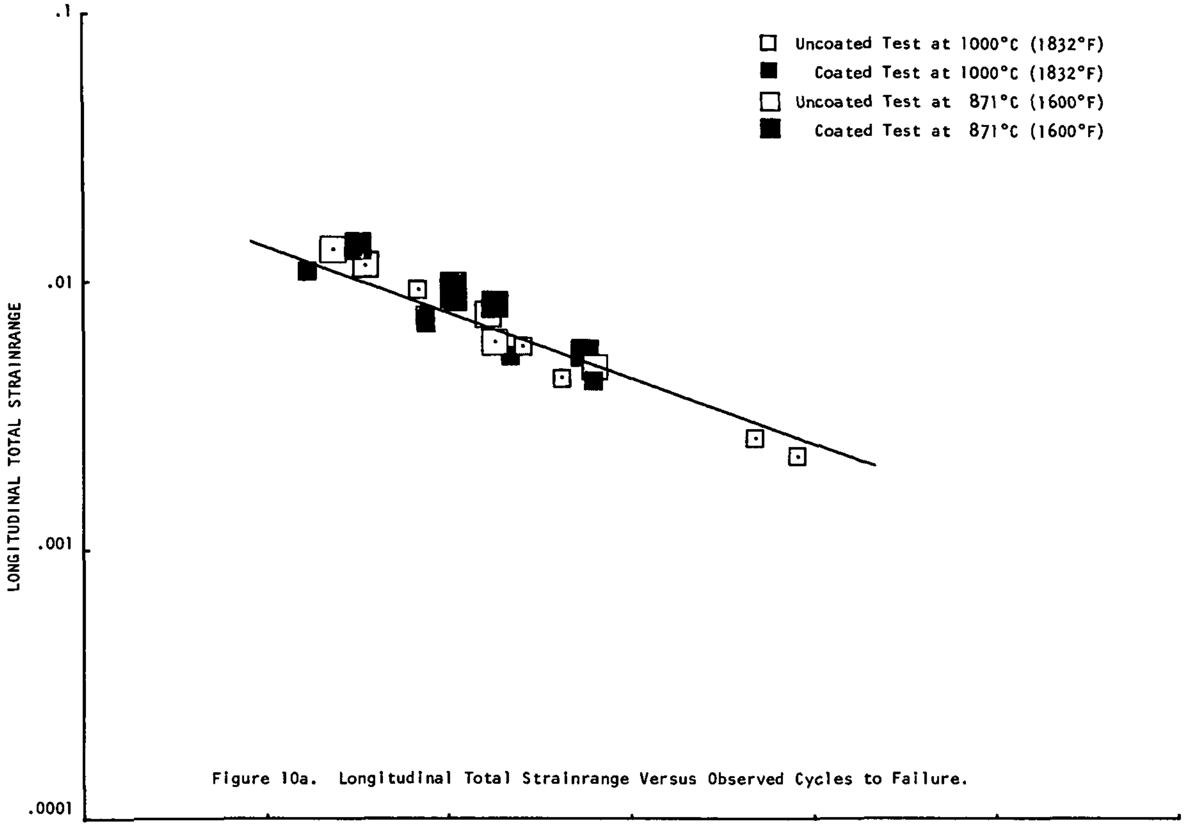

Figure 10a. Longitudinal Total Strainrange Versus Observed Cycles to Failure.

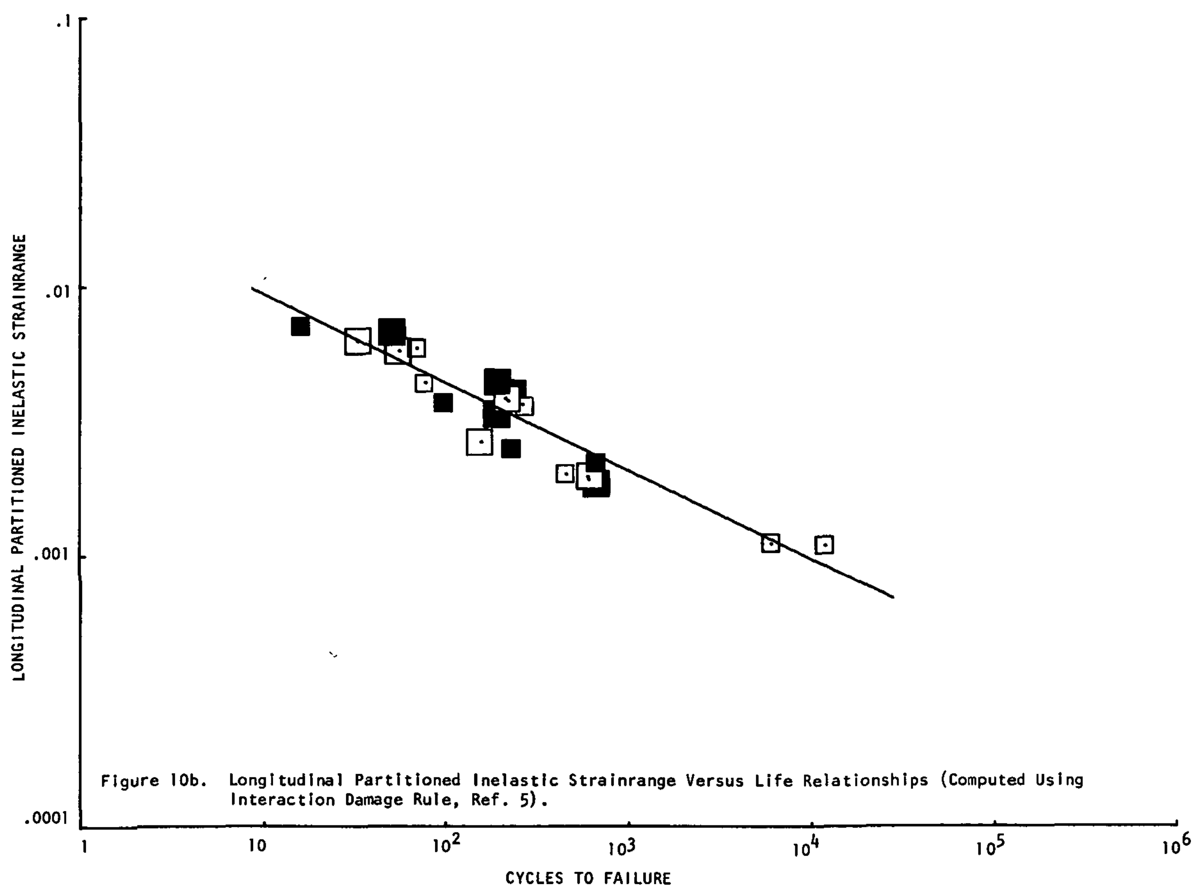

Figure 10b. Longitudinal Partitioned Inelastic Strainrange Versus Life Relationships (Computed Using Interaction Damage Rule, Ref. 5).

Figure 10. Rene' 80 Fatigue Test Results at 1000°C (1832°F) and 871°C (1600°F) for Uncoated and Coated Specimens Tested with the $\Delta\varepsilon_{cc}$ Type Deformation.

To summarize these fatigue results more clearly, the least squares lines shown in Figures 7-10 are included in the composite plot of Figure 11. These results indicate that PP deformation resulted in the least damaging type of cycling. When a time-dependent creep component was introduced into the cycle, however, an effect was observed which was dependent upon which portion of the cycle contained the creep component. The PC type deformation, in which creep was introduced in the compressive portion of the cycle, was most damaging, resulting in failure lives one order of magnitude below those for PP deformation. The CP type deformation, in which creep was introduced in the tensile portion of the cycle resulted in failure lives slightly higher than those for PC, i.e., slightly less than an order of magnitude below those for PP. The least damaging of the creep type cycling was CC in which creep occurred both in the tensile and compressive portions of the cycle. It resulted in failure lives approximately 1/2 an order of magnitude below those for PP.

The life results from Table VI for tests conducted at a number of different temperatures on uncoated material with the PP type deformation in a poorer vacuum (approximately 10^{-6} torr) are shown in Figure 12. This figure contains a plot of total strainrange versus observed cycles to failure and inelastic strainrange versus observed cycles to failure. No tests were conducted under these conditions at 871°C (1600°F) but the least squares lines from Figure 5 for the ultrahigh vacuum tests have been included for comparative purposes. The results for inelastic strainrange indicate a decrease in fatigue life as temperature is reduced. It has been generally acknowledged that in the absence of time dependent deformation (creep) a material's ductility will be an indicator of its relative fatigue resistance with a decrease in ductility usually resulting in a decrease in fatigue life (7). Ductility results for cast Rene' 80 indicate a decrease with temperature from 1000°C (1832°F) (8). Thus, the inelastic strainrange results for Rene' 80 do reflect the decrease in fatigue life with decreasing ductility.

B. Microstructural Observations

All the fatigue specimens failed within the hourglass areas. There was no evidence of the specimen geometry change known as "barrelling" which is characterized by an increase in specimen diameter adjacent to the center of the original hourglass configuration. This effect has been observed in 304 stainless steel (9) and tantalum base materials (3). Metallographic examination was conducted on selected specimens and included light and scanning electron microscopy to aid in the interpretation of the fatigue results. The results indicated that microstructural damage varied with cycle type, test temperature and surface condition (coated versus uncoated), Figures 13-18.

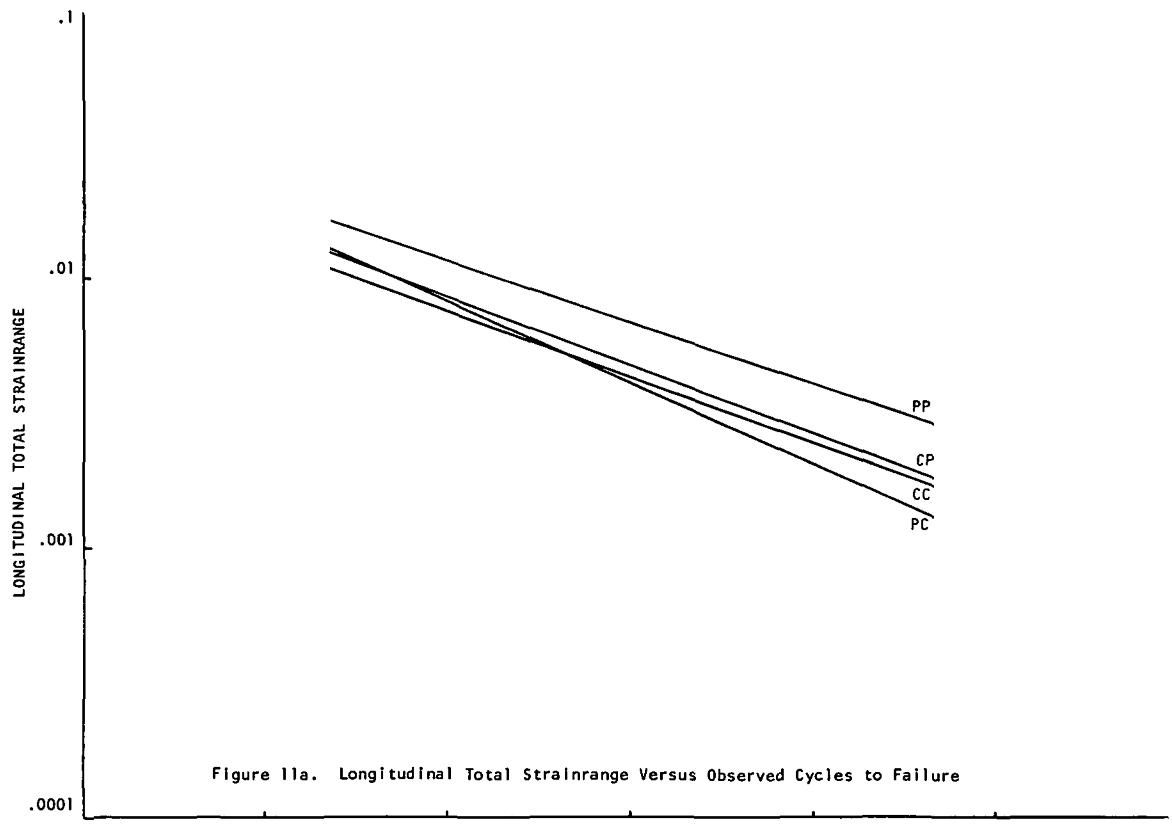

Figure 11a. Longitudinal Total Strainrange Versus Observed Cycles to Failure

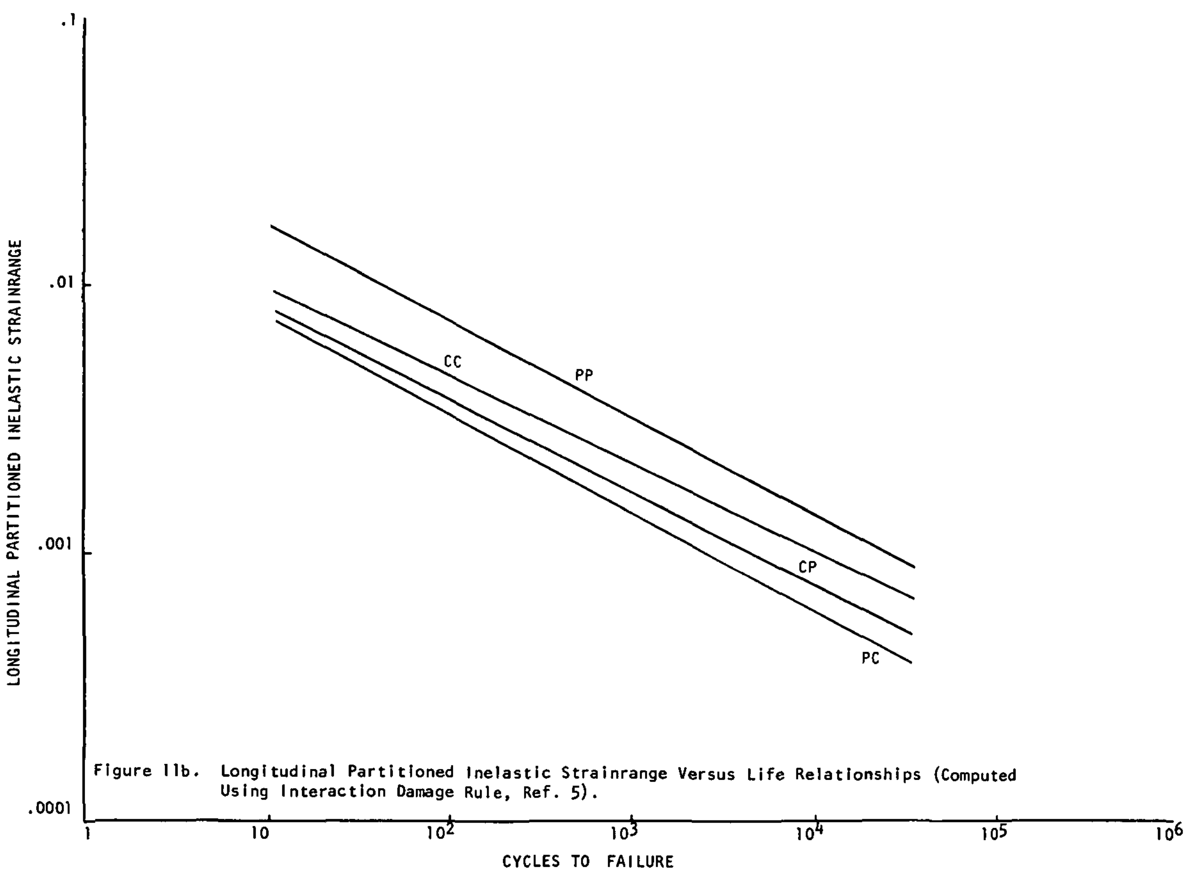

Figure 11b. Longitudinal Partitioned Inelastic Strainrange Versus Life Relationships (Computed Using Interaction Damage Rule, Ref. 5).

Figure 11. Composite Plot of Least Squares Lines Through Fatigue Data Shown in Figures 7-10.

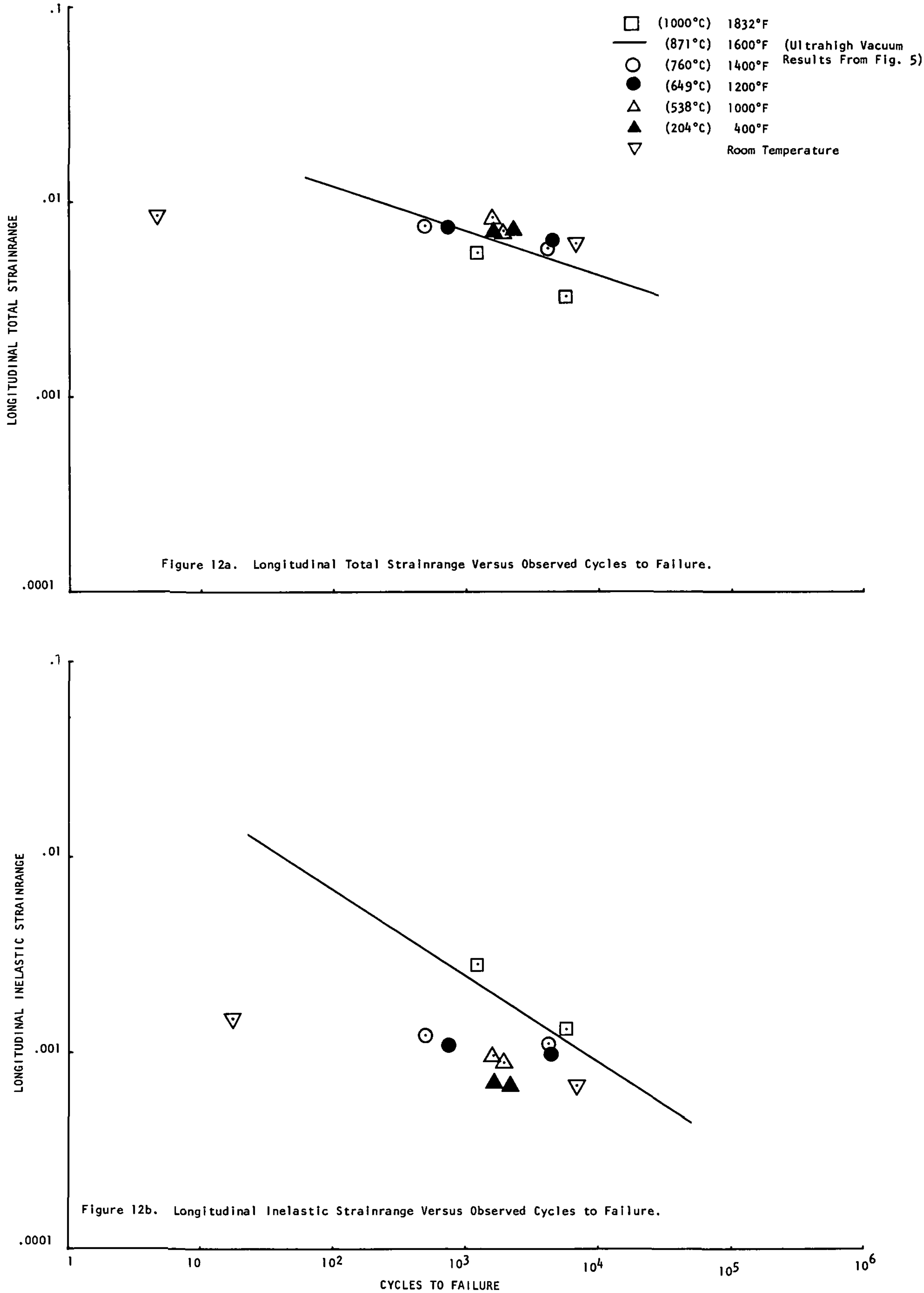

Figure 12a. Longitudinal Total Strainrange Versus Observed Cycles to Failure.

Figure 12b. Longitudinal Inelastic Strainrange Versus Observed Cycles to Failure.

Figure 12. Rene' 80 Fatigue Test Results at Various Temperatures for Uncoated Material Tested in Poorer Vacuum (Approximately 10^{-6} Torr) with the $\Delta\varepsilon_{pp}$ Type Deformation.

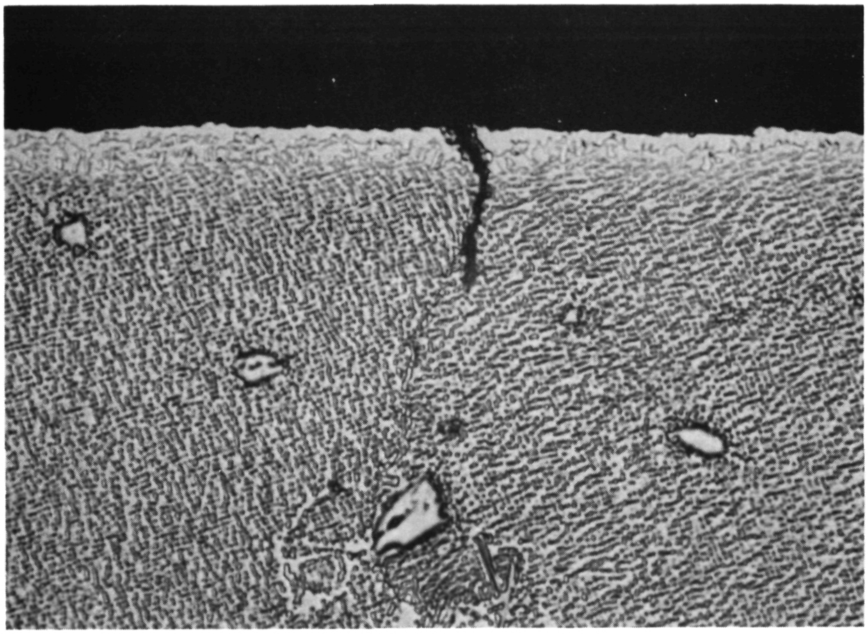

a) Surface Grain Boundary Crack Initiation with Crack Branching Off Into Matrix Region, 800X Magnification.

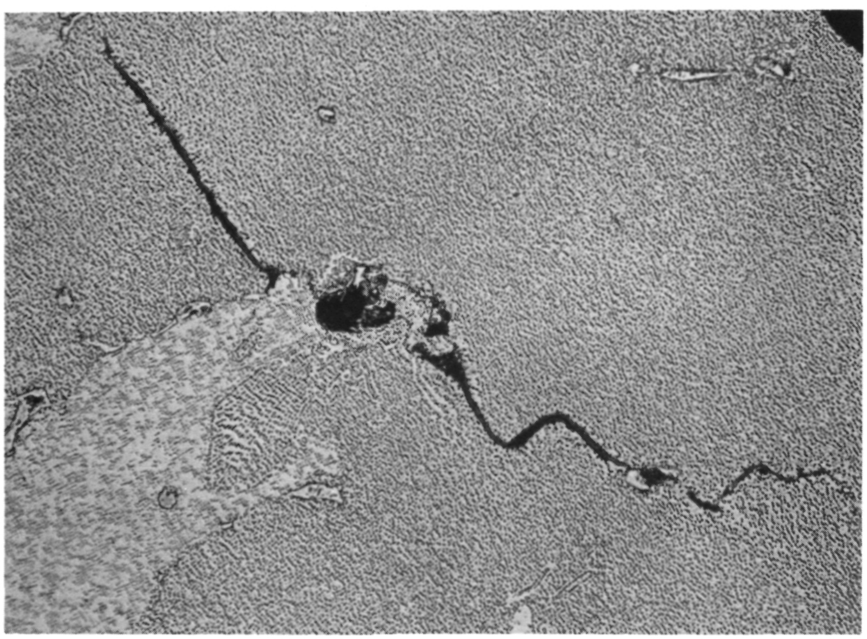

b) Grain Boundary Porosity Crack Initiation with Crack Branching Off Into Matrix Region, 400X Magnification.

Figure 13. Light photomicrographs of fatigue specimen 8U-PP-7, tested at 1000°C (1832°F), 1.033 Hz, total strainrange of 0.00247. Failure occurred after 22,115 cycles. Fry's etch.

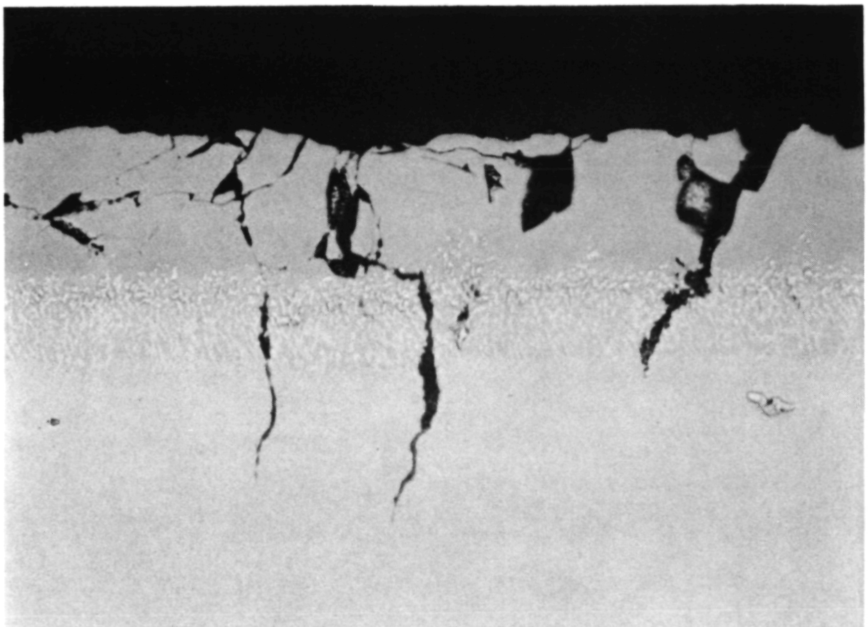

a) Unetched

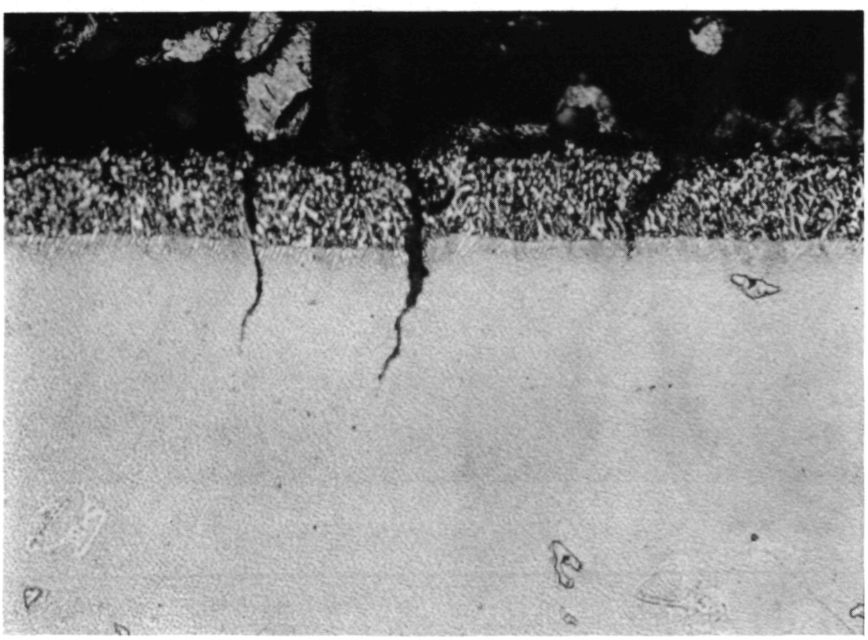

b) Fry's etch

Figure 14. Light photomicrographs of fatigue specimen 51C-PP-6, tested at 871°C (1600°F), total strainrange of 0.00672. Failure occurred after 1860 cycles. Note coating cracks propagating transgranularly into specimen, 500X magnification.

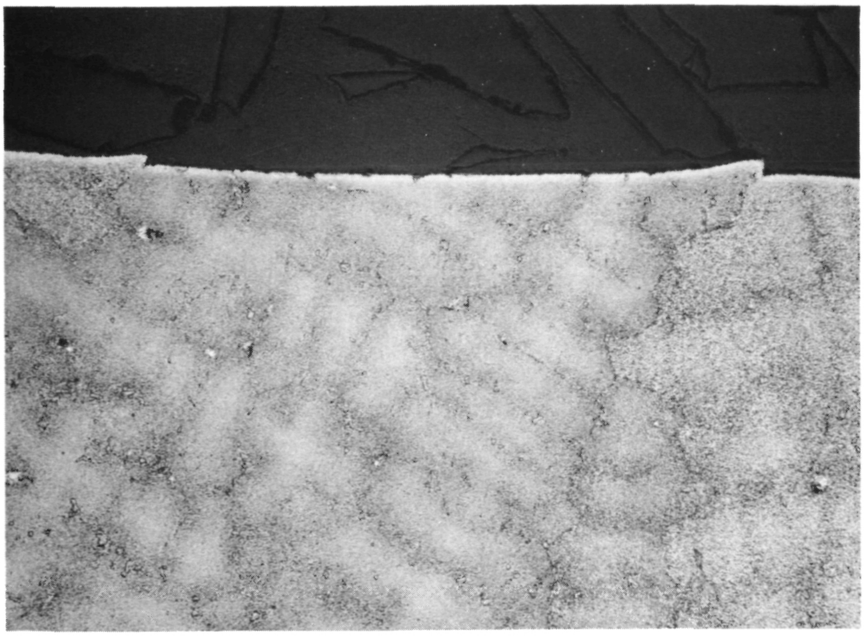

a) 80X Magnification

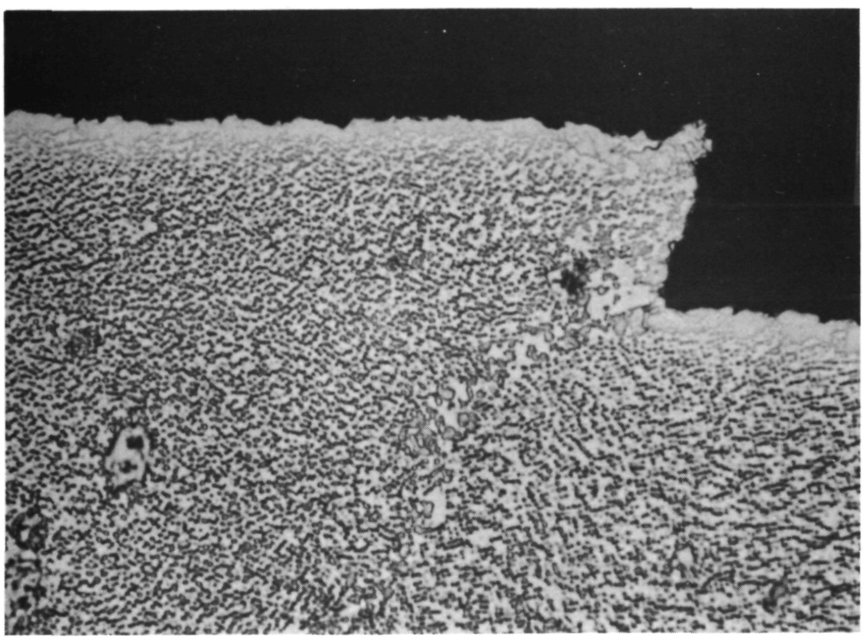

b) 800X Magnification

Figure 15. Light photomicrographs of uncoated fatigue specimen 10U-PC-2, tested at 1000°C (1832°F), total strainrange of 0.01999. Failure occurred after 19 cycles. Note grain extrusion as a result of PC deformation. Fry's etch.

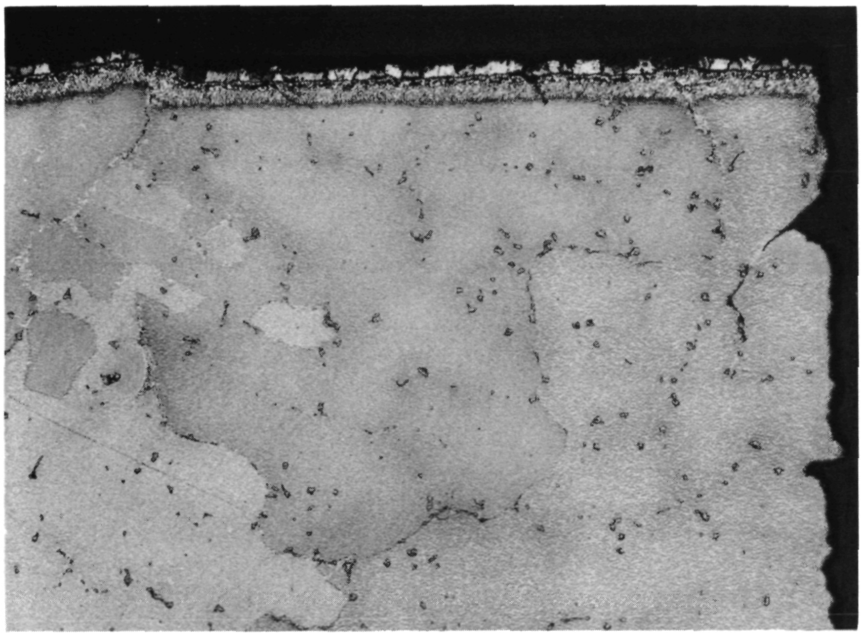

a) 100X Magnification

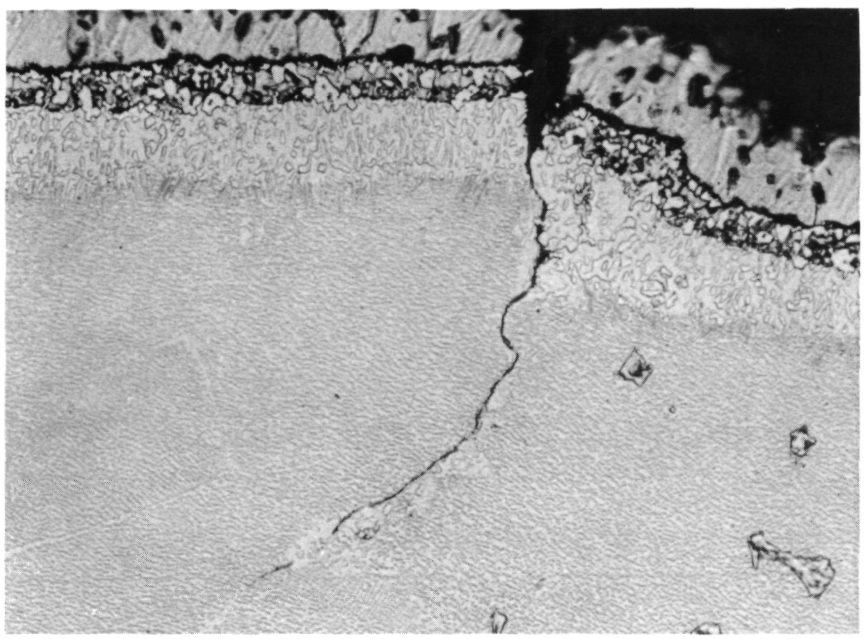

b) 500X Magnification

Figure 16. Light photomicrographs of coated fatigue specimen 57C-PC-2, tested at 1000°C (1832°F), total strainrange of 0.00450. Failure occurred after 386 cycles. Note grain extrusion and intergranular cracking as a result of PC deformation. Fry's etch.

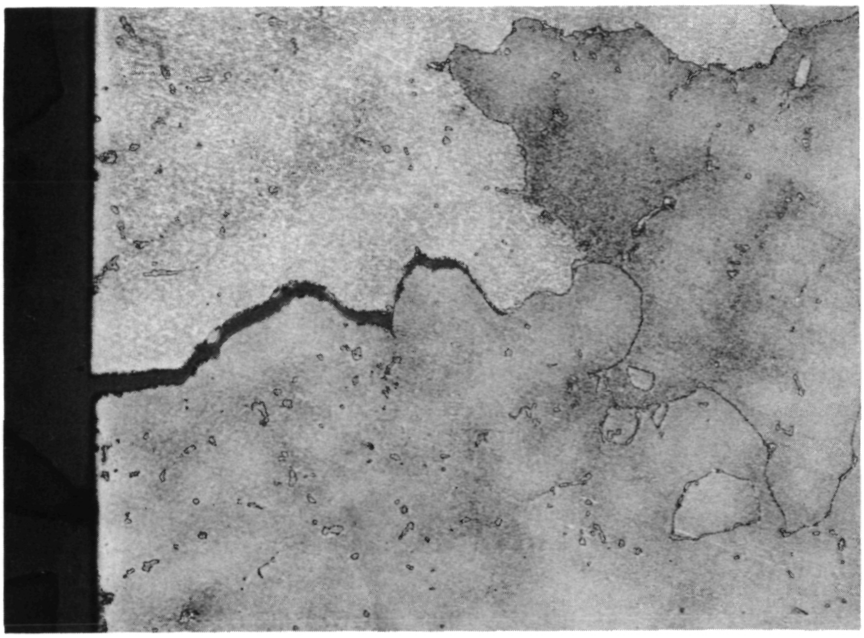

a) Uncoated specimen 31U-CP-6, tested at 871°C (1600°F), total strainrange of 0.00586, 530 cycles to failure.

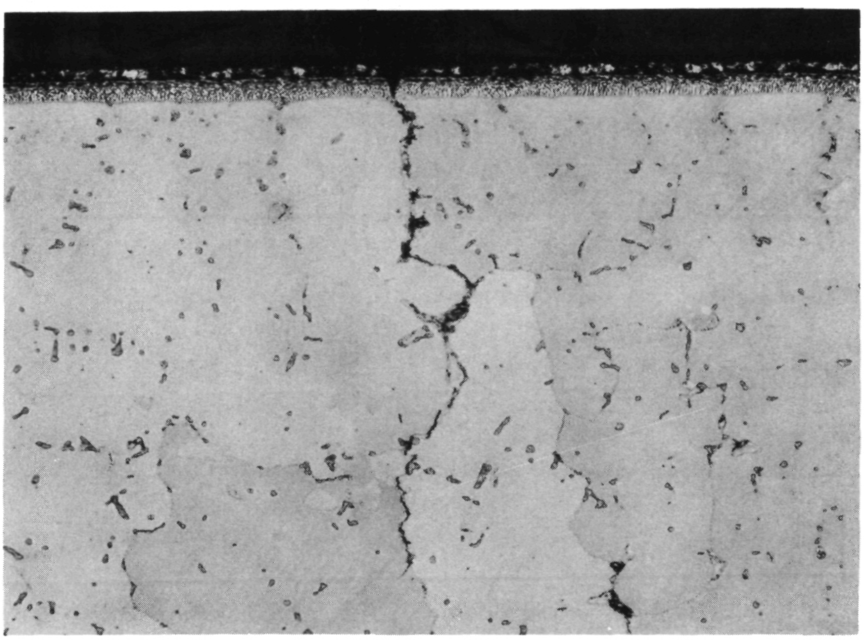

b) Coated specimen 62C-CP-1, tested at 871°C (1600°F), total strainrange of 0.00995, 150 cycles to failure.

Figure 17. Light photomicrographs of intergranular fracture mode in specimens tested with the CP type deformation. Fry's etch. 100X magnification.

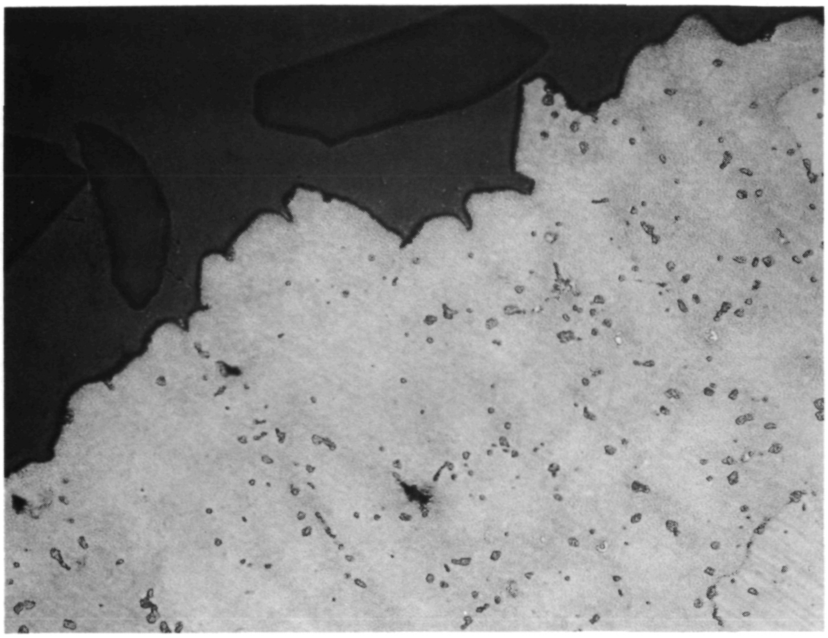

a) Intergranular Fracture Mode in Coated Specimen 68C-CC-1, Tested at 1000°C (1832°F), .01135 Total Strainrange, 17 Cycles to Failure 100X

b) Transgranular Fracture Mode in Coated Specimen 69C-CC-2, Tested at 871°C (1600°F), .01005 Total Strainrange, 108 Cycles to Failure. 500X

Figure 18. Light Photomicrographs Showing Examples of Fracture Modes for Specimens Tested with the CC Type Deformation. Fry's etch.

Specimens tested with the PP type deformation exhibited primarily a transgranular fracture mode for all test temperatures and surface conditions. This is a common fracture mode for materials tested at high frequencies where creep deformation is negligible. This fracture mode reflects the fact that the PP deformation resulted in the highest fatigue lives. Transgranular crack propagation in a highly alloyed cast nickel-base superalloy such as Rene' 80 is retarded by the heavy matrix precipitation of the gamma-prime strengthening phase. For uncoated specimens, grain boundary areas at the specimen surface were common crack initiation sites, with the cracks becoming transgranular after a short distance, Figure 13a. Crack initiation was also observed at grain boundary microporosity, Figure 13b. After initiation in the grain boundary region these cracks become transgranular. For coated specimens, considerable numbers of coating cracks were observed leading to transgranular crack propagation, Figure 14. Since the fatigue results for the PP type tests, Figure 7, indicated no appreciable differences in failure times as a function of surface condition, the presence of the aluminide coating and its attendant cracks did not degrade the low cycle fatigue properties of this alloy.

Specimens tested with the PC type deformation exhibited a predominantly intergranular fracture mode. In general, intergranular crack initiation and propagation occur at a faster rate than transgranular cracking in nickel-base superalloys and the presence of this fracture mode in PC specimens suggests why this type of strain cycling resulted in lower fatigue lives than the PP type. At 1000°C (1832°F) there was considerable evidence of grain boundary sliding which took place during the compressive (creep) portion of the cycle resulting in steps or grain extrusions along the sides of the specimens. Examples of these extrusions are shown in Figure 15 for the uncoated material and Figure 16 for coated material. Specimens tested at 871°C (1600°F) did not exhibit the extent of grain boundary sliding seen at 1000°C (1832°F). Considerable numbers of surface cracks were observed in the coated specimens, but, similar to the PP specimens, the presence of the aluminide coating and its attendant cracks did not degrade the low cycle fatigue properties of this alloy.

Specimens tested with the CP type deformation exhibited primarily an intergranular type of fracture mode both at 1000°C (1832°F) and 871°C (1600°F), Figure 17. Unlike materials such as iron base A-286 and 304 stainless alloys which exhibit intergranular fracture resulting from internal grain boundary "decohesion" as a consequence of CP cycling (4), specimens of Rene' 80 studied in the present investigation usually exhibited some form of surface grain boundary cracking into the specimen. High magnification SEM analyses of Rene' 80 specimens revealed no internal grain boundary "decohesion" or cavitation in this alloy. In addition, the CP specimens did not exhibit the grain boundary sliding observed in the PC specimens and this may explain why the CP failure lives were slightly higher. Similar to the results for the PP testing, the presence of numerous coating cracks did not result in an appreciable degradation in fatigue results, Figure 9.

Specimens tested with the CC type deformation exhibited different fracture modes depending on the test temperature. At 1000°C (1832°F) the fracture mode was primarily intergranular, while at 871°C (1600°F) the fracture mode was transgranular. Examples of these various modes are shown in Figure 18. There was no evidence of grain boundary extrusion at the specimen surface or of internal grain boundary decohesion or cavitation in these specimens.

C. Supplementary Mechanical Property Tests

The results of the supplemental vacuum tensile and creep rupture tests are presented in Appendix B in Tables B-1 and B-2.

VI SUMMARY

The results of ultrahigh vacuum low cycle fatigue tests conducted on uncoated and CODEP B-1 aluminide coated specimens of Rene' 80 nickel-base superalloy at 1000°C (1832°F) and 871°C (1600°F) indicated little effect of coating or temperature on the fatigue properties. There was, however, a significant effect on fatigue life as a function of strain cycle type. The method of Strainrange Partitioning offers an appropriate framework around which to correlate the effects of these strain cycle types. In terms of partitioned inelastic strainrange, the completely reversed plasticity type of strain cycling (PP) resulted in the highest fatigue lives. When a time-dependent creep component was introduced into the cycle, an effect was observed which was dependent upon which portion of the cycle contained the creep component. When creep was introduced in the compressive portion of the cycle (PC) failure lives were approximately one order of magnitude below those for PP deformation. When creep was introduced in the tensile portion of the cycle (CP), failure lives were slightly higher than those for the PC deformation, i.e., slightly less than an order of magnitude below those for PP. The least damaging of the creep type cycling was CC in which creep occurred both in the tensile and compressive portions of the cycle resulting in failure lives approximately 1/2 an order of magnitude below those for PP.

Metallographic evaluation indicated that microstructural damage varied with cycle type and test temperature. Specimens tested with the PP type deformation exhibited primarily a transgranular fracture mode. Specimens tested with the PC type deformation exhibited a predominantly intergranular fracture mode. At 1000°C (1832°F) there was considerable evidence of grain boundary sliding which took place during the compressive (creep) portion of the cycle resulting in steps or grain extrusions along the sides of the specimens. Specimens tested at 871°C (1600°F) did not evidence the same extent of grain boundary extrusion. Specimens tested with the CP type deformation exhibited an intergranular type of fracture mode at both test temperatures. Specimens tested with the CC type deformation exhibited different fracture modes depending on the test temperature. At 1000°C (1832°F) the fracture mode was intergranular while at 871°C (1600°F) the fracture mode was transgranular. At both test temperatures considerable evidence of surface cracking was observed in coated specimens for all the types of strain cycling.

V REFERENCES

1. M. Gell and G. R. Leverant, "Mechanisms of High Temperature Fatigue," Fatigue at Elevated Temperatures, ASTM STP 520, ASTM, 1973, pp. 37-67.

2. S. S. Manson, G. R. Halford and H. M. Hirschberg, "Creep-Fatigue Analysis by Strainrange Partitioning," Design for Elevated Temperature Environment, American Society of Mechanical Engineers, 1971, pp. 12-24.

3. K. D. Sheffler and G. S. Doble, "Influence of Creep Damage on the Low Cycle Thermal-Mechanical Fatigue Behavior of Two Tantalum Base Alloys," Final Report, Contract NAS-3-13228, NASA CR-121001, TRW ER-7592, 1 May 1972.

4. K. D. Sheffler, "Vacuum Thermal-Mechanical Fatigue Testing of Two Iron Base High Temperature Alloys," Topical Report No. 3, Contract NAS-3-6010, NAS-CR-13424, TRW ER-7696, 31 January 1974.

5. G. R. Halford and S. S. Manson, "Life Prediction of Thermal-Mechanical Fatigue Using Strainrange Partitioning," NASA TM X-71829, November 1975.

6. S. S. Manson and G. R. Halford, Discussion appearing in Journal of Pressure Vessel Technology, Trans. ASME, February 1976, p. 83, of paper by J. T. Fong, "Energy Approach for Creep-Fatigue Interactions in Metals at High Temperature," Journal of Pressure Vessel Technology, Trans. ASME, Vol. 96, Series J, No. 3, p. 214.

7. S. S. Manson, "Fatigue: A Complex Subject-Some Simple Approximations," Experimental Mechanics, July 1965, Vol. 5, p. 193.

8. L. J. Fritz, "Tensile and Creep-Rupture Properties of Engineering Alloys at Elevated Temperatures," Prepared for NASA-Lewis Research Center, Cleveland, Ohio 44135, NAS-3-18911.

APPENDIX A

HYSTERISIS LOOPS

TABLE A-1

MODULUS OF ELASTICITY USED TO CALCULATE ELASTIC STRAIN IN LOW CYCLE FATIGUE TESTS CONDUCTED IN THIS PROGRAM(1)

Test Temperature °F	Test Temperature °C	Modulus of Elasticity 10^6
Room	Room	29.98
400	204	28.78
1000	538	26.26
1200	649	25.29
1400	760	24.15
1600	871	22.76
1832	1000	20.90

(1) Modulus of elasticity data obtained from General Electric Co. Aircraft Engine Group, Materials Data Unit, Cincinnati, Ohio 45215, 10-8-74.

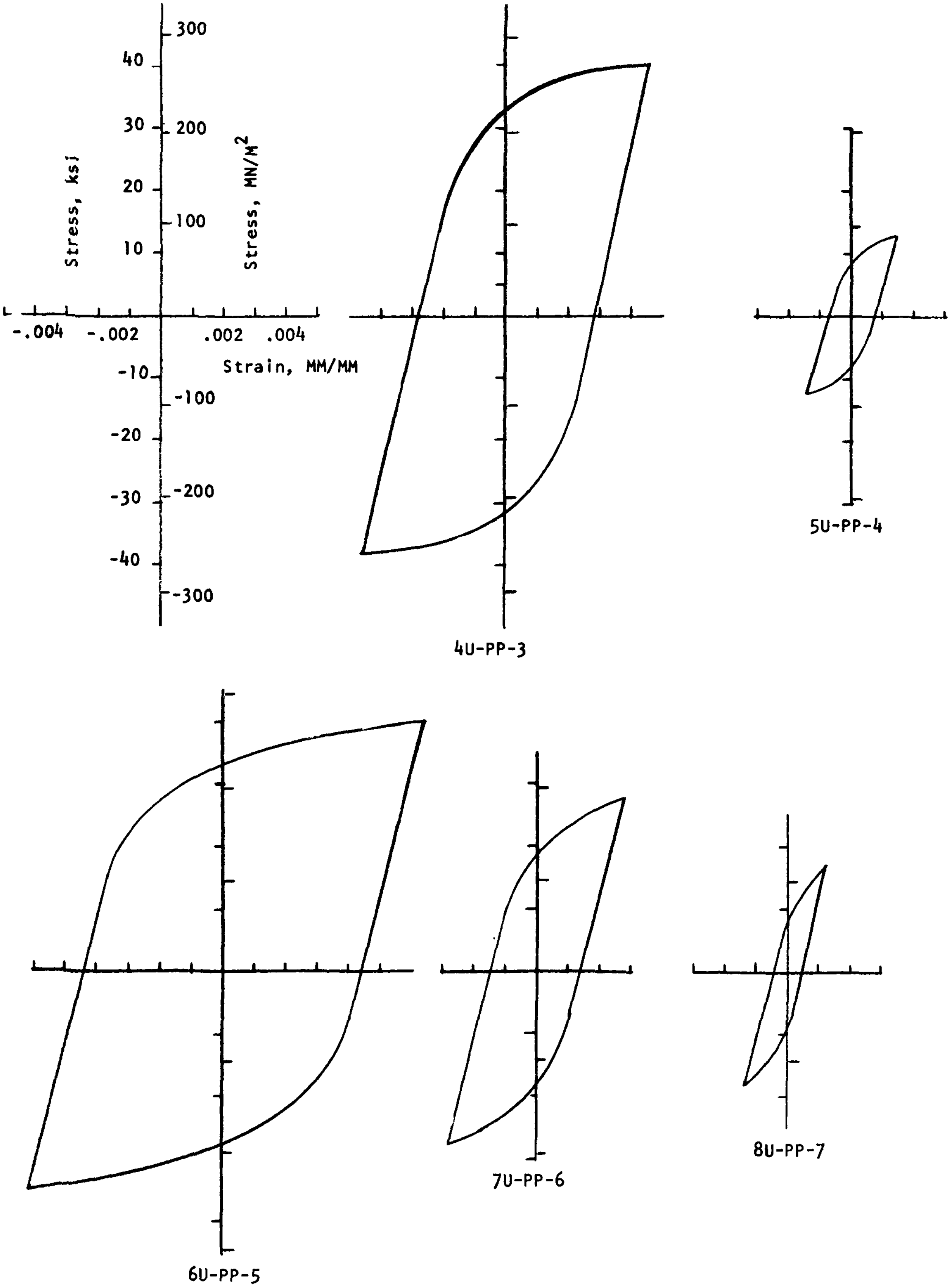

Figure A-1. Hysterisis Loops Observed for Uncoated Rene' 80 Tested at 1000°C (1832°F) with the $\Delta\varepsilon_{pp}$ Deformation.

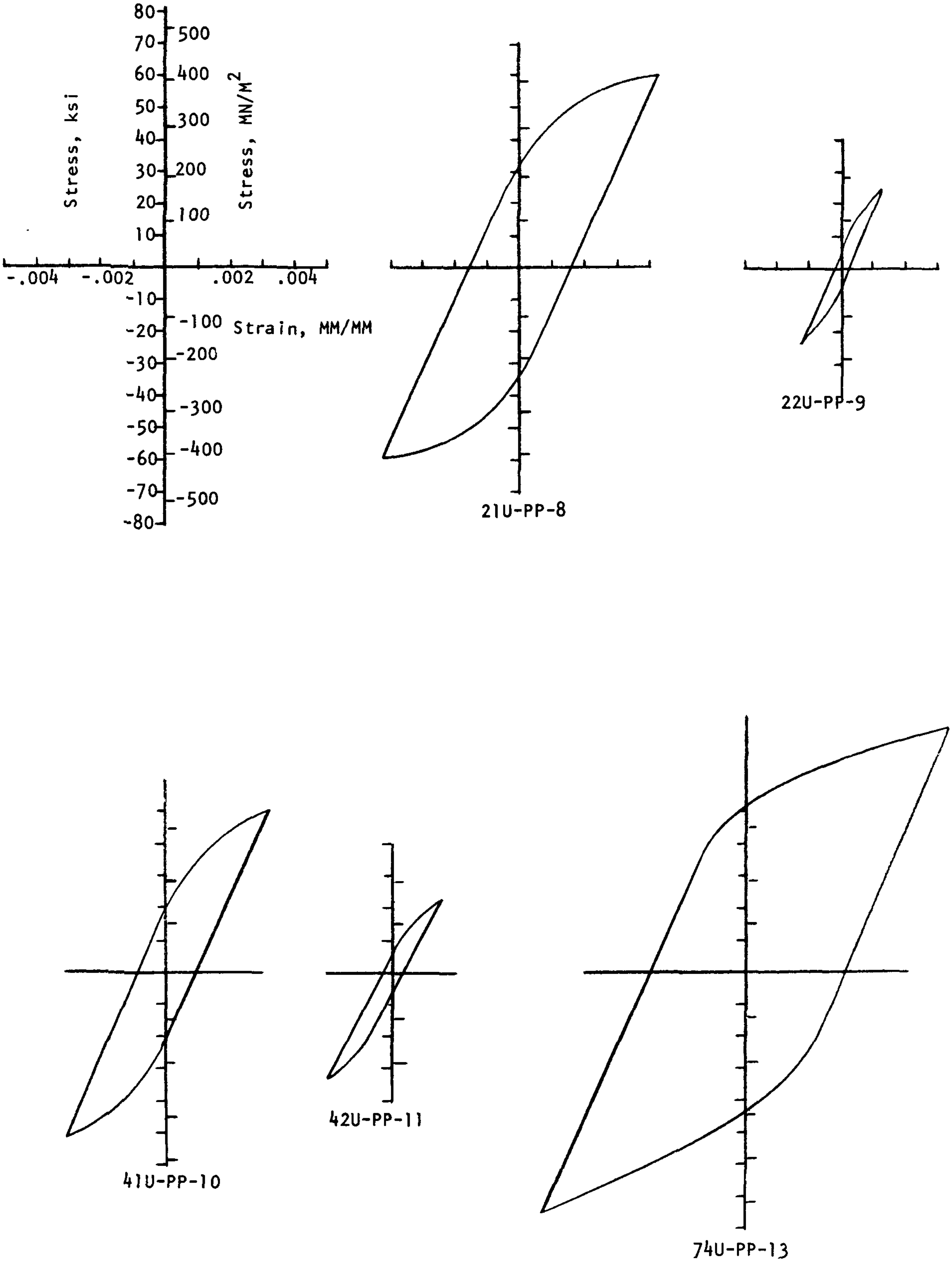

Figure A-2. Hysterisis Loops Observed for Uncoated Rene' 80 Tested at 871°C (1600°F) with the $\Delta\varepsilon_{pp}$ Deformation.

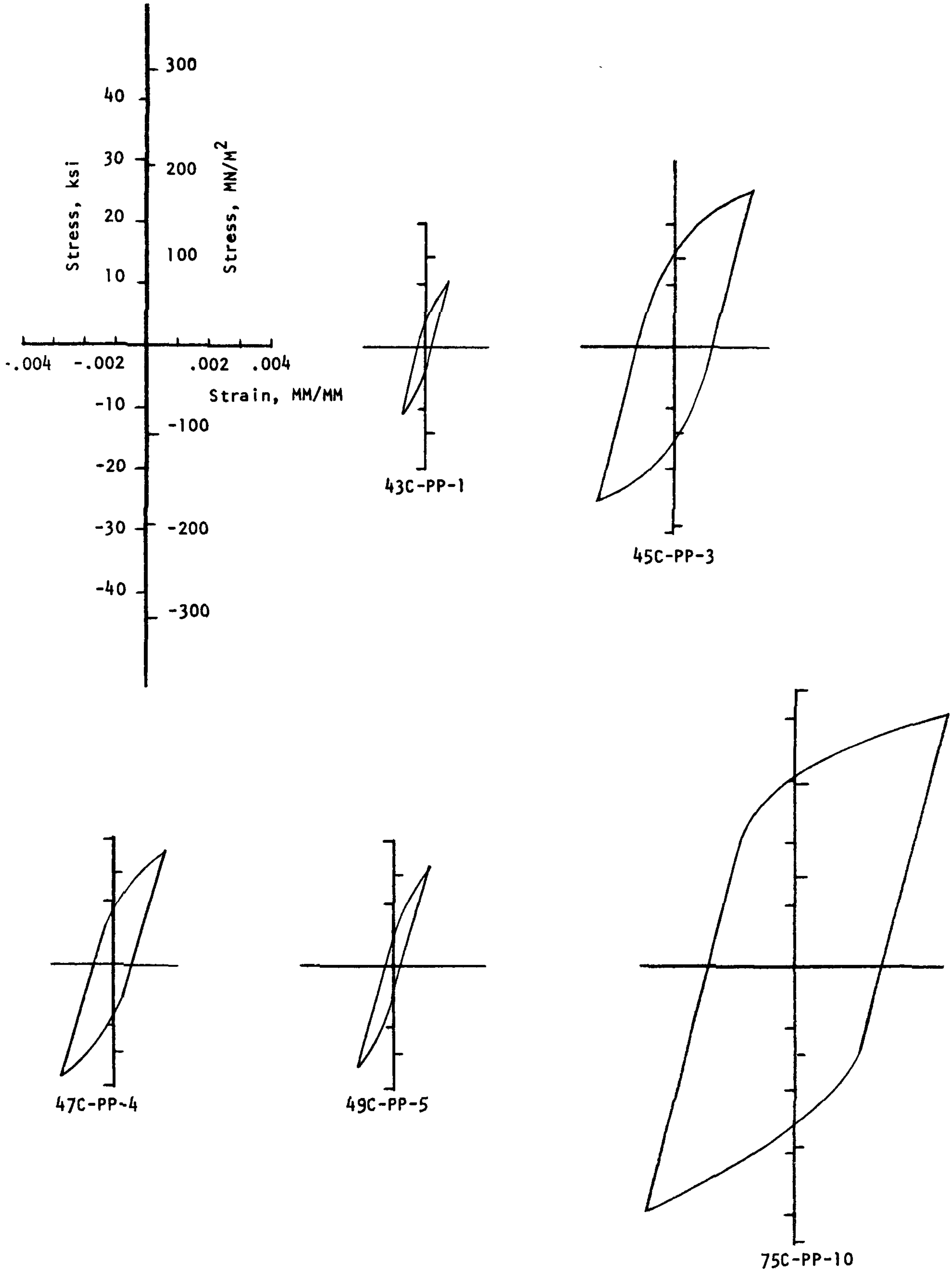

Figure A-3. Hysterisis Loops Observed for Coated Rene' 80 Tested at 1000°C (1832°F) with the $\Delta\varepsilon_{pp}$ Type Deformation.

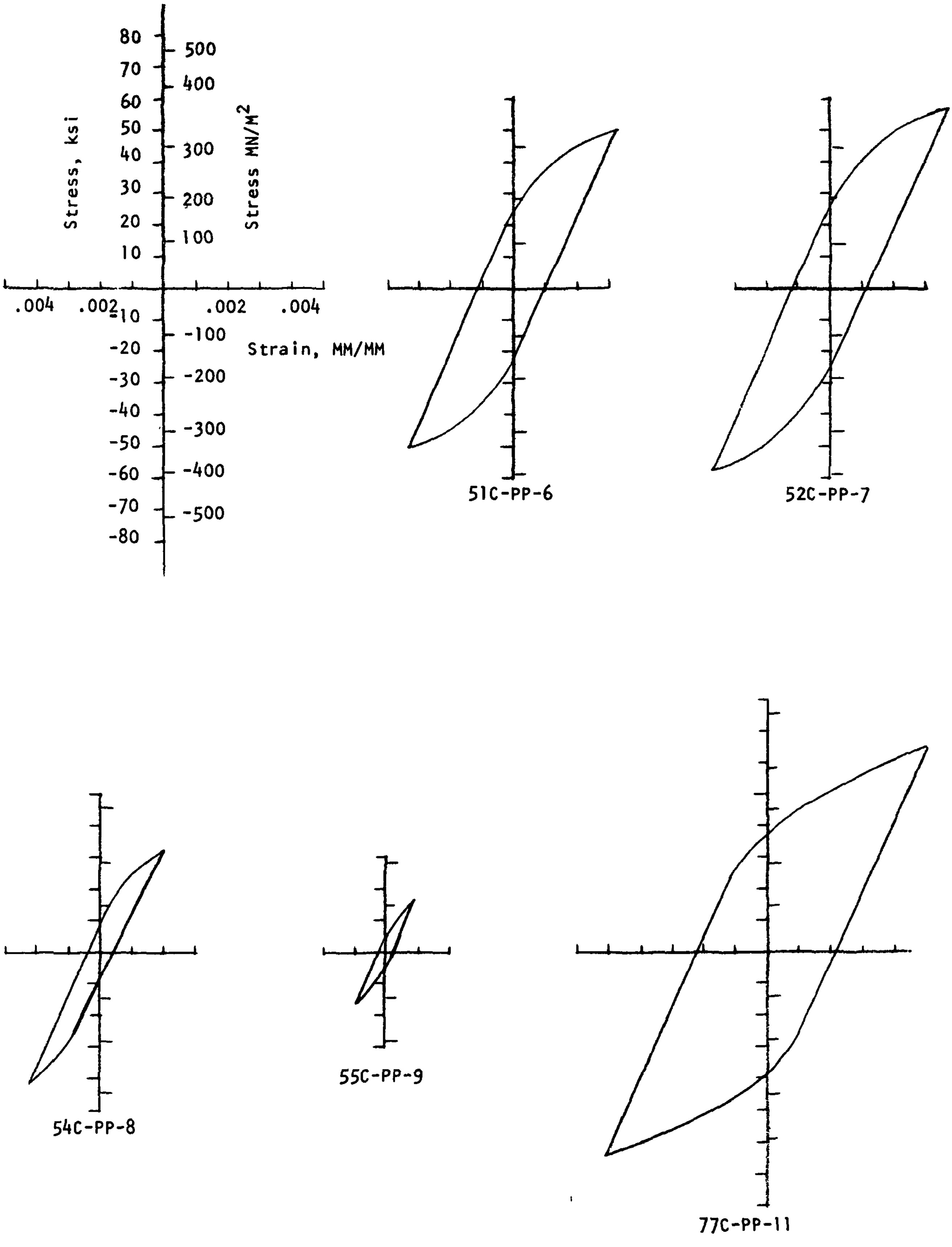

Figure A-4. Hysterisis Loops Observed for Coated Rene' 80 Tested at 871°C (1600°F) with the $\Delta\epsilon_{pp}$ Type Deformation.

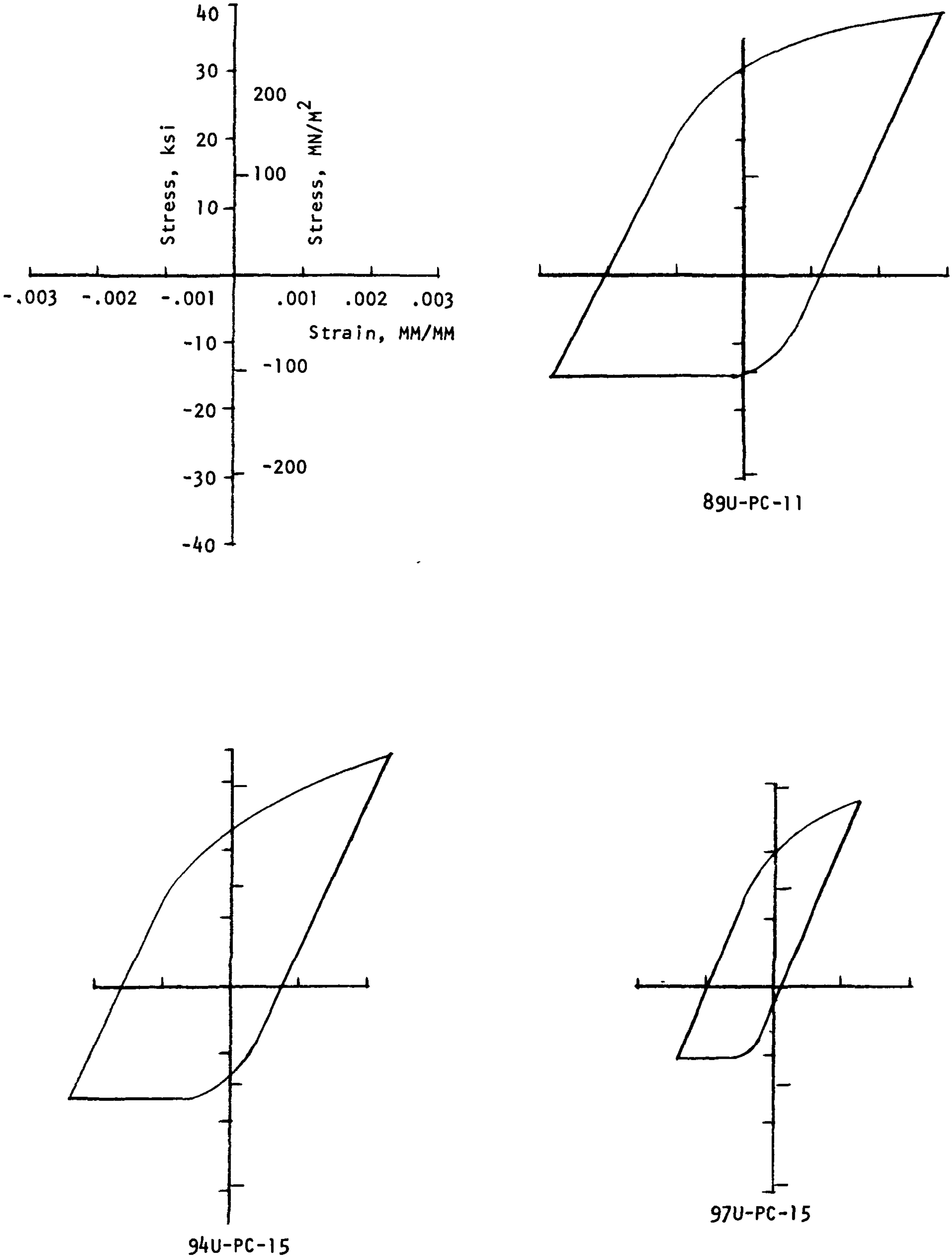

Figure A-5. Hysterisis Loops Observed for Uncoated Rene' 80 Tested at 1000°C (1832°F) with the $\Delta\varepsilon_{pc}$ Type Deformation.

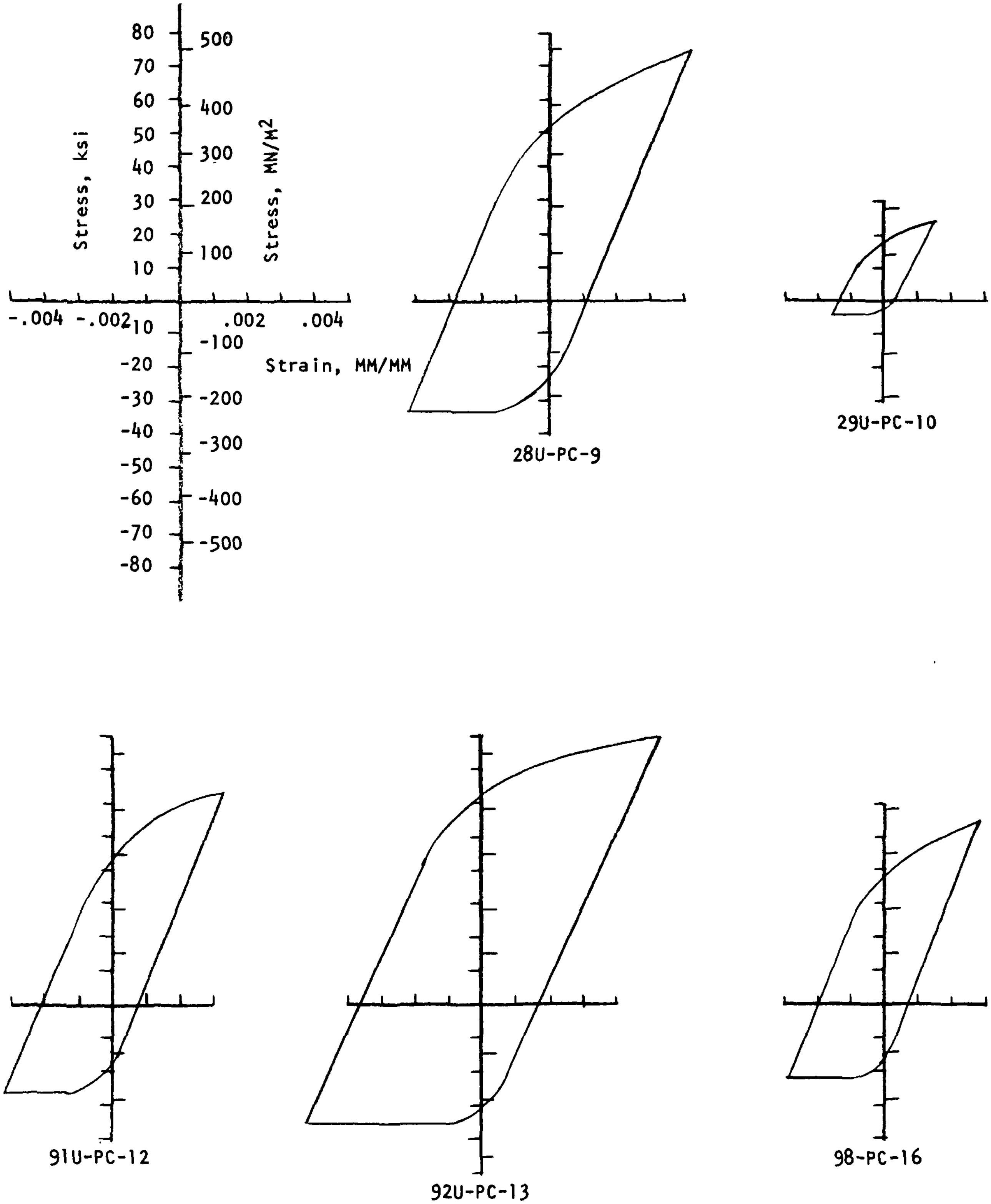

Figure A-6. Hysterisis Loops Observed for Uncoated Rene' 80 Tested at 871°C (1600°F) with the $\Delta\varepsilon_{pc}$ Type Deformation.

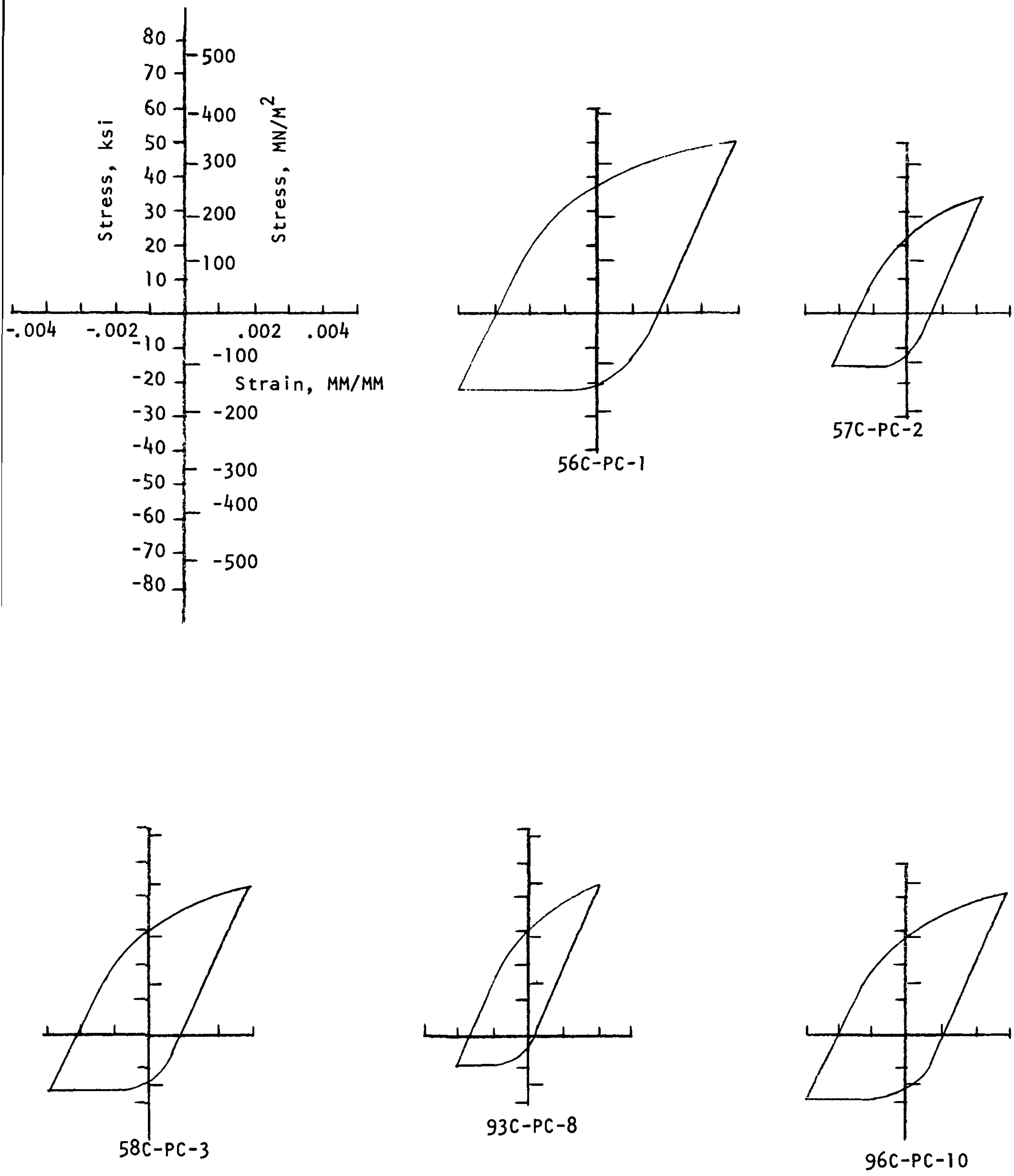

Figure A-7. Hysterisis Loops Observed for Coated Rene' 80 Tested at 1000°C (1832°F) With the $\Delta\varepsilon_{pc}$ Type Deformation.

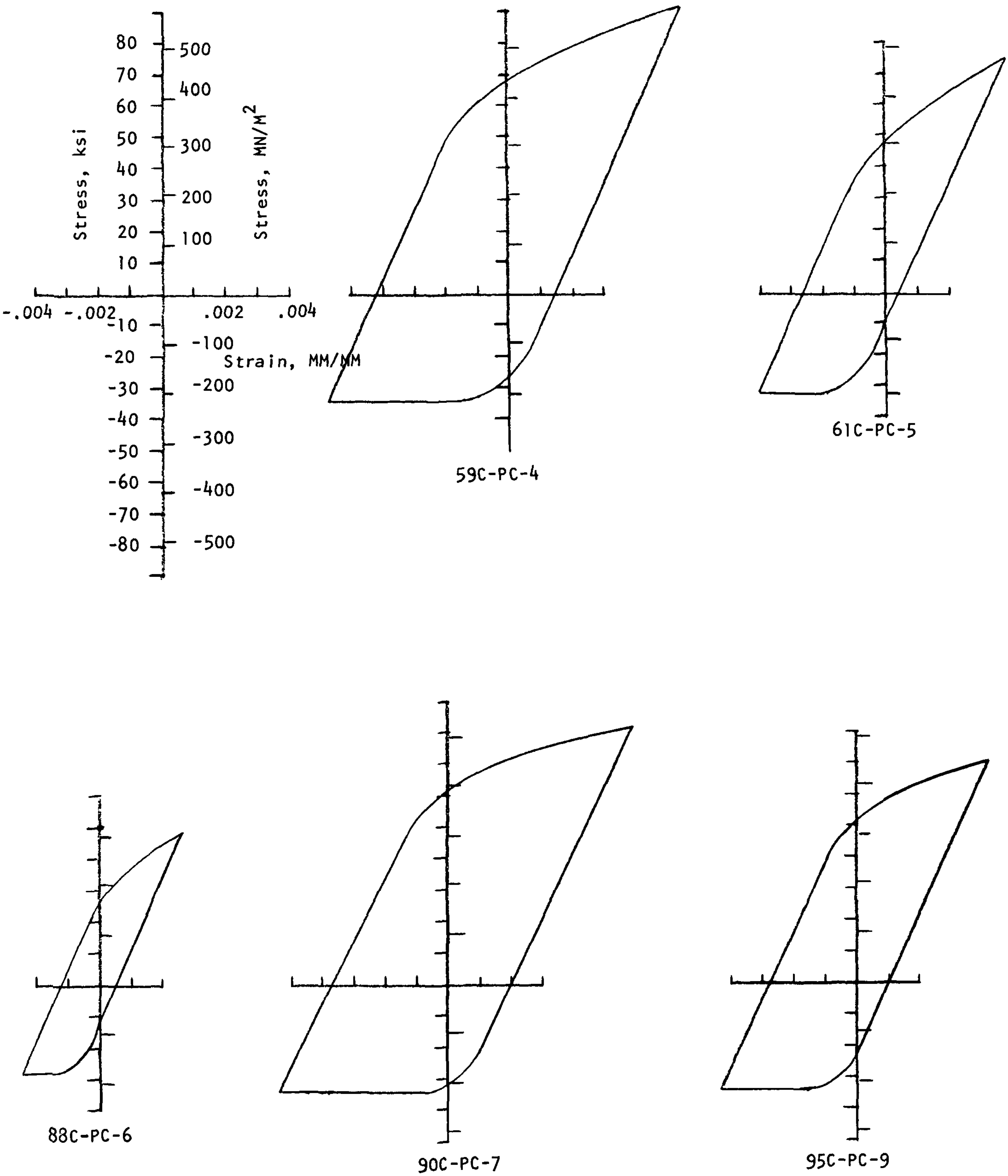

Figure A-8. Hysterisis Loops Observed for Coated Rene' 80 Tested at 871°C (1600°F) With the $\Delta\varepsilon_{pc}$ Type Deformation.

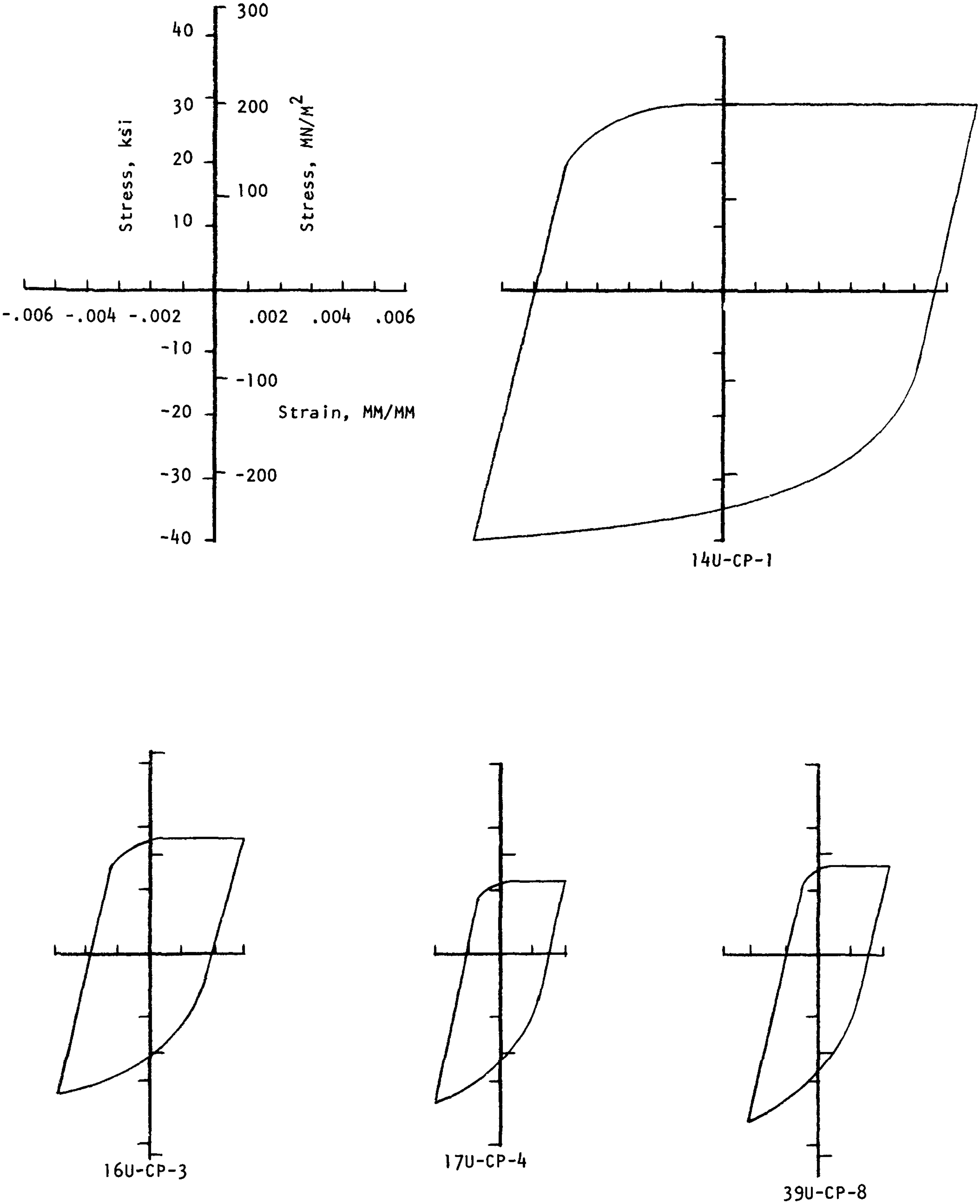

Figure A-9. Hysterisis Loops Observed for Uncoated Rene' 80 Tested at 1000°C (1832°F) with the $\Delta\varepsilon_{cp}$ Type Deformation.

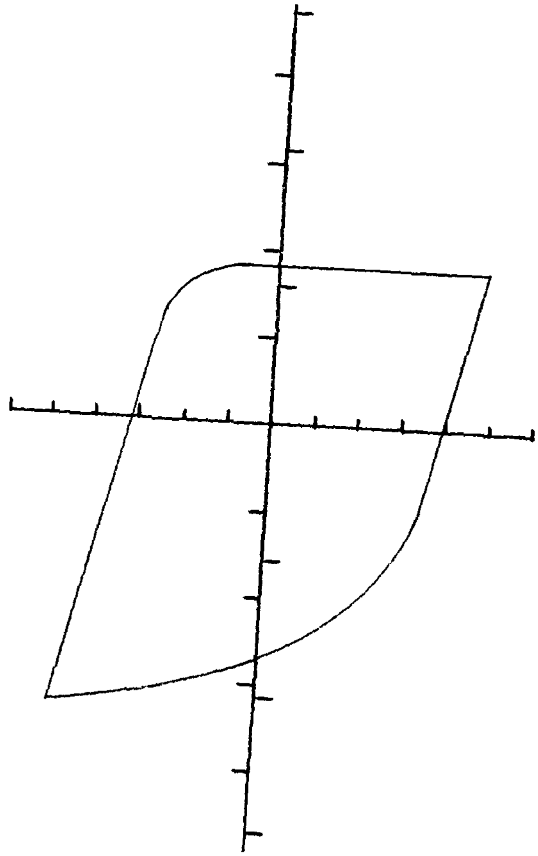

111U-CP-10

Figure A-9 continued.

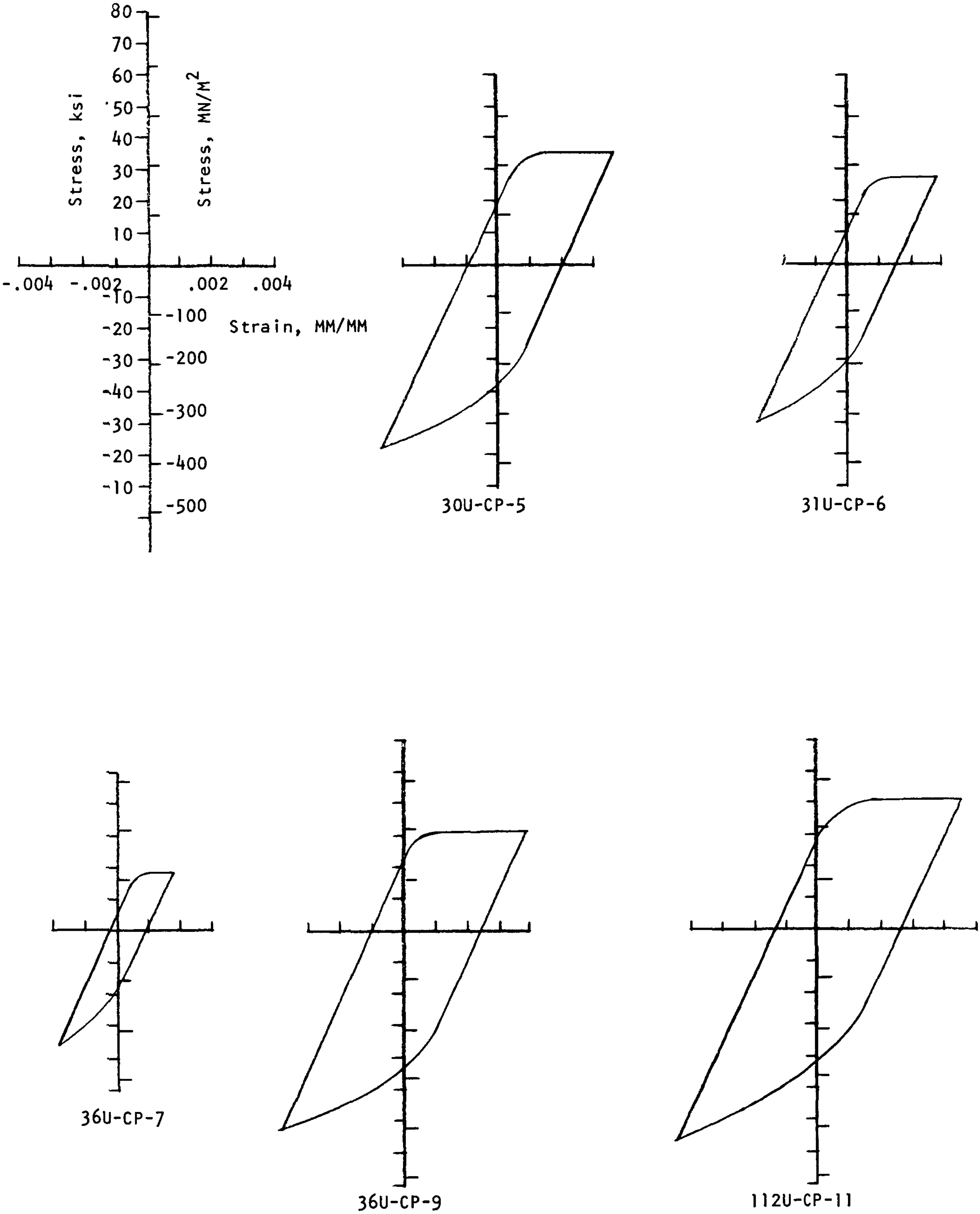

Figure A-10. Hysterisis Loops Observed for Uncoated Rene' 80 Tested at 871°C (1600°F) With the $\Delta\varepsilon_{cp}$ Type Deformation.

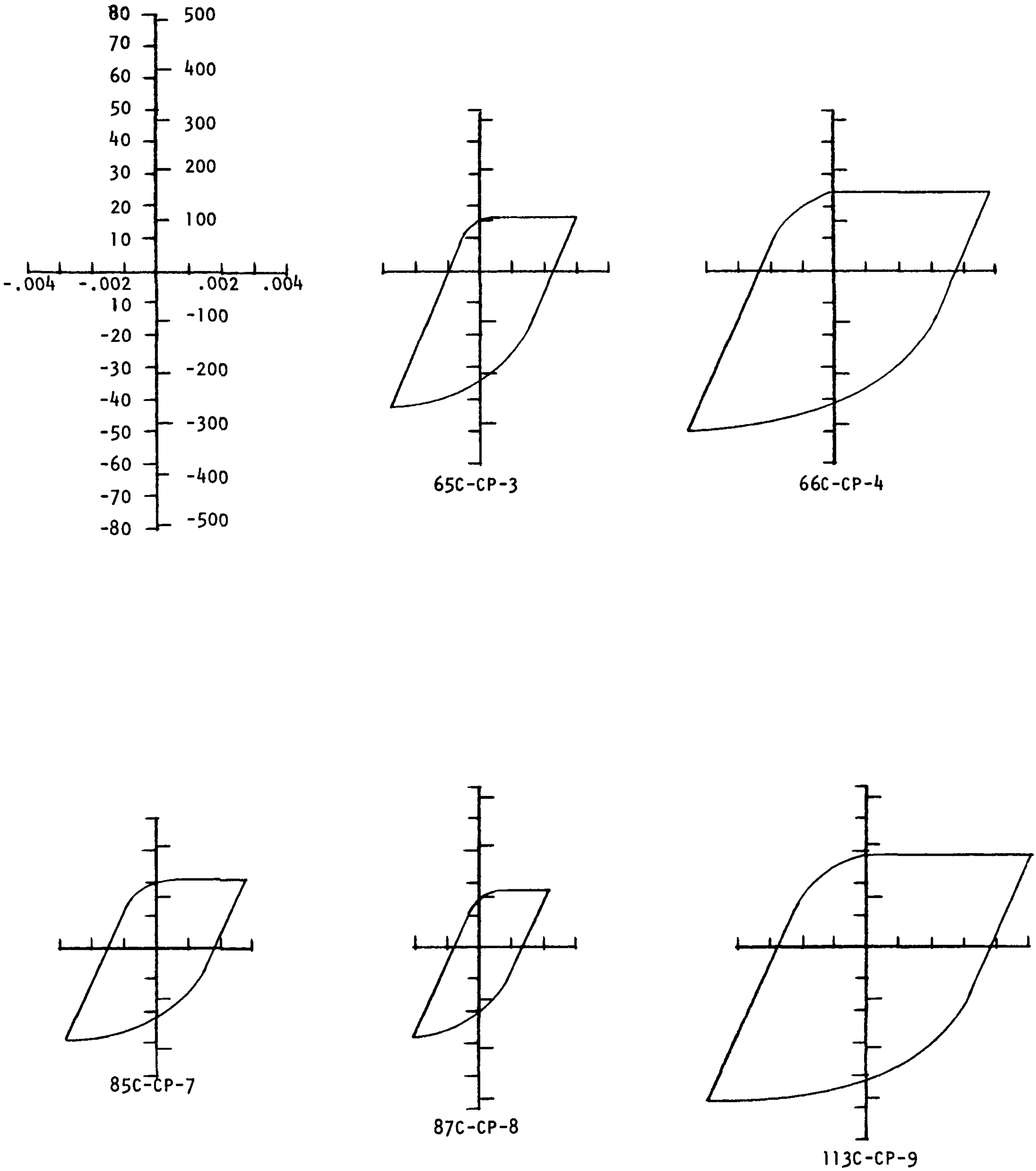

Figure A-11. Hysterisis Loops Observed for Coated Rene' 80 Tested at 1000°C (1832°F) With the $\Delta\varepsilon_{cp}$ Type Deformation.

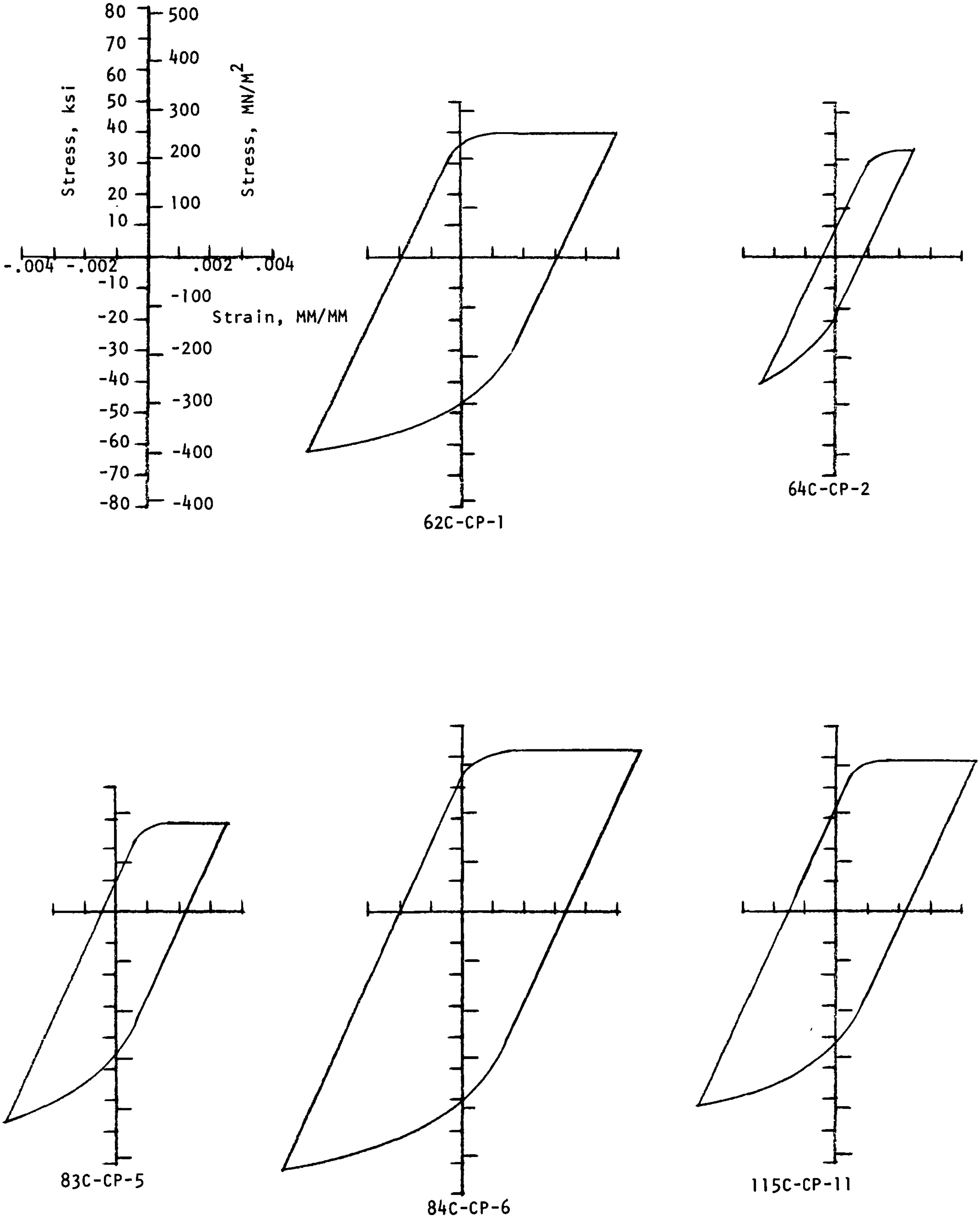

Figure A-12. Hysterisis Loops Observed for Uncoated Rene' 80 Tested at 871°C (1600°F) With the $\Delta\varepsilon_{cp}$ Type Deformation.

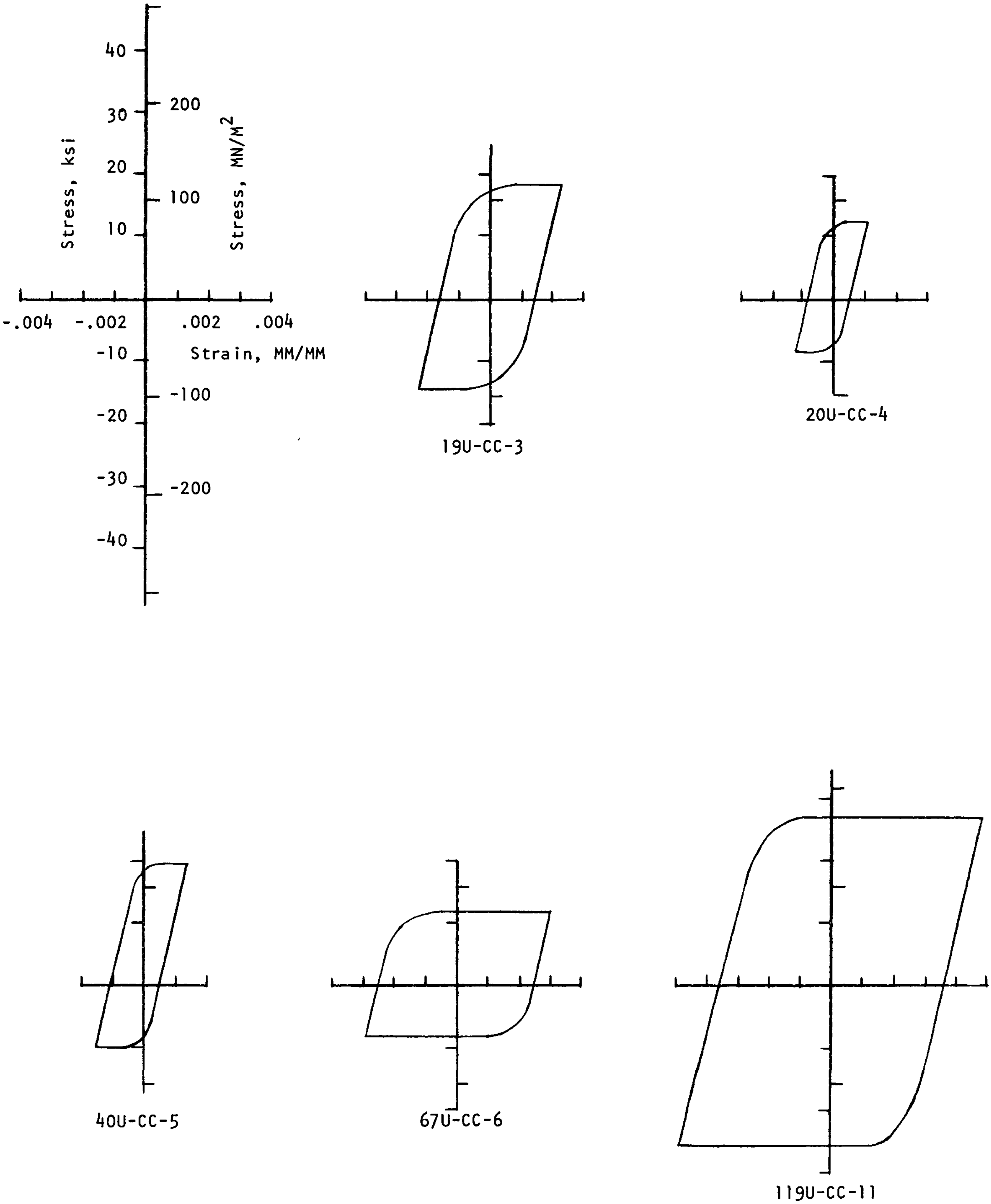

Figure A-13. Hysterisis Loops Observed for Uncoated Rene' 80 Tested at 1000°C (1832PF) With the $\Delta\varepsilon_{cc}$ Type Deformation.

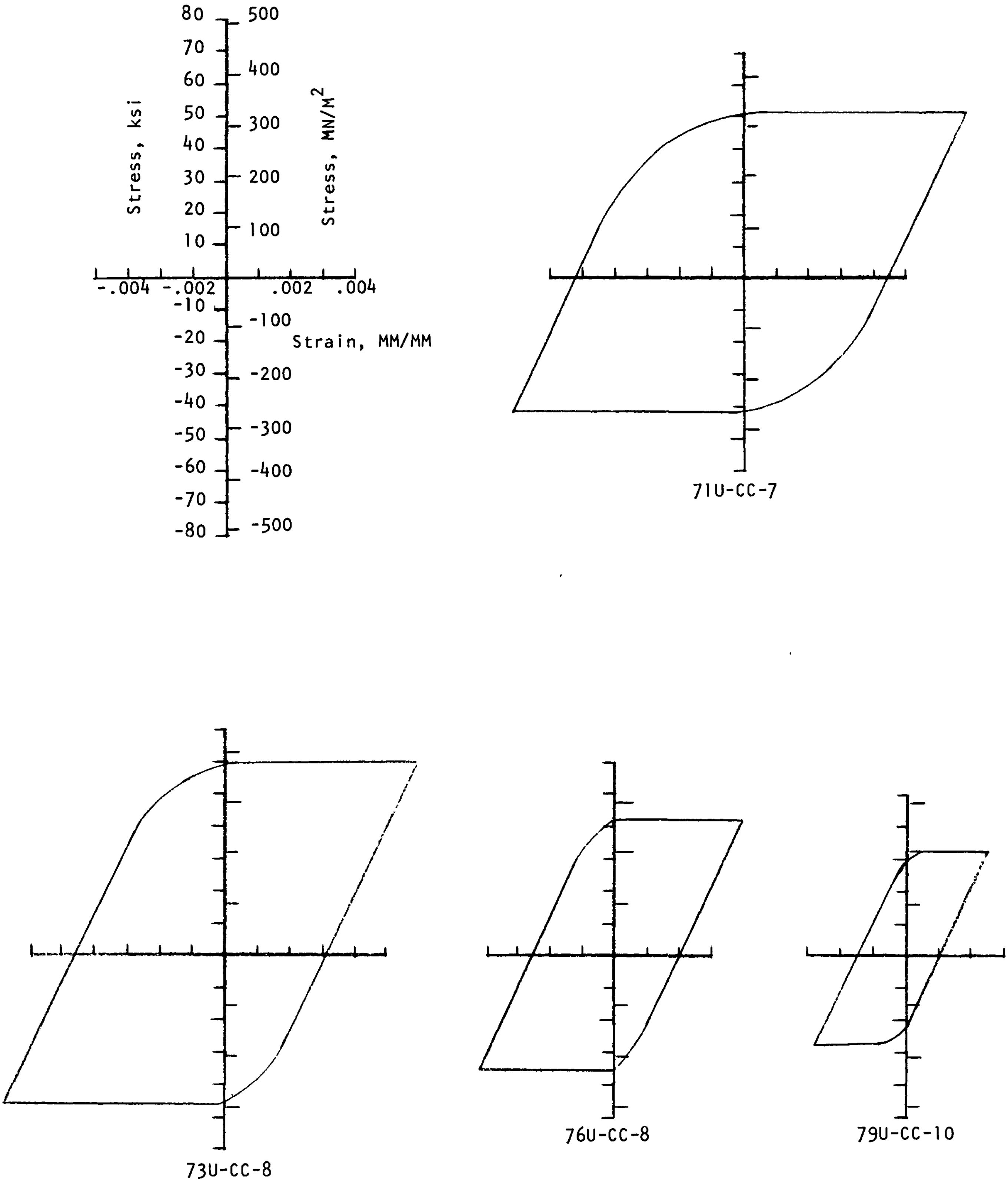

Figure A-14. Hysterisis Loops Observed for Uncoated Rene' 80 Tested at 871°C (1600°F) With the $\Delta\varepsilon_{cc}$ Type Deformation.

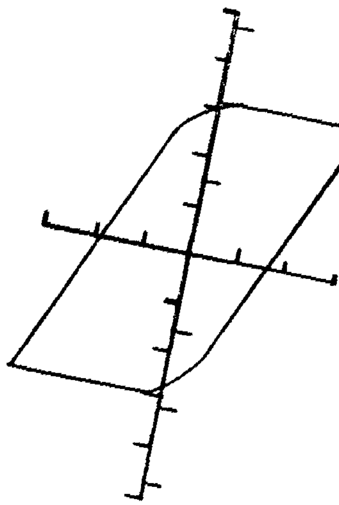

120U-CC-12

Figure A-14 (continued).

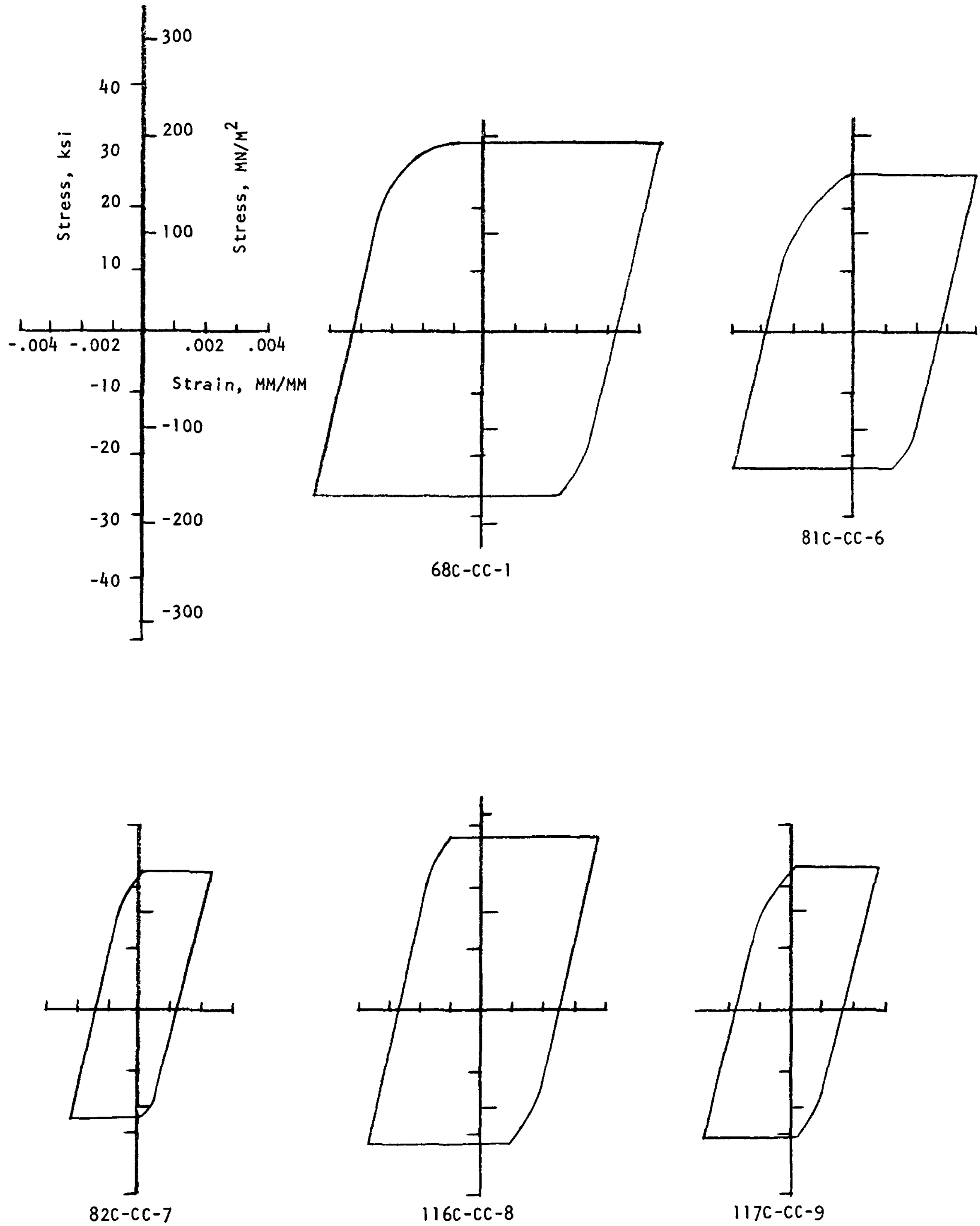

Figure A-15. Hysterisis Loops Observed for Coated Rene' 80 Tested at 1000°C (1832°F) With the $\Delta\varepsilon_{cc}$ Type Deformation.

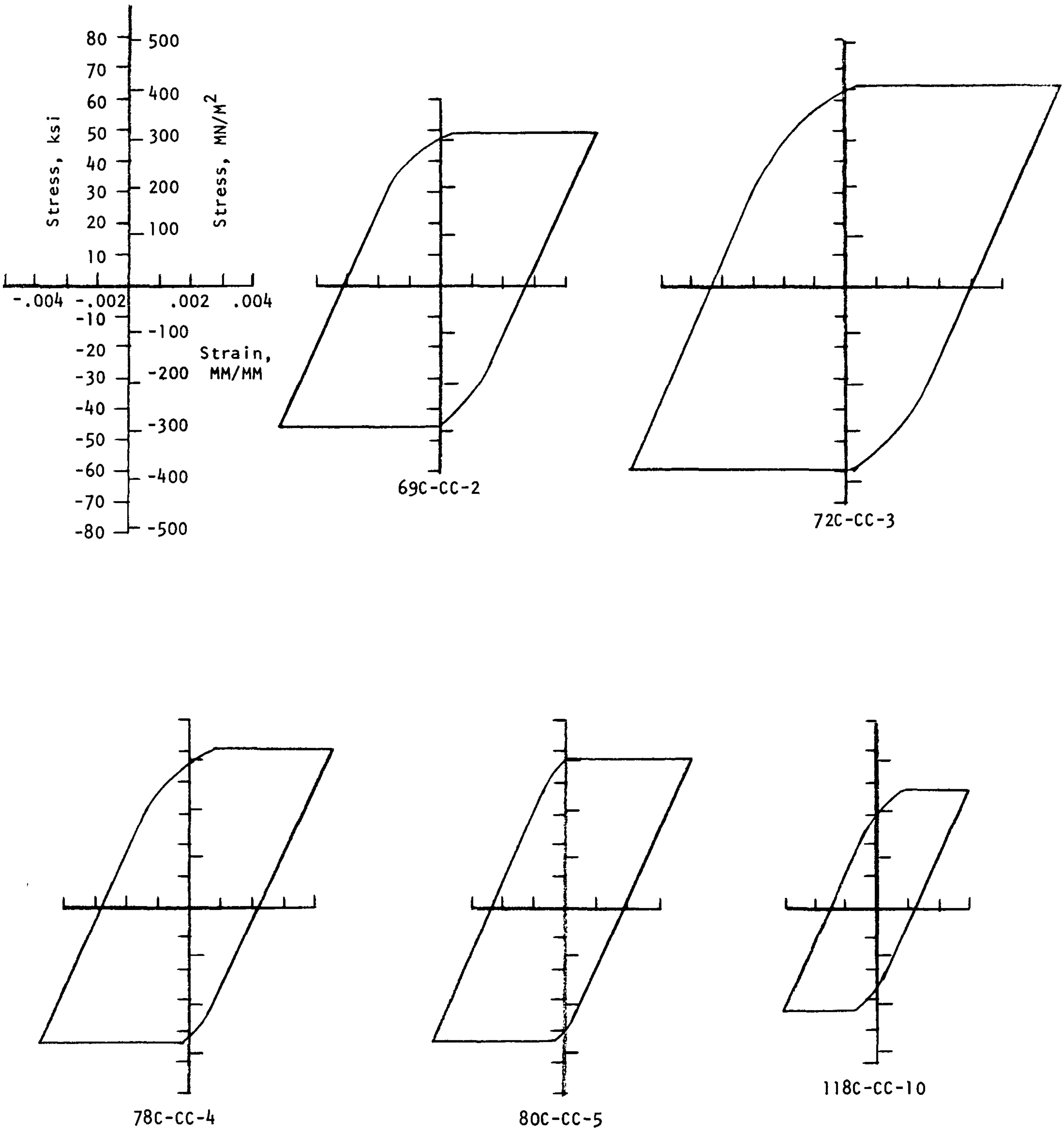

Figure A-16. Hysterisis Loops Observed for Coated Rene' 80 Tested at 871°C (1600°F) With the $\Delta\varepsilon_{cc}$ Type Deformation.

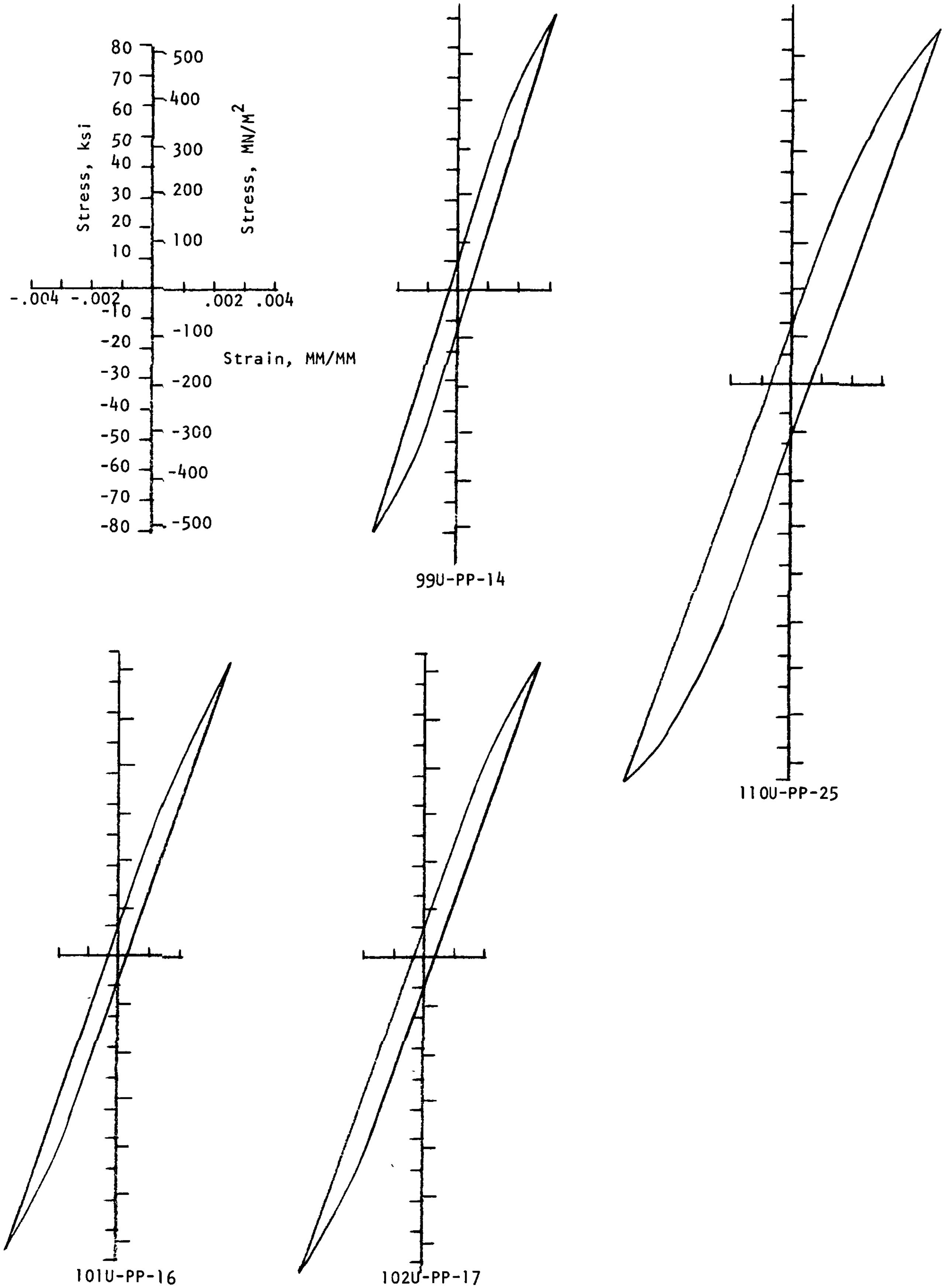

Figure A-17. Hysterisis Loops Observed for Uncoated Rene' 80 Tested at Various Temperatures with the $\Delta\varepsilon_{pp}$ Type Deformation.

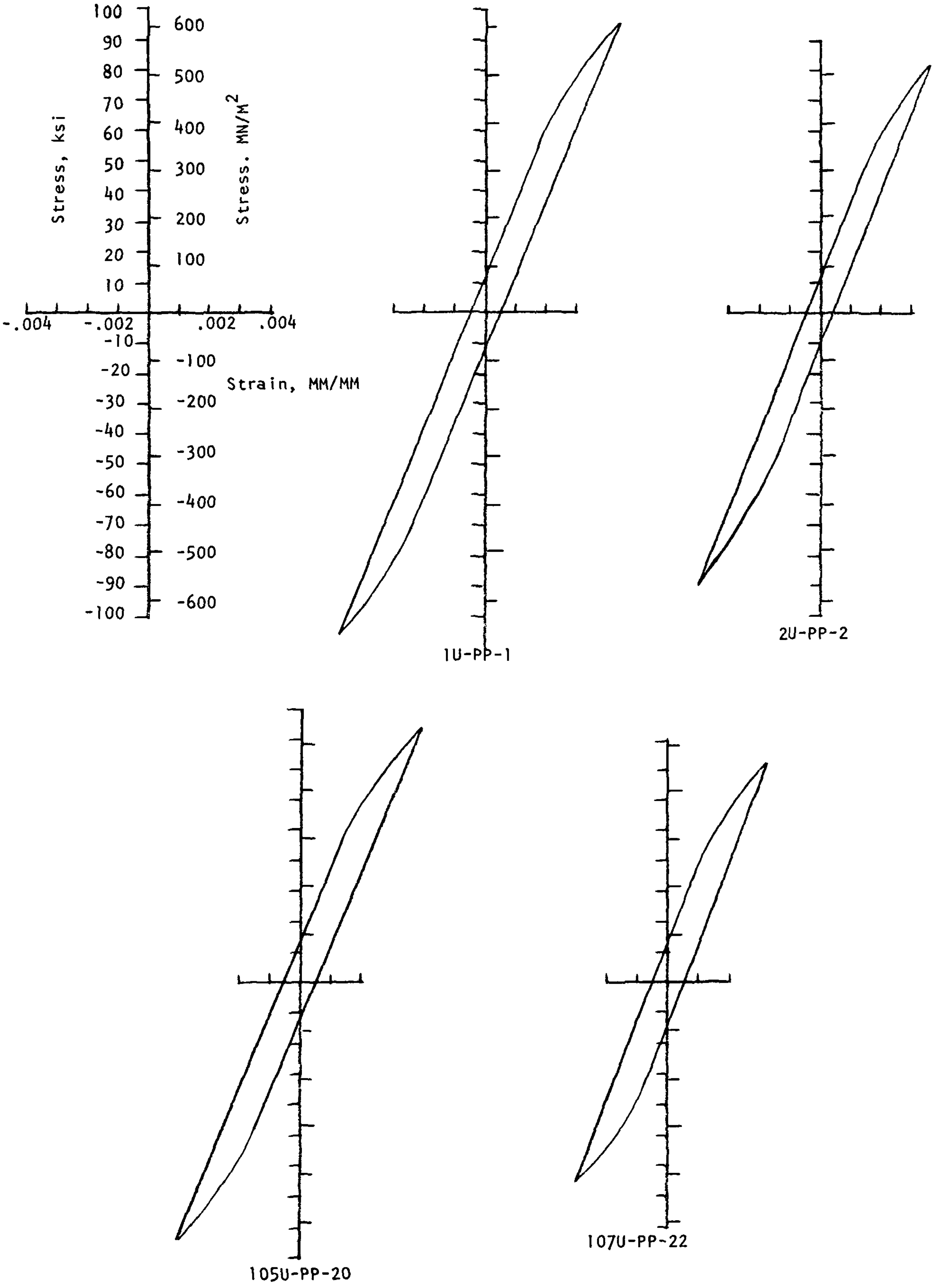

Figure A-17 (continued).

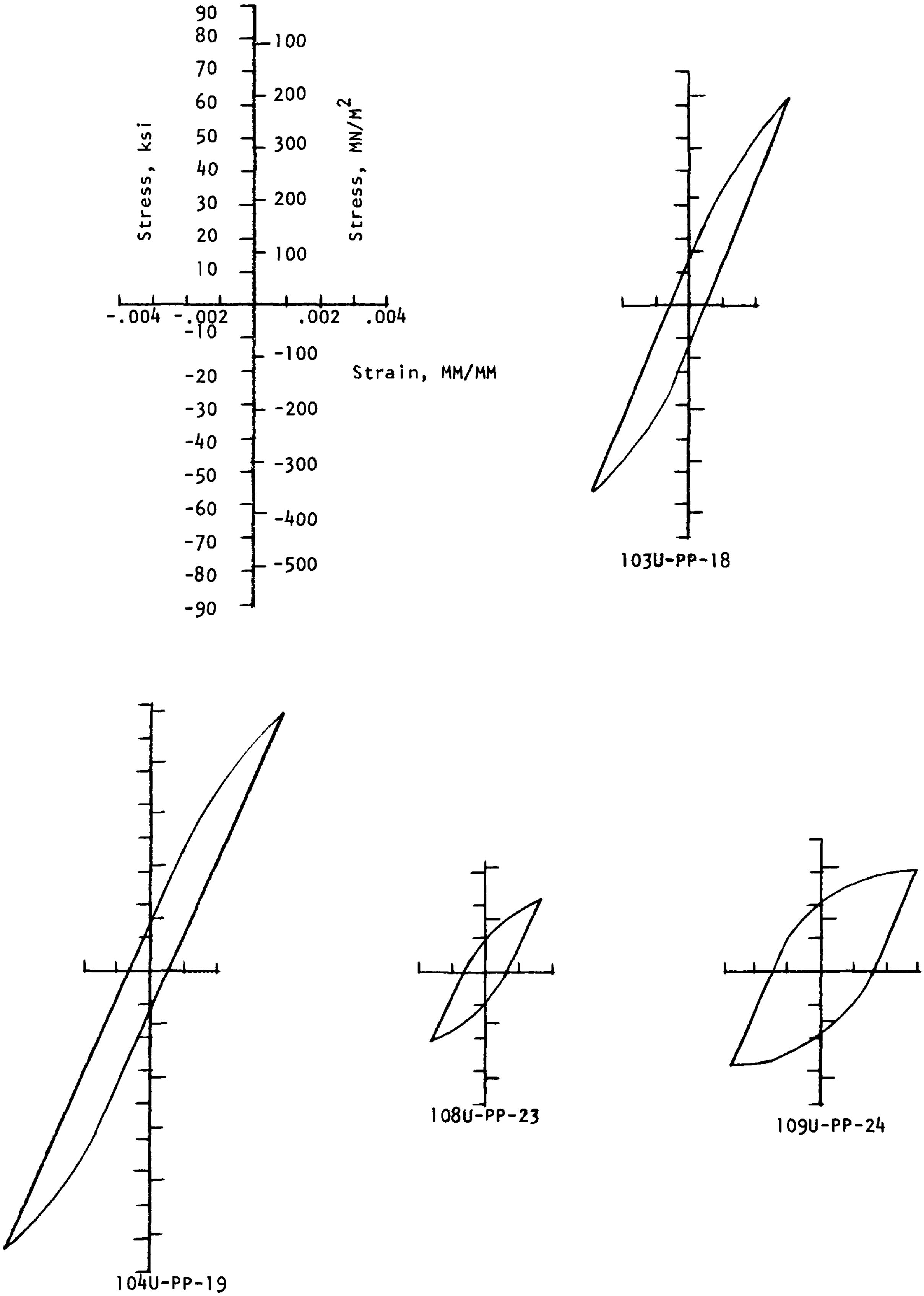

Figure A-17 (continued)

APPENDIX B

TABLE B-1

RENE' 80 TENSILE RESULTS

Specimen Number(1)	Temperature °F	Temperature °C	Ultimate Tensile Strength ksi	Ultimate Tensile Strength MN/M²	0.2% Yield Strength ksi	0.2% Yield Strength MN/M²	Percent Reduction Area %
123C-T-3	1600	871	110.4	761.2	83.4	575.1	27.8
124C-T-4	"	"	114.0	786.0	80.1	552.3	20.8
125U-T-1	"	"	106.8	736.3	79.3	546.8	27.5
126U-T-2	"	"	111.4	768.1	76.8	529.5	30.1
121C-T-1	1832	1000	67.5	465.4	33.4	230.3	29.7
122C-T-2	"	"	70.1	483.3	34.0	234.4	31.2
127U-T-3	"	"	62.2	428.9	34.2	235.8	33.5
128U-T-4	"	"	61.4	423.4	33.3	229.6	32.8

RENE' 80 CREEP RESULTS

Specimen Number(1)	Temperature °F	Temperature °C	Stress Level ksi	Stress Level MN/M²	Rupture Life hours	Percent Reduction Area
37U-C-7	1600	871	50.0	344.7	2.1	31.0
38U-C-8	"	"	35.0	241.3	84.8	23.0
53C-C-4	"	"	50.0	344.7	9.4	28.3
60C-C-5	"	"	45.0	310.3	66.6	20.6
25U-C-1	1832	1000	30.0	206.8	0.7	29.7
35U-C-6	"	"	25.0	172.4	1.0	31.1
33U-C-4	"	"	15.0	103.4	48.7	29.5
32U-C-3	"	"	15.0	103.4	52.6	32.1
63C-C-6	"	"	23.0	158.6	15.4	29.6
46C-C-1	"	"	15.0	103.4	60.0	31.1
48C-C-2	"	"	15.0	103.4	21.6	35.1

(1) The first letter in the specimen number designation stands for coated (C) or uncoated (U) material, while the second letter stands for a tensile (T) or creep (T) type of test.

DISTRIBUTION LIST

Allen, James M
Gas Turbine Eng Div -A605
Westinghouse
Lester, PA 19113

Anctil, Albert A
AMMRC
Watertown, MA 02172

Anderson, Allan F
G E - Evendale Plant
Interstate Highway 75
Mail Drop M87, Bldg 500
Cincinnati, OH 45231

Antolovich, Stephen D
Dept Matls Sci & Met Eng
489 Rhodes Hall
Univ of Cincinnati
Cincinnati, OH 45221

Barendreyht, Jerry A
G M Research Labs
12 Mile & Mound Rds
Warren, MI 48090

Barnes, Dr Robert A
Bldg 53, Room 334
G E
1 River Road
Schenectady, NY 12345

Beck, Robert
Teledyne CAE
Box 6971
Toledo, OH 43612

Bernstein, Martin D
Foster-Wheeler
110 S Orange Ave
Livingston, NJ 07039

Bowers, G W
AiResearch 93-336 J
402 S 36th St
Phoenix, AZ 85034

Bradley, E F
Chief Matl's Engineer
P&WA - United Tech Corp
400 Main St - Bldg 2-D
E Hartford, CT 06108

Brandt, D E
Bldg 53-317
G E
One River Rd
Schenectady, NY 12345

Brinkman, Dr C R (T-22)
O.R.N.L.
Box X
Oak Ridge, TN 37830
U.S.A.

Brodrick, Ronald F
Teledyne
303 Bear Hill Rd
Waltham, MA 02154

Brown, Dr E J
Office of Standards Dev
U S Nuclear Reg Comm
Washington, DC 20555

Bryan, David F
Boeing K 16-15
3801 S Oliver
Wichita, KS 67210

Cammett, Dr John T
MET-CUT
3980 Rosslyn Dr
Cincinnati, OH 45209

Campbell, Robert D
EDAC
2400 Michelson Dr
Irvine, CA 92715

Carden, Prof Arnold E
AME Dept
Box 2908
University, AL 35486

Carey, Robert S
Beckman Instruments
1117 California Ave
Palo Alto, CA 94304

Chow, Joe G Y
Brookhaven Nat Lab
Bldg 703
Upton, L I, NY 11973

Christensen, Roy H
McDonnell Douglas
Dept A3-215, MS 13-3
5301 Bolsa Ave
Huntington Beach, CA 92647

Ciuffreda, A R
EXXON Res & Engrg
Box 101
Florham Park, NJ 07932

Claudson, Dr T T
Westinghouse Hanford
Box 1970
Bldg 326 Area 300
Richland, WA 99352

Coffin, Dr Louis F Jr
G E - Corp R&D Lab
Box 8
Schenectady, NY 12301

Coles, Anton
G E M-87
Evendale, OH 45215
U.S.A.

Collins, Prof Jack A
Dept of Mech Engrg
Ohio State Univ
206 W 18th Ave
Columbus, OH 43210

Conn, Dr Andrew F
Hydronautics
7210 Pindell School Rd
Laural, MD 20810

Conrad, Dr Hans
Anderson Hall
Univ of Kentucky
Lexington, KY 40506

Conway, Dr Joseph B
Mar-Test
45 Novner Dr
Cincinnati, OH 45215
U.S.A.

Cooper, R A
Rocketdyne AC12
6633 Canoga Ave
Canoga Park, CA 91304

Corum, Dr J M
O.R.N.L.
Box Y
Oak Ridge, TN 37830

Crews, Dr John H Jr
NASA-Langley
Hampton, VA 23665

Crooker, Thomas W
Code 6384
Naval Research Lab
Washington, DC 20375

Curran, R M
G E Rm 238
273 North Ave
Schenectady, NY 12345

Dalcher, A W
G E Code S 77
310 DeGuigne Dr
Sunnyvale, CA 95030

Dalder, F
MS F-309
U.S.E.R.D.A.
Washington, DC 20545

DISTRIBUTION LIST (continued)

Davidson, Dr John R
MS-465
NASA-Langley
Hampton, VA 23665

Diercks, Dwight R
Matls Sci Div
Argonne Nat Lab
9700 S Cass Ave
Argonne, IL 60439

Dieter, Dr George E
Dir - Proc Res Inst
Carnegie-Mellon Univ
Scaife Hall
Pittsburgh, PA 15213

Donachie, Dr Matthew J
MERL J Mezz
P&WA - United Tech Corp
400 Main St
E Hartford, CT 06108

Doner, Mehmet
Detroit Diesel Allison
Box 894-W5
Indianapolis, IN 46206

Drake, Justin R
Tech Ctr
Cummins Engine
500 S Poplar St
Columbus, IN 47201

Duke, J M
Westinghouse
Box 19218
Tampa, FL 33616

Duquette, Dr D J
Matls Engrg Dept
R P I
Troy, NY 12181

Eisenstadt, Prof Ray
Mech Engrg Dept
Steinmetz Hall
Union College
Schenectady, NY 12308

Esztergar, E P
442 Westbourne St
La Jolla, CA 92037

Fiero, Ivan B
485-12
Combustion Engrg
Windsor, CT 06002

Finnie, Prof I
Dept Mech Engrg
Univ of Cal
Berkeley , CA 94720

Fitch, George E Fr
Rockwell Int'l
B-1 Div
Mail Code AD-34
Los Angeles, CA 90009

Fong, Jeffrey T
Bldg 101, Rm A302
N.B.S.
Washington, DC 20234

Frick, V (9770/2001)
Mgr, Matl's Eng
Aerojet Liquid Rocket
Box 13222
Sacramento, CA 95813

Fuchs, Dr Henry O
Mech Engrg Dept
Stanford Univ
Stanford, CA 94305

Fulton, Don
Rocketdyne
Rockwell Int'l
6633 Canoga Ave
Canoga Pk, CA 91304

Gain, Dr Brian R
G E - KAPL
Box 1072
Schenectady, NY 12301

Garofalo, Dr Frank
Inland Steel Res Lab
3001 E Columbus Dr
E Chicago, IN 46312

Gayley, Harry B
DeLaval Turbine
Nottingham Way
Trenton, NJ 08602

Gell, Dr M
MERL J Mezz
P&WA - United Tech Corp
400 Main St
E Hartford, CT 06108

Goldblatt, Dr B
AVCO - Lycoming Div
550 S Main St
Stratford, CT 06497

Goldhoff, Dr Robert M
Bldg 55, Rm 107
G E - M&P Lab
Schenectady, NY 12345

Gonyea, David C
Bldg 41, Rm 303
G E
1 River Rd
Schenectady, NY 12345

Gowda, Dr Byre
Westinghouse - ARD
Box 158
Madison, PA 15663

Grady, Harold F
Director - R&D
AVCO - Lycoming
550 S Main St
Stratford, CT 06497

Grant, Prof Nicholas J
Rm 13-2090, M I T
77 Mass Ave
Cambridge, MA 02139

Graves, Richard F
AiResearch
2525 W 190th St
Torrance, CA 90509

Greenstreet, W L
O.R.N.L.
Box Y, Bldg 9201-1
Oak Ridge, TN 37830

Griffin, Dr Donald S
Westinghouse - ARD
Box 158
Madison, PA 15663

Gross, Maj Larry
AFAPL/TBP
WPAFB
Dayton, OH 45433

Grosskreutz, Dr J C
Consultant
Black & Veatch
Box 8405
Kansas City, MO 64114

Harding, Walter L
Combustion Engrg
1000 Prospect Hill Rd
Windsor, CT 06095

Hardrath, Herbert F
MS-188M
NASA-Langley
Hampton, VA 23665

Hardrath, Herbert F
MS-188M
NASA-Langley
Hampton, VA 23665

Harris, John A
Box 2691, Loc. B-08
P&WA - United Tech Corp
W Palm Beach, FL 33402

Harrod, Dr D L
Westinghouse R&D Ctr
Beulah Rd
Churchill Boro
Pittsburgh, PA 15235

Heller, Robert A
Dept of Engrg Sci & Mech
VPI
Blacksburg, VA 24060

Herman, Dr Marvin
Detroit Diesel Allison
Box 894 - 5827 - W8
Indianapolis, IN 46206

Hillberry, Prof B M
School of Mech Engrg
Purdue Univ
W Lafayette, IN 47907

Hjelm, L
AFML/LL
WPAFB
Dayton, OH 45433

Hoeppner, David W
Engineering Dept
Univ of Missouri
Columbia, MO 65201

Holt, J M
MS-64
Research Ctr
U S Steel
Monroeville, PA 15146

Hopkins, Steven W
MERL
P&WA - United Tech Corp
Middletown, CT 06457

Howes, Dr M A H
Metals Div
IIT Res Inst
10 W 35th St
Chicago, IL 60616

Imig, Leland A
NASA - Langley
MS-188E
Hampton, VA 23665

Impellizzeri, L F
McDonnell-Douglas
Lambert Airfield
St Louis, MO 63166

Jakub, M T
General Atomic Co
Box 81608
San Diego, CA 92138

James, Lee A
Westinghouse Hanford
Box 1970
Richland, WA 99352

Jaske, Carl E
B M I
505 King Ave
Columbus, OH 43201

Jewett, Dr Robert P
Rocketdyne AC-29
6633 Canoga Ave
Canoga Pk, CA 91303

Johnson, H
AFML/LTM
WPAFB
Dayton, OH 45433

Kaye, Prof A L
Purdue Univ
Calumet Campus
2233 171st St
Hammond, IN 46323

Korth, G E
Aerojet Nuclear
550 2nd St
Idaho Falls, ID 83401

Kramer, I R
Martin Marietta Aerospace
Box 179
Denver, CO 80201

Krempl, Erhard
Mech & Aero Engrng Mech
R P I
Troy, NY 12065

Laird, Dr Campbell
Met & Matls Sci School
Univ of Penn
Philadelphia, PA 19174

Landgraf, Dr R W
Scientific Research Staff
Ford Motor
Box 2053
Dearborn, MI 48121

Langer, B F
Westinghouse
Nuclear Energy Systems
Box 355 - Penn Center
Pittsburgh, PA 15230

Lawton, Carl W
Dept 516-22
Combustion Engrg
1000 Prospect Hill Rd
Windsor, CT 06095

Lee, F F
22421 Philiprinn St
Woodland Hills, CA 91364

Leis, Brian
B M I
505 King Ave
Columbus, OH 43201

Leshenski, Steven J
Exp Mech Dept - Bldg 6
AVCO - Lycoming Div
550 S Main St
Stratford, CT 06497

Leven, Milton M
Westinghouse R&D Ctr
Buelah Road
Churchill Boroughs
Pennsylvania 15235

Leverant, Gerald R
MERL, Bldg 140
P&WA - United Tech Corp
Middletown, CT 06457
U.S.A.

Libertiny, Dr G Z
Bldg 5 Rm 1222
Ford Motor
20000 Rotunda Dr
Dearborn, MI 48121

Little, Prof Robert E
Engrg Div
Univ of Michigan
4901 Evergreen Rd
Dearborn, MI 48128

Liu, Prof H W
409 Link Hall
Syracuse Univ
Syracuse, NY 13210

Maiya, Dr P S
MSD 212
Argonne Nat Lab
Argonne, IL 60439

Mangano, Guy (PE62)
NAPTC/PEGZ
Trenton, NJ 08628

Manjoine, M J
Westinghouse R&D
Beulah Rd
Pittsburgh, PA 15235

Manson, S S
Dept Solid Mech&Struct
CWRU 314 Bingham Hall
10900 Euclid Ave
Cleveland, OH 44106

DISTRIBUTION LIST (continued)

Mar, Dr James W
Room 33-307
M. I. T.
Cambridge, MA 02139

Mauney, David A
Alcoa Labs
Alcoa Center, PA 15069

McConnelee, J E
G E - Matls & Proc Lab
55 North Ave
Schenectady, NY 12345

McEvily, Prof A J
Met Dept U-136
Univ of Conn
Storrs, CT 06268

Mehringer, Frank J
KAPL - GE
Box 1072
Schenectady, NY 12301

Miller, C R
Gas Turbine Res
Tech Ctr F-1
Caterpillar Tractor
Peoria, IL 61611

Miller, James
G E Bldg 24601
1000 Western Ave
Lynn, MA 01905

Miller, Roy W
Atkins & Merrill, Inc
Main St
Ashland, MA 01721

Mindlin, Dr Harold
B M I
505 King Ave
Columbus, OH 43201

Mitchell, M R
306-C Talbot Lab
TAM Dept
Univ of Illinois
Urbana, IL 61801

Moen, R G
Turbine Engrg
Nordberg Mfg
4608 N Marlborough
Milwaukee, WI 53211

Mogul, J
Dir - Matls Engrg
Curtiss-Wright
1 Passaic St
Wood-Ridge, NJ 07075

Moon, David M
Westinghouse
R&D Center
Beulah Rd
Pittsburgh, PA 15235

Morrow, Prof JoDean
321A Talbot Lab
Univ of Ill
Urbana, IL 61801

Moteff, Dr J
Dept Matls Sci & Met Eng
Location 12
Univ of Cincinnati
Cincinnati, OH 45221

Mowbray, Donald F
Bldg 55-219
G E
1 River Rd
Schenectady, NY 12345

O'Donnell, Dr W J
O'Donnell & Assoc
5100 Centre Ave
Pittsburgh, PA 15232

Opinsky, Dr A J
Bldg 14-1, GE
2901 E Lake Rd
Erie, PA 16531

Osias, Dr John
Engineering 3S-1
P&WA - United Tech Corp
400 Main St
E Hartford, CT 06108

Ostergren, Warren J
Bldg 53, Rm 317
Gas Turbine Dept
G E
Scenectady, NY 12345

Paquette, Walter J
General Dynamics
Grants Lane
Box 748 MZ 2829
Fort Worth, TX 76101

Pelloux, Prof Regi M
M I T, Rm 8-237
77 Mass Ave
Cambridge, MA 02139

Peterson, George P
Director, AFML (CC)
WPAFB
Dayton, OH 45433

Picklesimer, Dr M L
Chief, Mech Prop Sect
N B S
B120 Matls Bldg
Washington, DC 20234

Popp, Herbert G
Bldg 500, Mail Stop M-87
MPTL - AEG
G E
Cincinnati, OH 45242

Reemsnyder, Harold S
Homer Research Labs
Bethlehem Steel
Bethlehem, PA 18016

Reynolds, Dr E E
G M Technical Center
Warren, MI 48069

Rocker, James R
MS-374
NASA-Langley Res Ctr
Hampton, VA 23665

Rostoker, Prof William
Dept Matl's Engrng
Univ of Illinois
Box 4348
Chicago, IL 60680

Sandor, Prof Bela I
Dept Engrng Mech
2359 Engineering Bldg
Univ of Wisconsin
Madison, WI 53705

Schaefer, A O
M P C
United Engineering Center
345 E 47th St
New York, NY 10017

Schmidt, E H
AiResearch Ind Div
9225 Aviation Blvd
Box 92992
Los Angeles, CA 90009

Schultz, Carl C
B & W
R & D Division
Box 835
Alliance, OH 44601

Severud, I K
Mgr, Plant Analysis
Westinghouse-Hanford
Box 1970
Richland, WA 99352

Shahinian, P
Code 6305
Naval Research Lab
Washington, DC 20375

Sharpe, William N Jr
Dept Metallurgy Mechanics
and Materials Science
Mich State Univ
E Lansing, MI 48824

DISTRIBUTION LIST (continued)

Sheffler, Dr K D
MERL J Mezz
P&WA - United Tech Corp
400 Main St
E Hartford, CT 06108

Sherby, Prof Oleg D
Dept of Matls Sci
Stanford Univ
Stanford, CA 94305

Siegel, Howard J
Dept-247 Bldg-32 Level-2
McDonnell Aircraft Co
Box 516
St Louis, MO 63166

Sinclair, Prof G M
321 Talbot Lab
Univ of Ill
Urbana, IL 61801

Sines, Prof George
Matl's Dept, Engineering
U C L A
Los Angeles, CA 90024

Slot, Dr T
2 Yorkshire Terrace
Clifton Park, NY 12065

Smith, Dr Thomas E Jr
Mgr, Research Analysis
Waukesha Engine Div
St Paul Ave
Waukesha, WI 53186

Snow, Alfred L
12 Nottingham Dr
Greensburg, PA 15601

Sokol, George J
Bldg A-3 Rm 208
G E - KAPL
Schenectady, NY 12301

Solomon, H D
G E - Corp R&D Ctr
Box 8
Schenectady, NY 12305

Springer, W E U29A
Detroit Diesel
Allison Div GMC
Box 894
Indianapolis, IN 46206

Stetson, Alvin R
Solar Division
2200 Pacific Highway
San Diego, CA 92138

Stross, William J
MET-CUT
3980 Rosslyn Dr
Cincinnati, OH 45209

Sullivan, C P
CDS - MERL
P&WA - United Tech Corp
E Hartford, CT 06108

Swindeman, Dr Robert W
Metals & Ceramics Div
O.R.N.L. - Bldg 4500S
Box X
Oak Ridge, TN 37830

Tallan, Dr Norman M
Code AFML/LLM
WPAFB
Dayton, OH 45433
U.S.A.

Thevenow, V H
Detroit Diesel
Allison Div GMC
Box 894 W-8
Indianapolis, IN 46206

Throop, Joseph F
Benet Weapons Lab
Watervliet Arsenal
Watervliet, NY 12189

Timo, Dominic P
G E
Bldg 41, Rm 301
1 River Rd
Schenectady, NY 12345

Van Der Sluys, Dr W A
Research Ctr
B & W
Box 835
Alliance, OH 44601

Van Nimwegen, R R
AiResearch
402 S 36th St
Phoenix, AZ 85034

VanWanderham, Marvin C
United Technologies Corp
Box 2691, Loc B-08
W Palm Beach, FL 33402
U.S.A.

Vogel, William H (EB 2G4)
P&WA - United Tech Corp
400 Main St
E Hartford, CT 06108

Voorhees, Howard R
Matls Tech Corp
Box 358
Ann Arbor, MI 48107

Walker, Dr C D
Bldg 55, Rm 213
G E
Schenectady, NY 12345

Walker, W J
Air Force Off Sci Res
Directorate of Aero Sci
1400 Wilson Blvd
Arlington, VA 22209

Weertman, Prof Julia R
Dept of Mtl's Sci
Northwestern Univ
Evanston, IL 60201

Weiss, Dr Volker
409 Link Hall
Syracuse Univ
Syracuse, NY 13210

Wells, Dr Clifford H
Southwest Research
P.O. Drawer 28510
San Antonio, TX 78284

Wetzel, Richard M
MTS
Box 24012
Minneapolis, MN 55424

Williams, Dell P
Chief, Matls Sci Br
NASA Ames Research Ctr
Moffett Field, CA 94035

Woodford, Dr David A
G E - Corp R&D Ctr
Box 8
1 River Rd
Schenectady, NY 12301

Wundt, Boris M
2346 Shirl Lane
Schenectady, NY 12309

Zamrik, Prof Sam
Penn State Univ
121 Hammond Bldg
University Park, PA 16802
U.S.A.

NASA Sci&Tech Info (10)
Facility-Accession Dept
Box 8757
Balt/Wash Intnl Airport
Maryland 21240

Defense Documentation Ctr
Cameron Station
5010 Duke St
Alexandria, VA 22314

DISTRIBUTION LIST (continued)

MCIC
Battelle Memorial Inst
505 King Ave
Columbus, OH 43201

Tech Reports Library (3)
U S AEC
Washington, DC

Tech Info Service (3)
U S AEC
Box 62
Oak Ridge, TN

Project Manager (79)
NASA-Lewis
21000 Brookpark Rd
Cleveland, OH 44135

Library MS-185
NASA
Langley Research Ctr
Langley Field, VA 23365

Library
NASA
Marshall Space Flight Ctr
Huntsville, AL 35812

Tech Library / JM6
NASA
Manned Spacecraft Ctr
Houston, TX 77058

Library - Acquisitions
NASA - JPL
4800 Oak Grove Dr
Pasadena, CA 91102

Library
NASA
Goddard Space Flight Ctr
Greenbelt, MD 20771

Library
NASA
Flight Research Ctr
P O Box 273
Edwards, CA 93523

Library MS 202-3
NASA
Ames Research Ctr
Moffett Field, CA 94035

Technical Library
AFML/LAM
WPAFB
Dayton, OH 45433

Research Library
United Tech Corp
400 Main St
E Hartford, CT 06108

Library
P&WA
United Tech Corp
W Palm Beach, FL 33402

Library
General Electric Co
Box 8
Schenectady, NY 12301

Techn Info Ctr
AEG
General Electric Co
Cincinnati, OH 45215

Library
Detroit Diesel Allison
General Motors Corp
340 White Rover Pkwy
Indianapolis, IN 46206

Library
Denver Research Institute
University Park
Denver, CO 80210

Technical Library
Sargent & Lundy
Room 27P48
55 E Monroe St
Chicago, Il 60603

Aerojet Liquid Rocket Ctr
Tech Info Ctr 7362
c/o R Duncan
Box 1322
Sacramento, CA 95813

Technical Library
Hamilton Standard
Div of United Tech Corp
Windsor Locks, CT 06096

Technical Library
SKF Industries
1100 First Ave
King of Prussia, PA 19406

R&D Library
Huntington Alloy Prod Div
International Nickel
Huntington, WV 25720

Technical Library
Lockheed-California
Burbank, CA 91503

Technical Library
McDonnell-Douglas Corp
Missiles & Space Div
5301 Bolsa Ave
Huntington Beach CA 92647

Technical Library
North Amer Rockwell
6633 Canoga Ave
Canoga Pk, CA 91304

Technical Library
Northrop Corp
Aircraft Div
3901 West Broadway
Hawthorne, CA 90250

Technical Library
Philco-Ford Corp
Ford Road
Newport Beach, CA 92663

Technical Library
Sandia Corp
Albuquerque, NM 87115

Technical Library
AVCO-Space Systems Div
Lowell Industrial Pk
Lowell, MA 01851

Technical Library
Beech Aircraft
Wichita, KS 67201

Technical Library
Continental Aviation
127 Kercheval Ave
Detroit, MI 48215

Technical Library
Douglas Aircraft Co
3855 Lakewood Blvd
Long Beach, CA 90801

Technical Library
G E
1000 Western Ave
Lynn, MA 01905

Technical Library
U S AAMRDL
Fort Eustis, VA 23604

Technical Library
Solar
Div of Int'l Harvester
2200 Pacific Hwy
San Diego, CA 92101

DISTRIBUTION LIST (continued)

Library - Tech Ctr
Fisher Controls Co
205 S Center St
Marshalltown, IA 50158

Report Control Office
NASA MS 5-5
Lewis Research Ctr
21000 Brookpark Rd
Cleveland, OH 44135

Contracts Sect B
NASA MS 500-313
Lewis Research Ctr
21000 Brookpark Rd
Cleveland, OH 44135

Chief, Fracture Branch
MS 105-1
NASA-Lewis Research Ctr
21000 Brookpark Rd
Cleveland, OH 44135

Chief, Comp & Struct Br
MS 49-3
NASA-Lewis Research Ctr
21000 Brookpark Rd
Cleveland, OH 44135

Chief, Alloys Branch
MS 49-3
NASA-Lewis Research Ctr
21000 Brookpark Rd
Cleveland, OH 44135

Technical Library
Southwest Research
8500 Culebra Rd
San Antonio, TX 78284

Patent Council
NASA MS 500-311
Lewis Research Ctr
21000 Brookpark Rd
Cleveland, OH 44135

AAMRDL Office
MS 77-5
NASA Lewis Cesearch Ctr
21000 Brookpark Rd
Cleveland, OH 44135

Chief, Surr Protect Br
MS 49-3
NASA-Lewis Research Ctr
21000 Brookpark Rd
Cleveland, OH 44135

Chief, Mtls Appl Br
MS 105-1
NASA-Lewis Research Ctr
21000 Brookpark Rd
Cleveland, OH 44135

Head, Fatigue Res Sect
MS 49-1
NASA-Lewis Research Ctr
21000 Brookpark Rd
Cleveland, OH 44135

Technology Utilization
NASA MS 3-19
Lewis Research Ctr
21000 Brookpark Rd
Cleveland, OH 44135

Library (2)
NASA MS 60-3
Lewis Research Ctr
21000 Brookpark Rd
Cleveland, OH 44135

AFSC Liaison Office
MS 501-3
NASA Lewis Research Ctr
21000 Brookpark Rd
Cleveland, OH 44135

Assoc Chief, M&S Div
MS 105-1
NASA-Lewis Research Ctr
21000 Brookpark Rd
Cleveland, OH 44135

Chief, M&S Div 49-1
Report File
NASA-Lewis Research Ctr
21000 Brookpark Rd
Cleveland, OH 44135